To the Graduate Council:

I am submitting herewith a thesis written by William B. Cathey entitled "Implications of the Geology and Geochemistry of the Maclean Five Uranium Deposit, Three Rivers, Texas." I recommend that it be accepted in partial fulfillment of the requirements for the degree of Master of Science, with a major in Geology.

Kula C. Misra

Kula C. Misra, Major Professor

We have read this thesis
and recommend its acceptance:

Lawrence A. Taylor

Daman S. Walia

Fred B. Keller

Otto C. Kopp

Accepted for the Council:

L Evans Beck

Vice Chancellor
Graduate Studies and Research

IMPLICATIONS OF THE GEOLOGY AND GEOCHEMISTRY OF THE MACLEAN FIVE URANIUM DEPOSIT, THREE RIVERS, TEXAS

A Thesis

Presented for the

Master of Science

Degree

The University of Tennessee, Knoxville

William B. Cathey

June 1980

ACKNOWLEDGMENTS

I would like to express my appreciation to Exxon Minerals Company, U.S.A., for their cooperation in making this research possible. In particular, I would like to thank R. V. Spivey (former Operations Manager), Carl Oman, Steve Collings, and Ken Barrett (head mine geologist), who were instrumental in helping me obtain authorization through proper channels within Exxon. I would like to thank the present Operations Manager, Larry Hayes, for authorizing the release of hydrocarbon data from the Live Oak County area. I would also like to acknowledge helpful discourse provided by several experienced Exxon engineers and geologists, including Mike Barker, Bob Pickens, Bob Davids, Richard Barr, Steve Young, and Bill MacIntire. I would especially like to thank Brenda Bombers of Texas A & M, who unselfishly provided the core samples for the study.

I am indebted to Louis Pogorski, president of Chemical Projects, Ltd., for authorizing expensive hydrocarbon analyses free of charge, and to Oak Ridge Associated Universities, for providing fellowship assistance and access to NAA equipment. I would like to specifically acknowledge Damon Walia and Clayton Gist for their guidance while I was in residence at ORAU. I would also like to thank Todd Butz of the Union Carbide Corporation, NURE program, for providing standards for comparison with NAA values.

Finally, I would like to thank Dr. Kula Misra, my advisor, for his support and guidance, and my committee members, Dr. L. A. Taylor, Dr. F. B. Keller, Dr. O. C. Kopp, and Dr. D. Walia for their helpful

suggestions. I also owe the typist, Patsy Bivens, of Oak Ridge, Tennessee, a debt of gratitude for her perseverence. Last but not least, I am indebted to my devoted wife, Ann, who stood by me through five long, difficult years of college, and to my parents, who graciously provided financial assistance through much of my college career.

ABSTRACT

The Maclean five uranium deposit is an unusual "dike-like" accumulation of uranium and molybdenum minerals in the Miocene fluvial Oakville Sandstone, along a down-to-coast normal fault that displaces both the Catahoula and Oakville Formations. The fault-related configuration of these ores presents a marked contrast with adjacent roll-front and tabular deposits to the north.

Petrographic analysis of the barren host rock reveals a composition including 17.3% limestone rock fragments (LRF's), 22.2% volcanic rock fragments (VRF's), and 19.4% calcite cement. The percentage of calcite cement decreases significantly away from the fault, suggesting the bulk of cementing solution was introduced through the fault zone. The preservation of details in calcite fossil detritus, the calcite cement, and the groundwater geochemistry reflect alkaline conditions during the evolution of the Oakville Sandstone. Alkaline leaching of VRF's, especially glassy fragments, led to mobilization of metallic elements such as U. Bulk rock calculations based on U concentrations of volcanics in the source area (Big Bend, Texas) show considerable amounts of uranium may have been leached from the Oakville during diagenesis, providing an internal source for mineralizing fluids.

X-ray diffraction and electron microprobe analyses indicate the ore assemblage to be predominantly uraninite and cofffinite, with subordinate sphalerite and marcasite (rare pyrite). The high molybdenum content of the ore suggests the presence of Mo minerals or mineraloids. Ore textures reflect dissolution, replacement, and precipitation in

voids, and indicate drastic local fluctuations in pH. Ore-stage minerals almost invariably replace the calcite cement, proving that much of the calcite was an early or pre-ore phase.

Neutron activation analysis (NAA) data establish that elements fixed in inherent host rock minerals are pseudonormally or normally distributed, whereas elements associated with uranium are lognormally distributed. Depth-concentration plots show three vertical zones of uranium enrichment. Uranium in the core samples displays highly significant positive correlations with Mo and As.

The Maclean Five deposit differs from roll-front and tabular uranium deposits in several important respects: (1) dike-like distribution of mineralization; (2) strong positive correlation of U with associated elements; (3) unusually high concentrations of U and Mo, implying a sharp depositional gradient; (4) rarity of pyrite and abundance of marcasite. These deviations are significant in terms of U geochemistry, and warrant forumlation of a new ore-model.

The proposed "fault-trap" model of ore formation includes three phases: (1) dissolution of pre-existing mineralized bodies in response to weathering and stream erosion; (2) discharge of uraniferous carbonate solutions to a restricted fault zone; (3) precipitation of calcite within the microenvironments of pre-existing cement and deposition of ore-stage minerals, due to sharp, local reductions in pH. Eh remains relatively constant at the fault zone due to a continual influx of reducing gases from hydrocarbon deposits at depth.

Narrow linear anomalies of U, Mo, and As in geochemical sampling media should serve as potential pathfinders for this deposit-type.

Considering the numerous regional normal faults along the Gulf Coast, it seems highly probable that similar deposits exist elsewhere. Application of the fault-trap model of uranium mineralization may lead to exciting new discoveries, even in areas of extensive previous exploration.

TABLE OF CONTENTS

CHAPTER		PAGE
I.	INTRODUCTION	1
	Scope of the Research	1
	Geology of the Maclean Five Pit	4
	Objectives of the Thesis Research	6
	Methodology	6
	Field Methods	6
	Radiometric measurements	7
	Lithologic sampling	11
	Sampling for hydrocarbon analyses	11
	Core sampling	11
	Laboratory Methods	11
	Petrography	11
	Trace element analysis	12
	Practical Limitations	12
	Previous Investigations	13
	Live Oak County Uranium Deposits	13
	Felder Mine	13
II.	GEOLOGIC SETTING	17
	Regional Geology	17
	Local Stratigraphy	18
	Structural Styles	22
III.	SEDIMENTARY PETROLOGY	24
	Introduction to the Oakville Petrology	24
	Lithologic Constituents	24
	Quartz	24
	Feldspars	25
	Limestone Rock Fragments (LRF's)	25
	Volcanic Rock Fragments (VRF's)	30
	Authigenic Sulfides	31
	Cement	31
	Miscellaneous	32
	Modal Analyses	32
	Interpretation and Discussion	35
	Chemical Alteration	35
	Silicification	35
	Clay formation	39
	Sulfidization	39
	Cementation	40

CHAPTER PAGE

Pre-Ore Paragenetic Sequence 42
Host Rock Geochemistry 44
Uranium Source for the Oakville 45

IV. ORE PETROLOGY 48

Mineralogy 48
Ore Textures 49
Dissolution 49
Replacement 49
Co-Precipitation 54
Deposition in Voids 55
Sequential Deposition 55
Ore-Stage Paragenetic Sequence 55
Mineral Stabilities 56

V. TRACE ELEMENT ANALYSIS 60

Interpretation of Element Data 60
Error Analysis 60
Summary Statistics 60
Depth-Concentration Plots 61
Pearson Correlation Matrix 68
Element-Element Plots for Linear Correlation 70
Comparison of Maclean Five Deposit with Some Other Uranium Deposit-Types 72
Trends in Common Types of Uranium Deposits 72
Roll-front deposits 72
Tabular deposits 74
Trends in the Maclean Five Deposit 77

VI. MODEL FOR FAULT-TRAP MINERALIZATION 79

Background Information 79
Genetic Evidence 79
Reductant Source 81
Aqueous Hydrocarbon Associations 81
Model of Ore Genesis 82
Geochemical Considerations 82
Host Rock Preparation 86
Stage I: Roll-Front Development 87
Stage II: Weathering and Stream Erosion 87
Stage III: Fault-Trap Mineralization 90
Oxidation and Supergene Enrichment 91
Timing of Ore Emplacement 91
Application to Exploration 92

CHAPTER PAGE

VII. SUMMARY AND CONCLUSIONS 94

Summary 94
Conclusions 96

REFERENCES 98

APPENDICES 103

APPENDIX A. ERROR CALCULATION FOR MODAL ANALYSIS 104

APPENDIX B. HOST ROCK GEOCHEMICAL DATA 108

APPENDIX C. NEUTRON ACTIVATION PROCEDURE AND DATA PRESENTATION . 110

APPENDIX D. AQUEOUS HYDROCARBON DATA 125

VITA 126

LIST OF TABLES

TABLE		PAGE
5.1.	Error Calculations for Element Data	61
5.2.	Summary Statistics for Maclean Five Element Data (ppm)	62
5.3.	Correlation Matrix for Element Data, Maclean Five Deposit	69
6.1.	Summary Statistics for Hydrocarbon Data	83
6.2.	Correlation Matrix for Maclean Data	84
6.3.	Hydrocarbon Correlation Matrix for Live Oak County	85
A-1.	Modal Analysis by Grain Type	105
A-2.	Statistics for T-Test Comparison of Means, Calcite Cement	107
B-1.	Live Oak County Groundwater Data, Oakville Formation	108
B-2.	Uranium Concentrations for Some Extrusive Igneous Rock Types, Big Bend Area, Texas	109
C-1.	Sample Parameters for Neutron Activation Analysis	113
C-2.	Chart of Pertinent Radionuclides	116
C-3.	Table of Standards for NAA Data	117
C-4.	Element Data for Maclean Five Deposit (ppm)	119
C-5.	Summary Statistics for Supplementary Data	120
C-6.	Correlation Matrix for Supplementary Data	121
D-1.	Hydrocarbons	125

LIST OF FIGURES

FIGURE		PAGE
1.1.	Comparison of Maclean Five deposit with other South Texas deposit-types	2
1.2.	Location of the study area	3
1.3.	Stragraphic relations in the Maclean Five pit, looking northeast	5
1.4.	Sample locations, Maclean Five pit	8
1.5.	Radiometric map of Maclean Five pit	9
1.6.	Histogram of radiometric readings, Maclean Five pit	10
1.7.	Distribution of uranium deposits, Live Oak County area, Texas (modified after Eargle et al., 1975)	14
1.8.	Disposition of uranium deposits in the Felder ore trend, Live Oak County (modified after Klohn and Pickens, 1970)	16
2.1.	Geologic map of South Texas — Live Oak County area (after Eargle et al., 1975; Nichols et al., 1977)	19
2.2.	Schematic stratigraphic section, Live Oak County (after Bailey and Childers, 1977)	20
3.1.	Photomicrographs of framework grains (located by arrows), Oakville Sandstone	26
3.2.	Histogram of framework grain types, Oakville Sandstone, Three Rivers, Texas	33
3.3.	QFR compositions of Oakville Sandstone according to Folk's (1974) classification scheme	34
3.4.	Photomicrographs of chemical alterations (located by arrows), Oakville Sandstone	36
3.5.	Average modal composition of carbonate grains by traverse	41
3.6.	Pre-ore paragenetic sequence, Oakville Sandstone, Maclean Five pit	43
3.7.	Bulk-rock calculation for uranium availability in Oakville sediments	46

FIGURE PAGE

4.1. Ore textures (reflected light), Maclean Five deposit 50

4.2. Ore-stage paragenetic sequence, Maclean Five deposit 57

4.3. Schematic overlay of pertinent mineral stability fields . . . 59

5.1. Histograms of element data from a vertical suite of core samples, Maclean Five deposit 63

5.2. Depth-concentration plots for element data, Maclean Five deposit 65

5.3. Correlation plots of uranium with associated elements 71

5.4. Trace element zonation in a typical roll-front uranium deposit 73

5.5. Comparison of U-Mo distributions in roll-front deposits (Harshman, 1974) with that of the Maclean Five deposit . . . 75

5.6. Vertical variations of elements in a tabular orebody 76

6.1. Map view of the Felder roll-front and fault-trap uranium ores showing influence of Sulphur Creek drainage on their dispositions 80

6.2. Evolution of Eh-pH conditions for fault-trap ore model . . . 88

6.3. Time-space diagram for model of fault-trap uranium mineralization 89

C-1. Histograms of supplementary element data 122

C-2. Depth concentration plots for supplementary data 123

C-3. Correlation plots for supplementary data 124

CHAPTER I

INTRODUCTION

I. SCOPE OF THE RESEARCH

Sedimentary uranium deposits in the Gulf Coast occur as tabular orebodies associated with regional unconformities or salt domes and as cresent-shaped roll fronts updip from extensive normal faults. In these deposits uranium minerals fill the interstices in fluvial or beach sandstones and replace detrital grains or organic debris (Bunker and MacKallor, 1973; Eargle et al., 1975).

Four prominent uranium districts are recognized in South Texas: the Karnes District, the Northeast and Southwest Live Oak County Districts, and the Duval County District. Initial uranium discoveries in the Karnes District were tabular in plan, although later exploration discovered numerous roll-front orebodies. Mineralization in the Northeast and Southwest Live Oak County Districts is exclusively of the roll-front type. The Duval County District includes roll-front mineralization in the Catahoula Formation (Miocene), and tabular mineralization in the Goliad Sand (Pliocene) around the Palangona salt dome.

The Maclean Five uranium deposit is an unusual "dike-like" accumulation of uranium and molybdenum minerals impregnating the fluvial Miocene Oakville Sandstone (Figure 1.1). The deposit is located in the Northeast Live Oak County District, seven miles (11 km) northeast of Three Rivers, Texas, near state highway 72 (Figure 1.2). Significant mineralization is limited to the downthrown block of the Oakville fault,

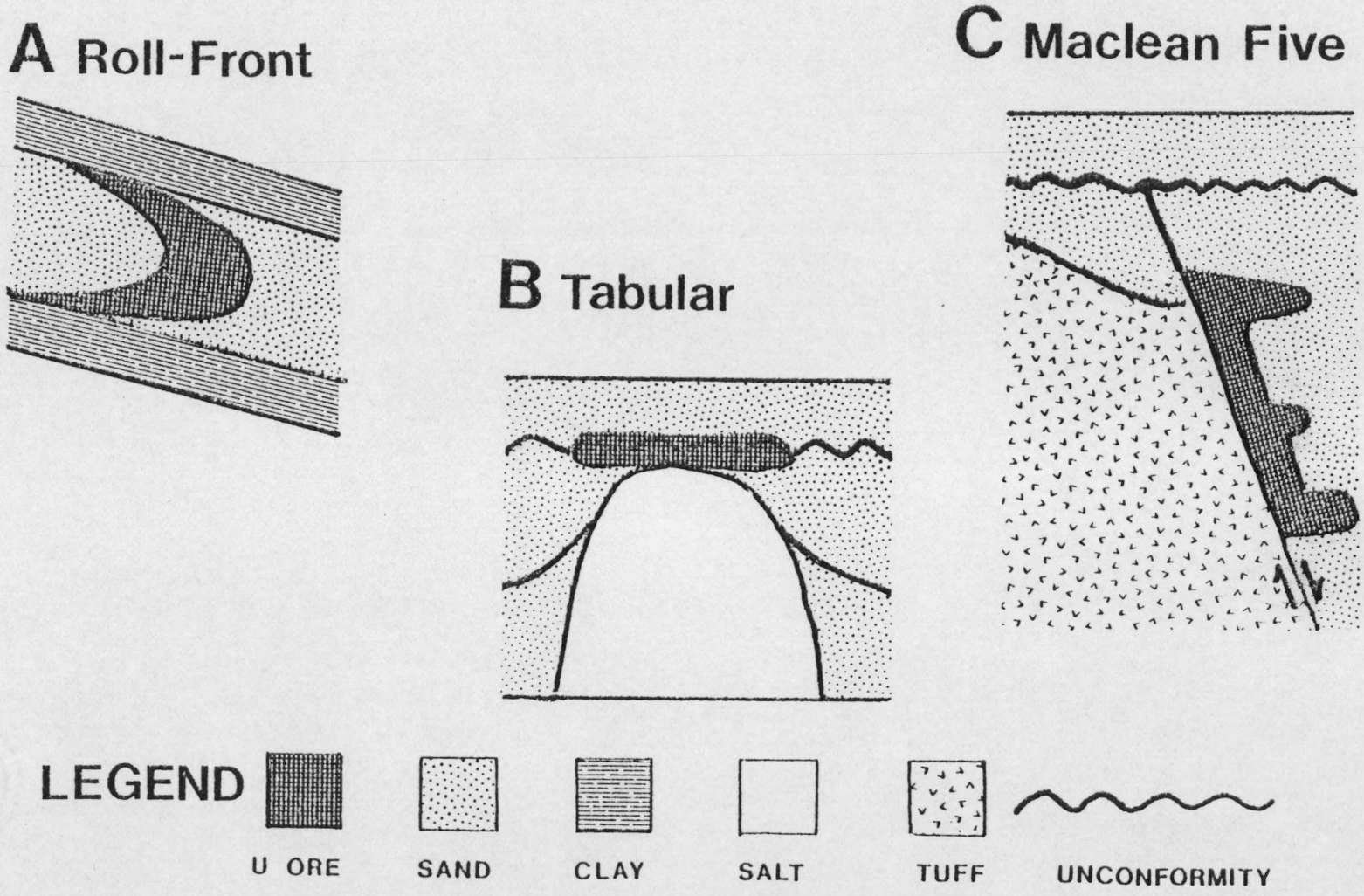

Figure 1.1. Comparison of Maclean Five deposit with other South Texas deposit-types.

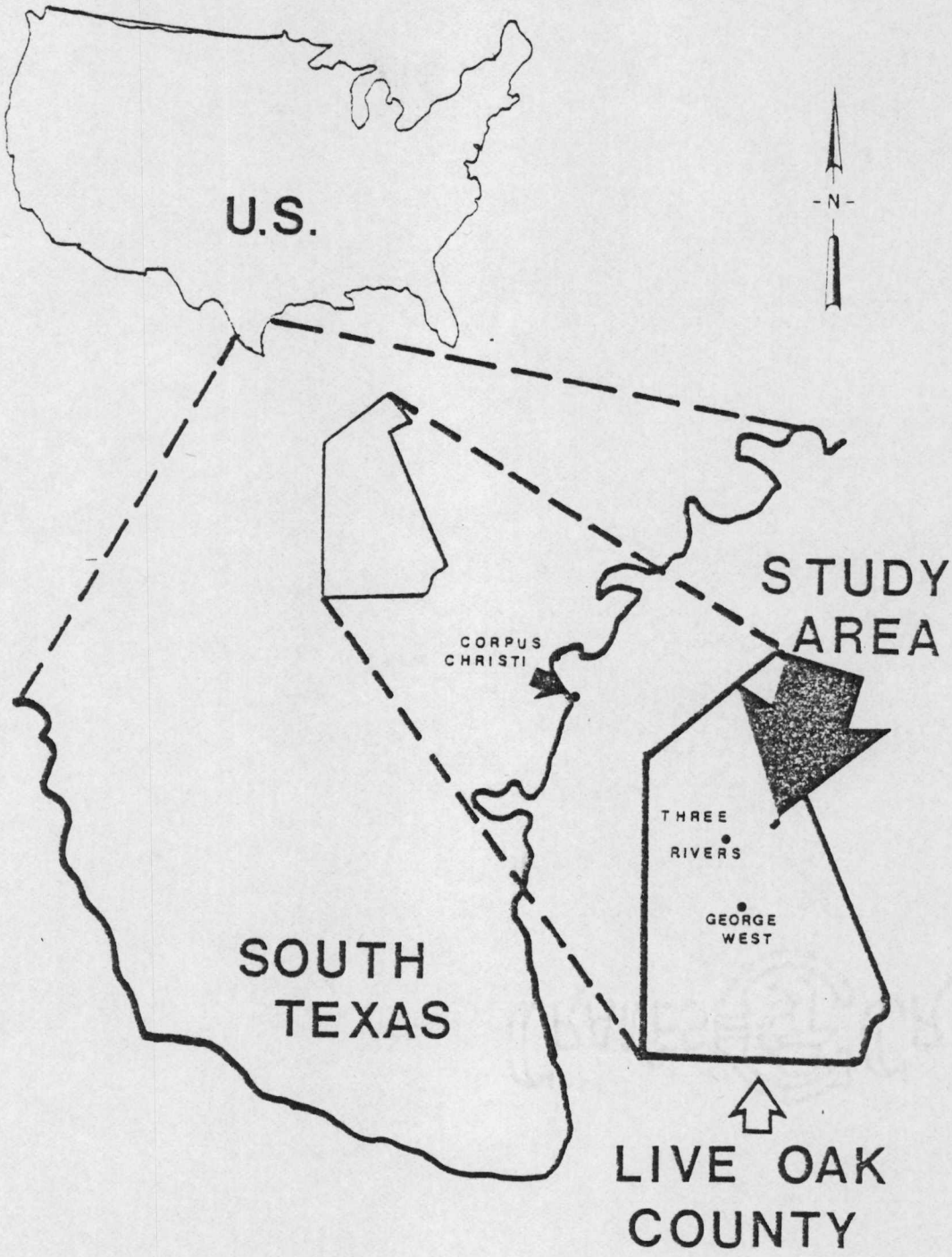

Figure 1.2. Location of the study area.

a down-to-coast normal fault which extends laterally for several miles subparallel to the coastline. The fault-related spatial distribution of these ores apparently does not conform to genetic models that have been proposed for the roll-front or tabular uranium deposits. The description, analysis, and characterization of this and other similar deposits are necessary to understand the nature of fault-related uranium mineralization in sedimentary host rocks.

Geology of the Maclean Five Pit

The Maclean Five deposit is exposed within a shallow open-pit mine excavated by the Felder Mining Operations group of Exxon Minerals Company, U.S.A. The Oakville fault transects the pit and is exposed in both the northeastern and southwestern walls, as well as the pit floor. In map view this fault trace separates upthrown tuffaceous claystones of the Catahoula Formation from footwall litharenites of the Oakville. In cross section the fault is truncated by the Mio-Pliocene unconformity, which separates the Oakville and Catahoula from the overlying Goliad and younger sediments (Figure 1.3). The Oakville Sandstone in the downthrown block is capped by several impermeable clay beds which separate oxidized ground from the lower reduced zone.

Black and dark blue surficial blooms generally associated with uranium and molybdenum minerals are only observed in sands directly adjacent to the fault plane. Chemical analyses of the ore reveal that U and Mo are concentrated together in significant quantities, whereas in adjacent roll-front type deposits Mo has been removed from the ore zone. Iron sulfides and gypsum are also abundant in the immediate vicinity of

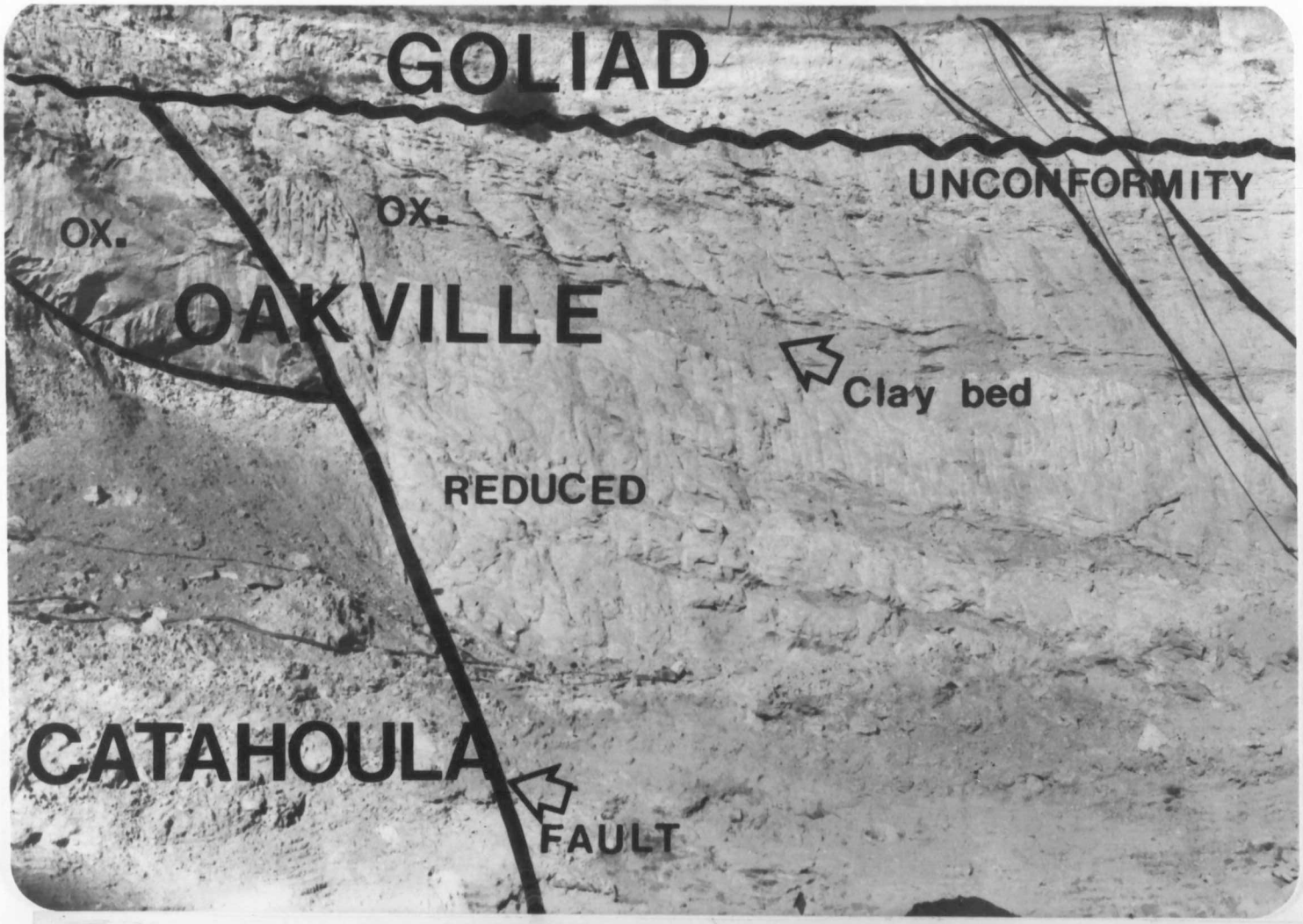

Figure 1.3. Stragraphic relations in the Maclean Five pit, looking northeast. Width represented by photograph about 150 ft.

the fault and are generally absent at a distance. Sandstones overlying the upthrown block are strongly altered, suggesting that fluids migrated through them along the less permeable clays below and passed into the fault zone. Thus, fault control of ore distribution is strongly indicated by field evidence.

Objectives of the Thesis Research

The thesis research has the following objectives:

(1) to recognize and describe the mineralogy and alteration within the barren host rock;

(2) to define more precisely the spatial distribution of ore and gangue minerals and their relation to the fault plane;

(3) to determine the source and nature of the ore-forming solution;

(4) to develop a model for ore deposition.

These objectives are examined in sequential order to provide a comprehensive picture of the ore-forming process.

II. METHODOLOGY

Field Methods

The field work was designed to test the hypothesis that the distribution of uranium in the Maclean Five pit was fault-controlled. The azimuth of the fault transecting the northeast and southwest pit walls measured N 51° E and N 30° E, respectively. A control line or traverse was constructed along the pit floor on a bearing N 29° E, roughly parallel to the fault trace. Five supplemental traverses were constructed parallel to the fault at 25 ft (7.6 m) intervals to the

southeast. A series of consecutively numbered stations were located along the traverses, establishing a grid network from which comparative data were collected (Figure 1.4). A single traverse labeled "a" was constructed northwest of the fault-line along the pit wall.

Samples and geiger-counter readings taken along traverses A, B, C, and D came from the 99 ft (30.2 m) contour level, while traverses RS and WL represented the 109 ft (33.2 m) level along the access road. Mike Barker, a mine geologist, donated a few sulfide-rich samples from the 79 ft (24.1 m) and 90 ft (27.4 m) horizons.

Radiometric measurements. Geiger counter readings were taken from 30 of the previously defined stations in and near the ore zone. Although the accuracy of the measurements as absolute uranium concentrations is questionable, high and low values are reliable as indicators of ore and barren ground, since they corresponded to analogous zones designated by the grade stakes. The results of the radiometric survey are shown in Figure 1.5.

Levinson (1974) reported that background is usually chosen equal to the mode of the frequency distribution of geochemical values for a given study, and Boyle (1971) defined an anomaly as a value twice the background or normal value. Examination of a histogram representing radiation levels in the mine reveals a lognormal-shaped distribution around a mode of 0.25 mR/hr (Figure 1.6). It is evident that only values along the fault are anomalous, ranging from 2.8 to 14 times the background. There is a progressive decrease in radiation in a perpendicular direction away from the fault-line.

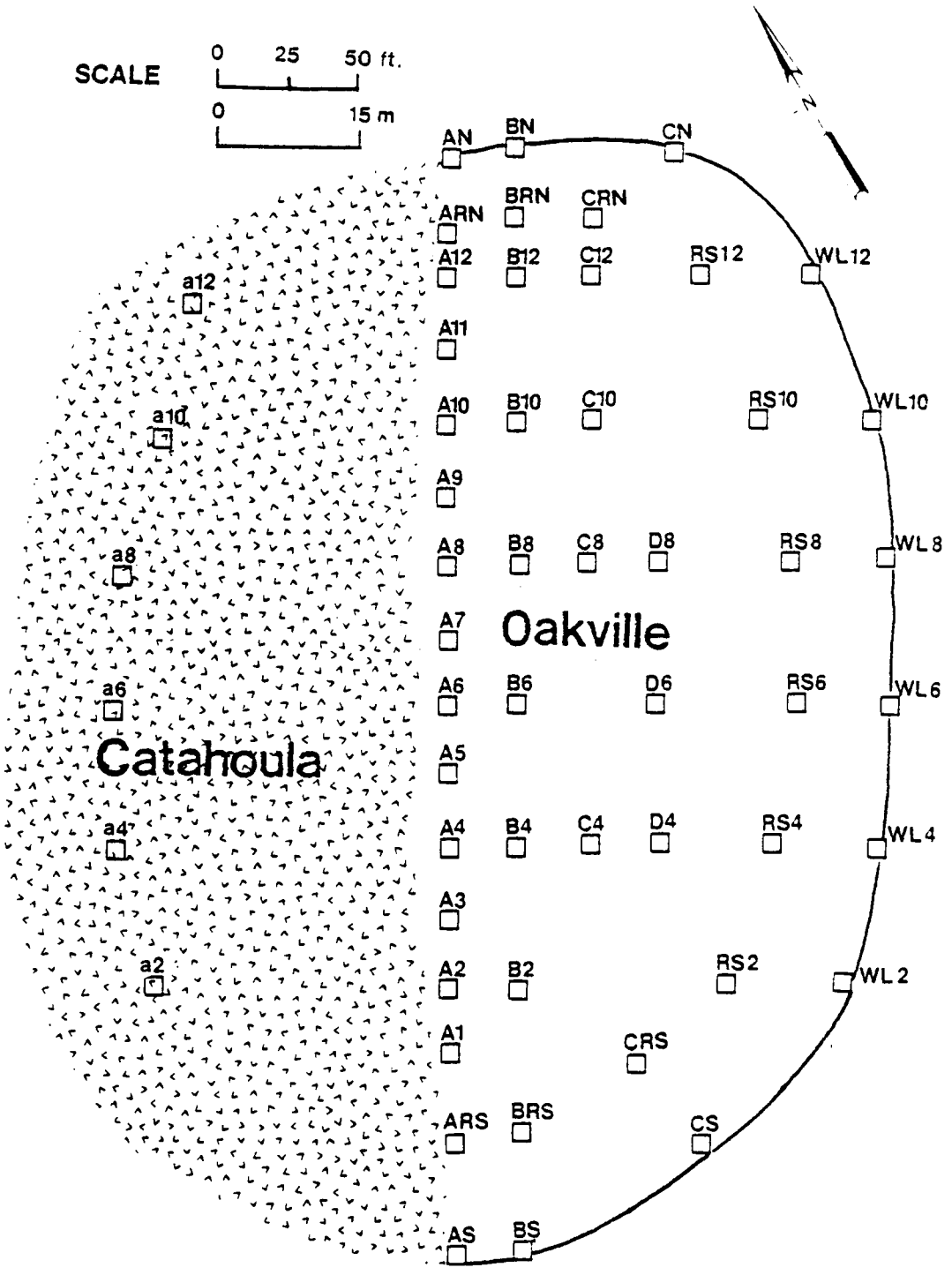

Figure 1.4. Sample locations, Maclean Five pit.

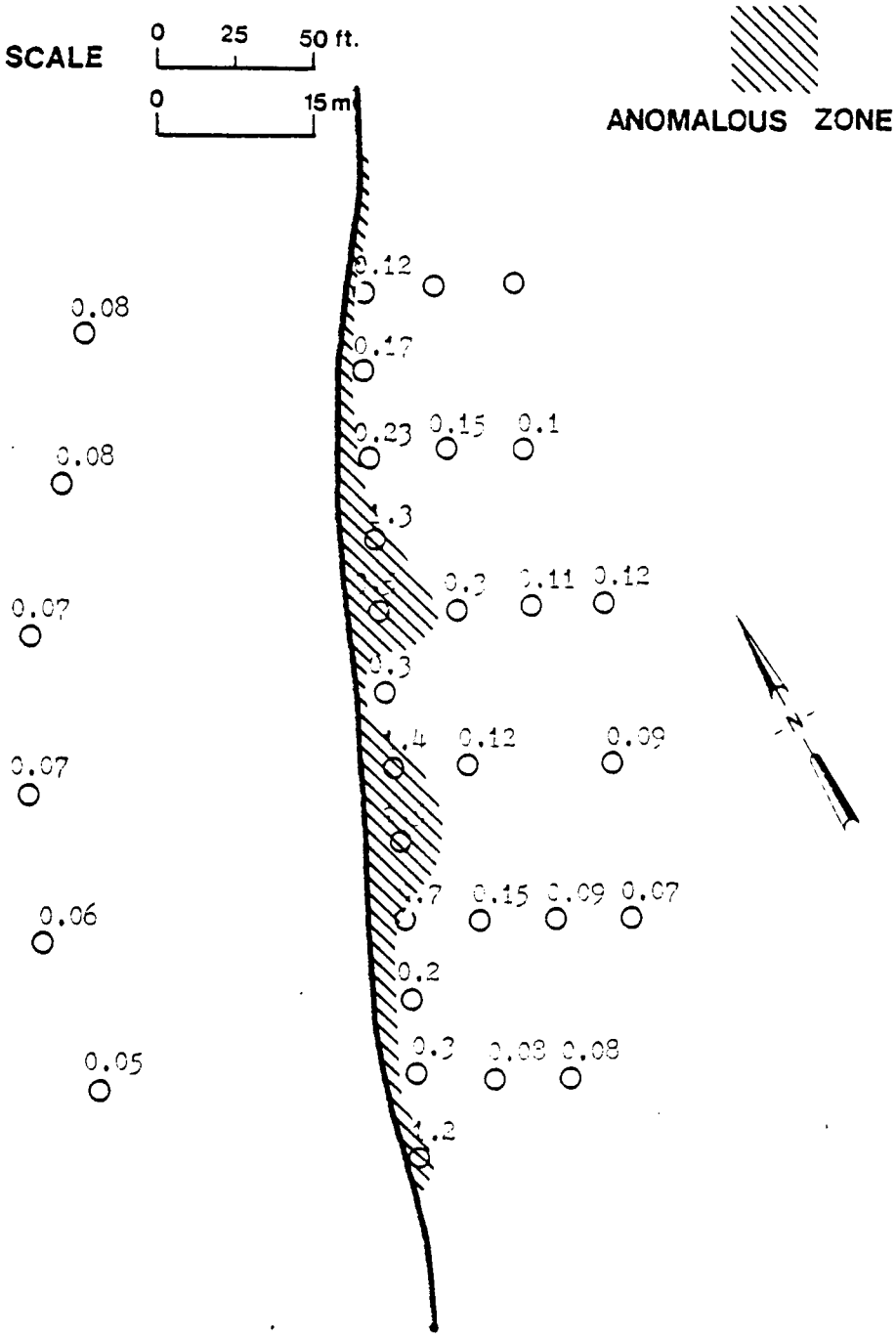

Figure 1.5. Radiometric map of Maclean Five pit. Cross-hatched area greater than 1 mR/hr.

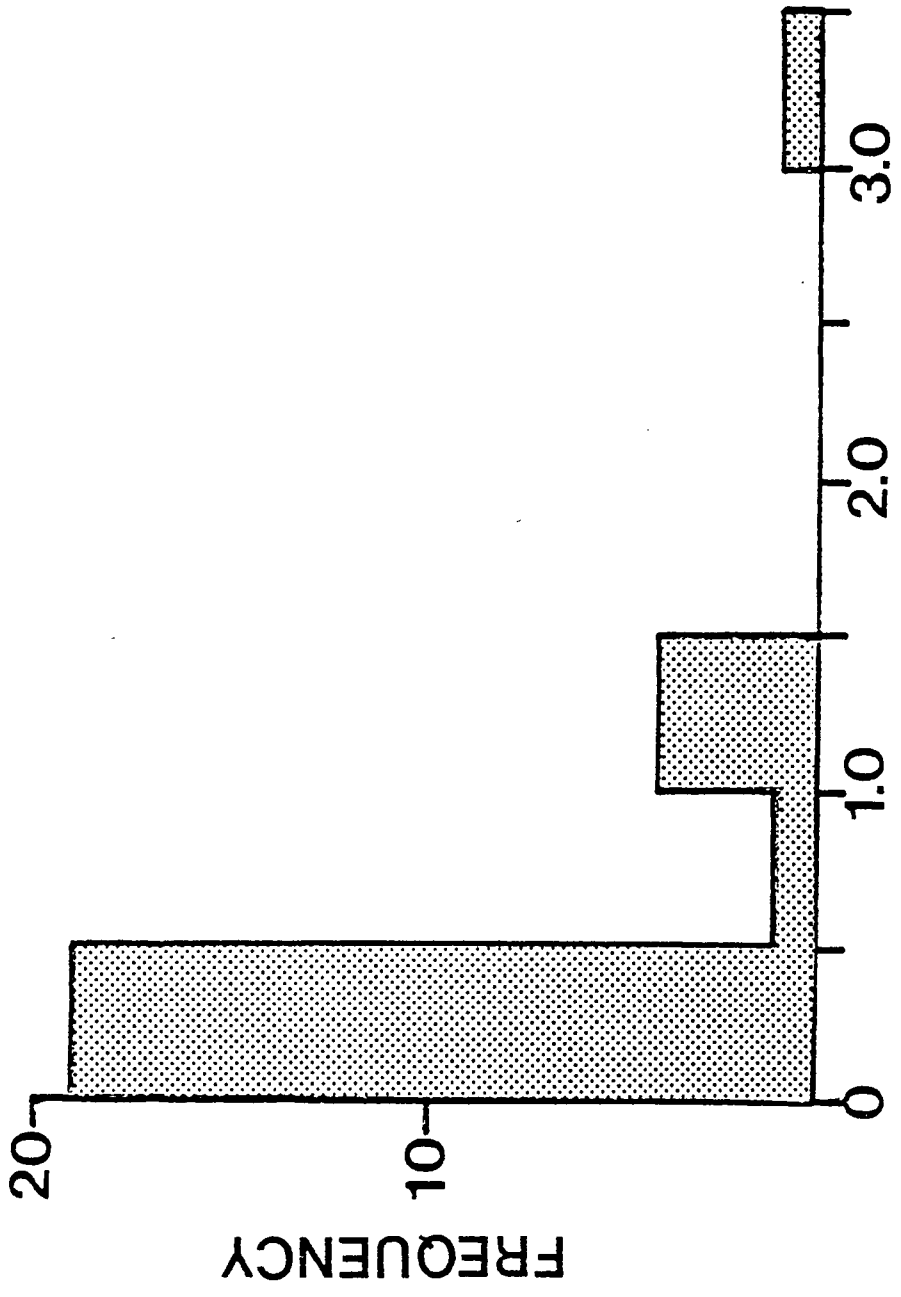

Figure 1.6. Histogram of radiometric readings, Maclean Five pit.

Lithologic sampling. A suite of rock samples was collected from the pit, each sampling station represented by two to three samples (Figure 1.4). Only specimens which showed no indication of alteration due to mining processes were selected.

Sampling for hydrocarbon analyses. To determine the nature of sour gases (H_2S, CH_4) given off by mine waters, samples of natural groundwater seepage were collected using a patented technique developed by Pogorski and Quirt (1976). Water was sealed in aluminum canisters to prevent leakage during shipping. The samples were analyzed for methane and ethane by Chemical Projects Limited, Ontario, Canada. Exxon Minerals Company, U.S.A., contributed analytical data from an additional 20 groundwater samples from the surrounding area for comparison.

Core sampling. Powdered core samples from an Exxon drillhole penetrating the deposit were used for the study. The core suite included 51 samples, ranging from depths of 3 ft (0.9 m) to 87 ft (26.5 m). The samples are numbered according to their depth of origin in feet.

Laboratory Methods

Petrography. Thin sections from 35 rock specimens representing 20 different sampling stations in the barren zone were analyzed petrographically to determine mineralogy, alteration, and paragenesis. Modal analysis was conducted on 20 sections to quantify percentages of constituents, each section characterized by identification of 200 points. When necessary, identifications of some of the phases were verified by

x-ray diffraction or electron microprobe analysis. Petrographic analysis of the barren sediments was undertaken to understand the nature of the original host rock and to search for overprints of mineralizing processes.

A total of 40 polished thin sections and 33 polished sections were prepared from specimens in the ore zone and examined to determine assemblages of ore minerals and their paragenetic sequence. Optically ambiguous phases were verified by x-ray or electron microprobe techniques.

Trace element analysis. Neutron activation analysis (NAA) was performed on 51 powdered core samples to determine concentrations of trace elements commonly associated with uranium ores, including U, Mo, As, and Mn (Harshman, 1974). Qualitative x-ray fluorescence analysis was also conducted on a few samples to obtain supplemental data on trace element contents not detectable through NAA procedures (e.g., Co, Ni, V, and Se).

Practical Limitations

The foremost limitation of the study is that the bulk of samples studied represent only a 224 ft (68.3 m) by 377 ft (114.9 m) area. In addition, the vast majority of radiometric readings and rock samples come from the 109 ft (33.2 m) and 99 ft (30.2 m) contour intervals, because rock material above that level had been removed and rocks high on the pit wall were inaccessible. The core samples provide the vertical control necessary to quantify ore-forming processes. The multifaceted approach to the thesis project should compensate for areal limitations proposed by the restricted nature of the data base.

III. PREVIOUS INVESTIGATIONS

Live Oak County Uranium Deposits

Uranium deposits of the Live Oak County area were reviewed by Eargle et al. (1975). Ores consisting of uraninite and coffinite in typical roll-front configuration (Adler, 1974) occur in the sandstone of the Miocene Oakville Sandstone at several localities in the county, usually some distance updip from down-to-coast or up-to-coast normal faults, but in regional association with them (Figure 1.7). Eargle and Weeks (1961) proposed that the faults supplied the reductants necessary for uranium precipitation through the migration of petroliferous gases from hydrocarbon deposits at depth.

In addition to the Maclean Five deposit, uranium mines in the vicinity include the Kopplin, Felder, Maclean One, Maclean Two, Clay West, and Burns' operations. Displacement along the Oakville fault is also visible in the pit walls of the Kopplin and Maclean One deposits. Uranium mineralization lies updip from the fault in the Kopplin mine, but extends to the fault plane in the Maclean One pit. The remainder of the deposits are found in sand units along redox interfaces somewhat removed from faults.

Felder Mine

Uranium mineralization most proximal to the Maclean Five deposit is exposed in the Felder mine, approximately one mile (1.6 km) to the northeast. The Felder ores display striking dissimilarities with those of the Maclean Five, and provide a good basis for comparison of the deposit types.

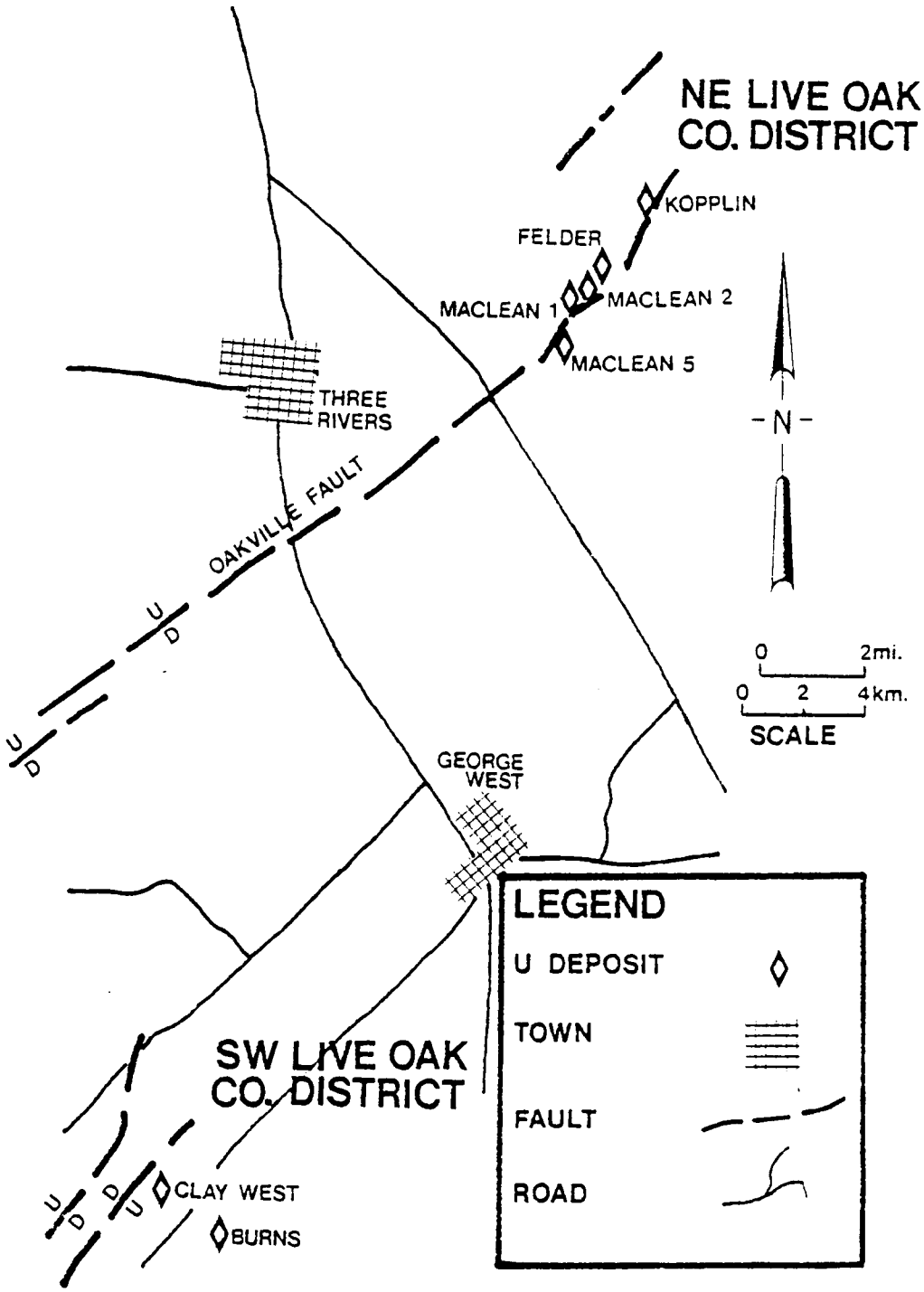

Figure 1.7. Distribution of uranium deposits, Live Oak County area, Texas (modified after Eargle et al., 1975).

Since the detailed report by Klohn and Pickens (1970), the Felder mine has become one of the most widely known in South Texas. Before the mine was opened, the Felder deposits were estimated to contain 5,000,000 pounds (2,268,000 kg) of U_3O_8, along sinuous geochemical fronts 1500 ft (457.2 m) northwest of the Oakville fault (Figure 1.8).

Ore-grade mineralization, averaging 0.35% U_3O_8, forms a crescentric roll-front trend 150 ft (46 m) wide, 2400 ft (732 m) long, and 25 ft (8 m) to 40 ft (12 m) thick, converging to the southeast. The wings of the roll are of variable thicknesses, and the upper wing has been partially removed, implying remobilization of ore by surficial weathering. The position of mineralized trends adjacent to the Felder tract suggests the ore migrated downdip to its present position in conjunction with erosional lowering of the surface (Klohn and Pickens, 1970). Mineralization fades below the economic cutoff down-dip from the convergent zone, although anomalous radioactivity may be detected 1000 ft (305 m) away.

Pyrite gangue is reported as ubiquitous to the ore zone, averaging 2-3%. A broad molybdenum halo is also associated with the ore, reaching its maximum concentration 1000 ft (305 m) down-dip from the convergent margin.

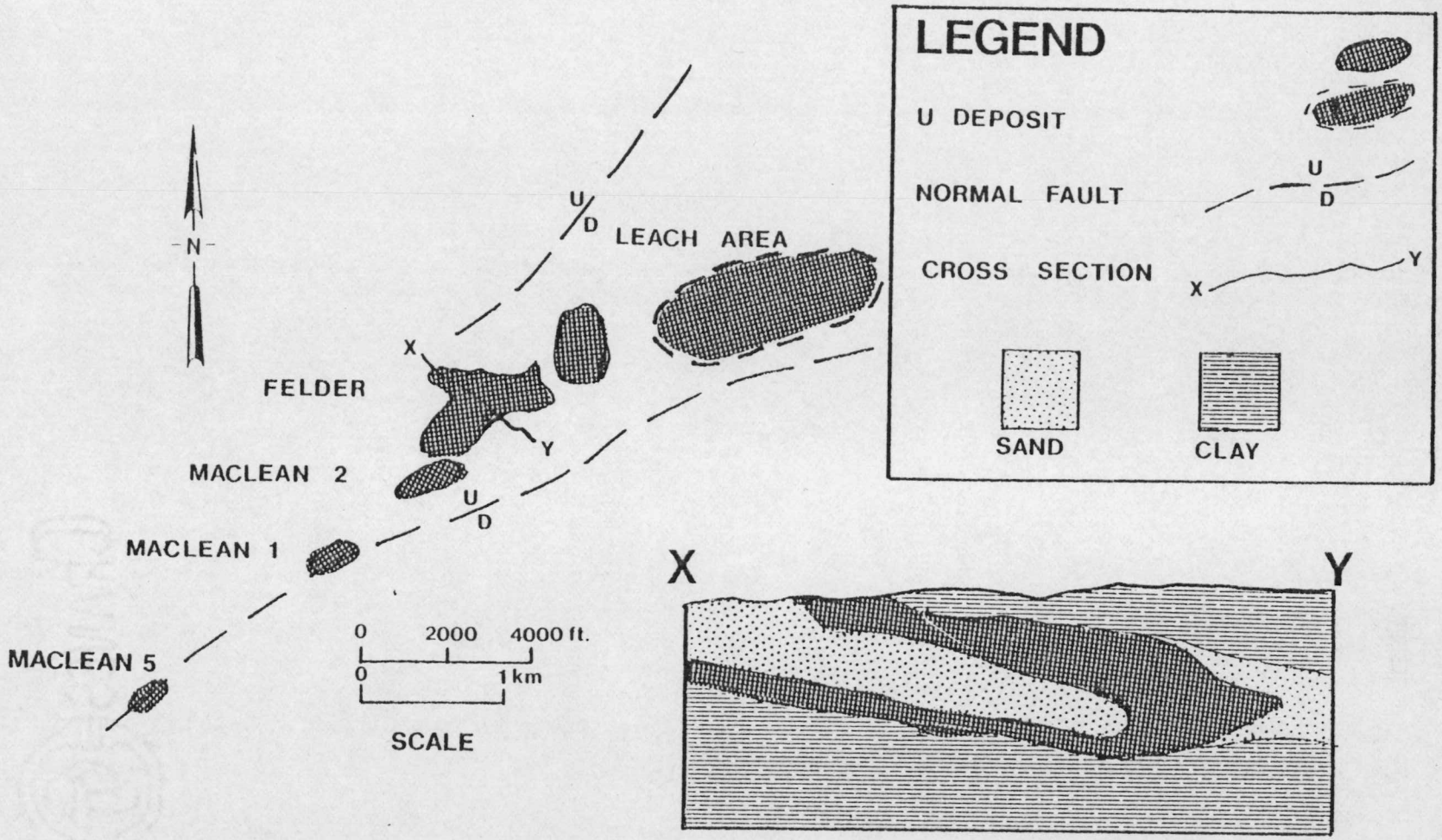

Figure 1.8. Disposition of uranium deposits in the Felder ore trend, Live Oak County (modified after Klohn and Pickens, 1970).

CHAPTER II

GEOLOGIC SETTING

I. REGIONAL GEOLOGY

Cenozoic stratigraphic units in Texas crop out along arcuate belts which are roughly concentric to the present margin of the Gulf of Mexico and, in their recent topographic configuration, form broad flat alluvial plains interspersed with gentle rolling hills and occasional buttes. The disposition of major paleodepocenters was controlled by pre-existing uplifts and other topographic highs (e.g., Llano Uplift and Edwards Plateau), major areas of subsidence, and tectonic pulsations with associated volcanism in west and southwest Texas. Volcanism and erosion of igneous and metamorphic highlands provided vast quantities of sediment for transport to the gulf. Beds of volcanics are found interstratified with fossiliferous Cenozoic beds in the Trans-Pecos region (Sellards et al., 1932), demonstrating contemporaneity between extrusive events and development of sedimentary basins.

Streams carrying arkosic, tuffaceous sediments emptied from the eroding highlands and deposited regressive deltaic sequences along the coast. Periodic quiescence and differential subsidence resulted in less extensive intervals of transgression, accompanied by development of microtidal shorelines (e.g., Jackson Group). Three major phases of regression are represented in the stratigraphic record by the Rockdale, Yegua, and the Miocene Catahoula and Oakville Formations. The less

predominant marine sediments introduced in excess of 1,200,000,000 barrels of crude oil into the Cenozoic section.

II. LOCAL STRATIGRAPHY

Eargle et al. (1975) reviewed the stratigraphy of uranium-bearing units along the Gulf Coast. A geologic map and stratigraphic cross section of units exposed in Live Oak County are shown in Figures 2.1 and 2.2.

The Upper Eocene Jackson Group is conformable with the underlying Claiborne Group and is overlain unconformably by the Catahoula Formation and Frio Clay. Individual units contain significant amounts of tuff and pyroclastic debris, indicating the initiation of powerful eruptions from volcanoes to the west. Jackson sediments represent shallow-water marine and beach sandstones and claystones, occasionally transected by delta distributary sands. Lithologic components include fine- to medium-grained, thin-bedded sands and tuffaceous clays.

The Oligocene Frio Clay lies unconformably on the sandstones and arenaceous claystones of the Jackson Group (Fayette Formation). The unit is composed of unevenly stratified green to tan clays, and conspicuously lacks fossils, suggesting a fluvial origin. The Frio is 150 ft (46 m) thick in Live Oak County.

The Miocene Catahoula Formation (Tuff) overlies the Jackson Group and Frio Clay unconformably, and is overlain unconformably by the Oakville and Lagarto Formations. Volcanism in the source area culminated in the Miocene, depositing vast sheets of tuffs and ash (Eargle et al., 1975).

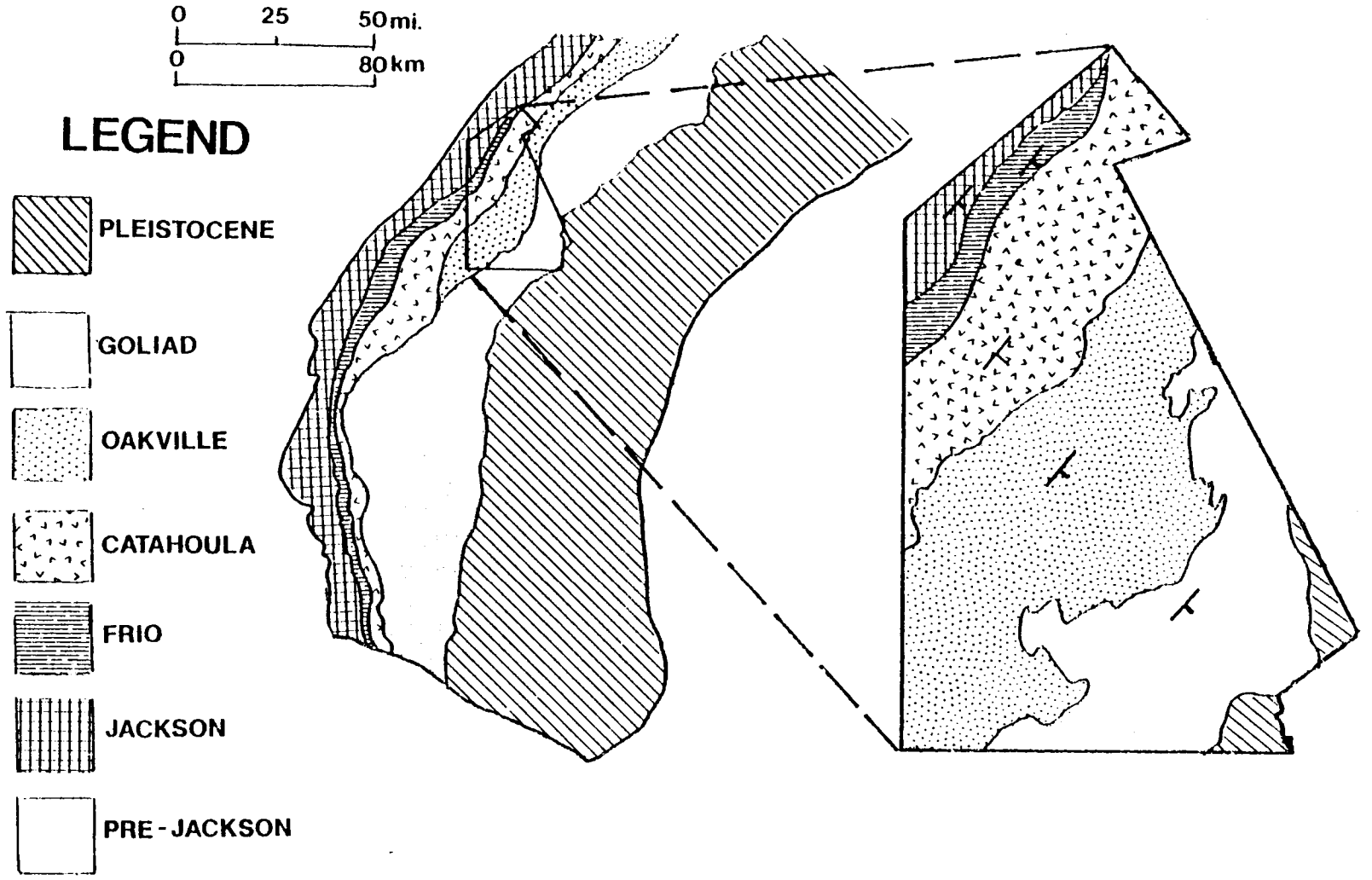

Figure 2.1. Geologic map of South Texas — Live Oak County area (after Eargle et al., 1975; Nichols et al., 1977).

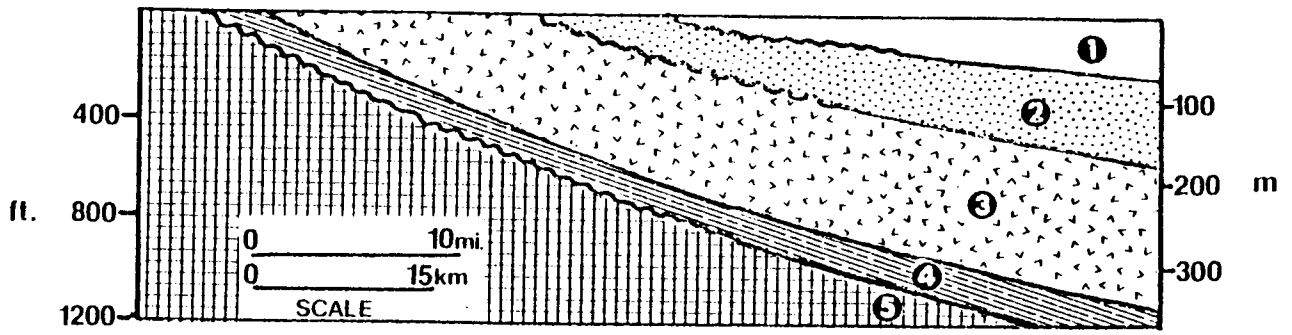

LEGEND

PLIOCENE	1 Goliad Sand — light gray to white sand, coarse at base; fine- to medium-grained; pinkish clay; beds of caliche; fluvial deposits.
MIOCENE	2 Oakville Sandstone (Fleming Formation) — gray to reddish-brown sandstone, fine- to coarse-grained; green to tan clays; beds of fossil pebbles and tuff-ball conglomerate; silica and calcite cements; beds locally contain horse-like mammal fossils; fluvial deposits.
?	3 Catahoula Formation (Tuff) — interbedded pink to white tuff, sandy conglomerate containing pebbles of volcanics, bentonitic clays; sandy units contain abundant tree fossils; fluvial and lacustrine environments.
OLIGOCENE	4 Frio Clay — pink to gray-green clays; montmorillonitic, tuffaceous, zeolitic; channel sandstones; fluvial and lacustrine.
EOCENE	5 Jackson Group — red to gray, fine- to medium-grained, thin-bedded sandstone; tuffaceous claystones; primary tuffs; strand plain and distributary environments.

Figure 2.2. Schematic stratigraphic section, Live Oak County (after Bailey and Childers, 1977). Lithologic descriptions after Eargle et al., 1975.

Three sub-units of the Catahoula are recognized in South Texas, the Fant, Soledad, and Chusa Members. The Fant Member comprises well-consolidated tuffs and ash interlayered with clay beds. The Soledad Member is a conglomerate composed of reddish to greenish-brown pebbles of trachyandesite, trachyte, pumice, tuff, and chert. The Chusa Member includes unstratified, noncalcareous to marly, poorly indurated, pisolitic or lumpy bentonitic claystone.

The Oakville Sandstone lies above the Oligo-Miocene unconformity, and is conformably overlain by the Lagarto Formation. Rejuvenated streams originating on the Edwards Plateau and Llano Uplift delivered remarkably heterogeneous sediments to emerging deltaic complexes along the gulf. It appears that deposition of extensive ash during the earlier Miocene denuded the vegetation on the plateau, rendering Cretaceous carbonates susceptible to rigorous alkaline weathering.

The Oakville consists of fine- to coarse-grained sandstones and tuffs with lentils of clay and clay-ball conglomerates. Basal conglomerates include rounded pebbles of redeposited Cretaceous fossils. Oakville sediments crop out continuously from southeast Texas north of Houston to an area just south of the Live Oak County line, and are covered by Pliocene sediments from Duval County southward. Sandstones of the Oakville grade upward into the Lagarto Formation, which is strikingly similar, but contains more shale. In southeast Texas the Oakville and Lagarto are undifferentiable and are referred to as the Fleming Group or Formation.

Sands and gravels of the Pliocene Goliad Sand unconformably overlie the Lagarto Clay; however, the Goliad is in many places one of

the more indistinguishable stratigraphic units on the Gulf Coast, grading upward imperceptibly into Pleistocene outliers and terrace gravels. For this reason, it has only been mapped generally in many localities. Where recognizable, the Goliad includes whitish to pinkish gray sands and minor basal gravels. Strata overlying the Oakville and Lagarto in Live Oak County are best identified as undifferentiated Goliad-Pleistocene sediments.

III. STRUCTURAL STYLES

Two major tectonic events affected the stratigraphic development of Cenozoic sediments in the Gulf Coast, mountain-building to the west and southwest of the basin, and regional normal faulting associated with overpressured shale at depth (Bruce, 1972). Development of growth faults within the Gulf Coast exerted an immediate influence on basin geometry and stratigraphic thicknesses.

Bruce (1973) recognized three major structural mechanisms which propagate regional normal faults:

(1) contemporaneous differential compaction on seaward limbs of overpressured shale masses;

(2) gravitational sliding along steepened slopes of anticlinal shale masses;

(3) post-depositional compaction.

Most uranium deposits in northeastern Live Oak County are associated with extensions of the Oakville fault. Identification of the structural mechanism responsible for this displacement provides a handle on the

timing of host-rock preparation by reducing gases from hydrocarbon deposits at depth.

The Oakville fault apparently resulted from postdepositional compaction. The Oakville Sandstone in vicinity of the Felder mine does not exhibit thickening in the downthrown fault-block, although there is evidence of drag. This would indicate reduction began after deposition of the unit was complete. In contrast, it is possible this isopach zone represents a hinge point along the fault and that downthrown strata might thicken to the south. Stratigraphic data to test this possibility were not available.

CHAPTER III

SEDIMENTARY PETROLOGY

I. INTRODUCTION TO THE OAKVILLE PETROLOGY

The Oakville Sandstone consists of about 50% sandstone and conglomerate and 50% bentonitic or calcareous claystone, with lentils of tuff-ball conglomerate (Sellards et al., 1932, p. 734). The sandstone is predominantly light gray, medium-grained, and intricately cross-bedded. Calcite cement is common where the sand is well-indurated, although chalcedony and opal are recognized at some localities. These latter cements are usually found associated with volcanic ash and tuffs, indicating the leaching of silica from reactive pyroclastic debris.

Petrologic data and interpretations are here limited to the basal sandstones of the Oakville exposed in the Maclean Five pit.

II. LITHOLOGIC CONSTITUENTS

The framework grains are sand-sized, fine- to coarse-grained (ranging from 0.15 to 0.66 mm), and moderately- to well-sorted. The mode of the grain-size distribution is approximately 0.33 mm (medium-grained). Quartz, feldspar, limestone rock fragments, and volcanic rock fragments are the dominant constituent particles. Calcite cement is abundant.

Quartz

Quartz grains are largely angular to subangular. Minor portions exhibit corroded boundaries where in contact with calcite cement.

Although polycrystalline and volcanic quartz varieties were identified in trace amounts, "common" monocrystalline quartz is predominant (Folk, 1974, p. 74). Many quartz grains contain various inclusions, including rutile needles, microlites, and fluid vacuoles. Reworked sedimentary quartz is also present in small amounts (Figure 3.1, A). Quartz diversity reflects multiple source areas.

Feldspars

K-spar was identified by cleavage and microcline twinning. These grains are generally moderately weathered, subangular to subrounded, and retain subhedral crystallographic boundaries. Severely weathered K-spar is altered to plate-like clays or micas. Minor overgrowths of potassic feldspar are occasionally observed surrounding detrital K-spar grains. Twinned and zoned plagioclase was also recognized. Plagioclase grains are moderately weathered and subangular to subrounded in shape.

Limestone Rock Fragments (LRF's)

Carbonate rock fragments are important constituents of the Oakville. Alizarin red stain reveals their mineral composition to be calcite, hence the abbreviation "LRF." LRF's tend to be elongate and well rounded, implying transport. Many authors (e.g., Sellards et al., 1932) cite the Cretaceous Edwards Group as the source of reworked carbonates deposited in the Miocene. LRF grain boundaries are cloudy and poorly defined, indicating dissolution along their margins. Cathodoluminescence petrography (CL) demonstrates that LRF's served as nuclei for early cementation by calcite.

Figure 3.1. Photomicrographs of framework grains (located by arrows), Oakville Sandstone.

A. Well-rounded detrital quartz with authigenic quartz overgrowth. Scale is representative of remaining photographs.

B. Echinoderm plate.

C. Detrital LRF, exhibiting remarkable preservation of relict fossil structures.

D. Elongate detrital LRF. Again note the well-preserved cellular internal structure.

E. Felsitic VRF. Shows intergrowth texture of plagioclase and quartz.

F. Microlitic VRF. Note parellel alignment of plagioclase laths in groundmass of clay.

G. Lathlike VRF with clay groundmass.

H. Lathlike VRF (Basalt). Note clay alteration of ferromagnesian minerals.

I. Vitric tuff, altered to clay. Note flow banding.

J. Crystal vitric tuff with quartz phenocrysts and relict glass shards.

K. Vitric tuff, altered to green clay. Note relict glass shards (1) and characteristic bubble-wall texture (2).

L. Sulfides (opaque minerals), surrounding and joining VRF's together.

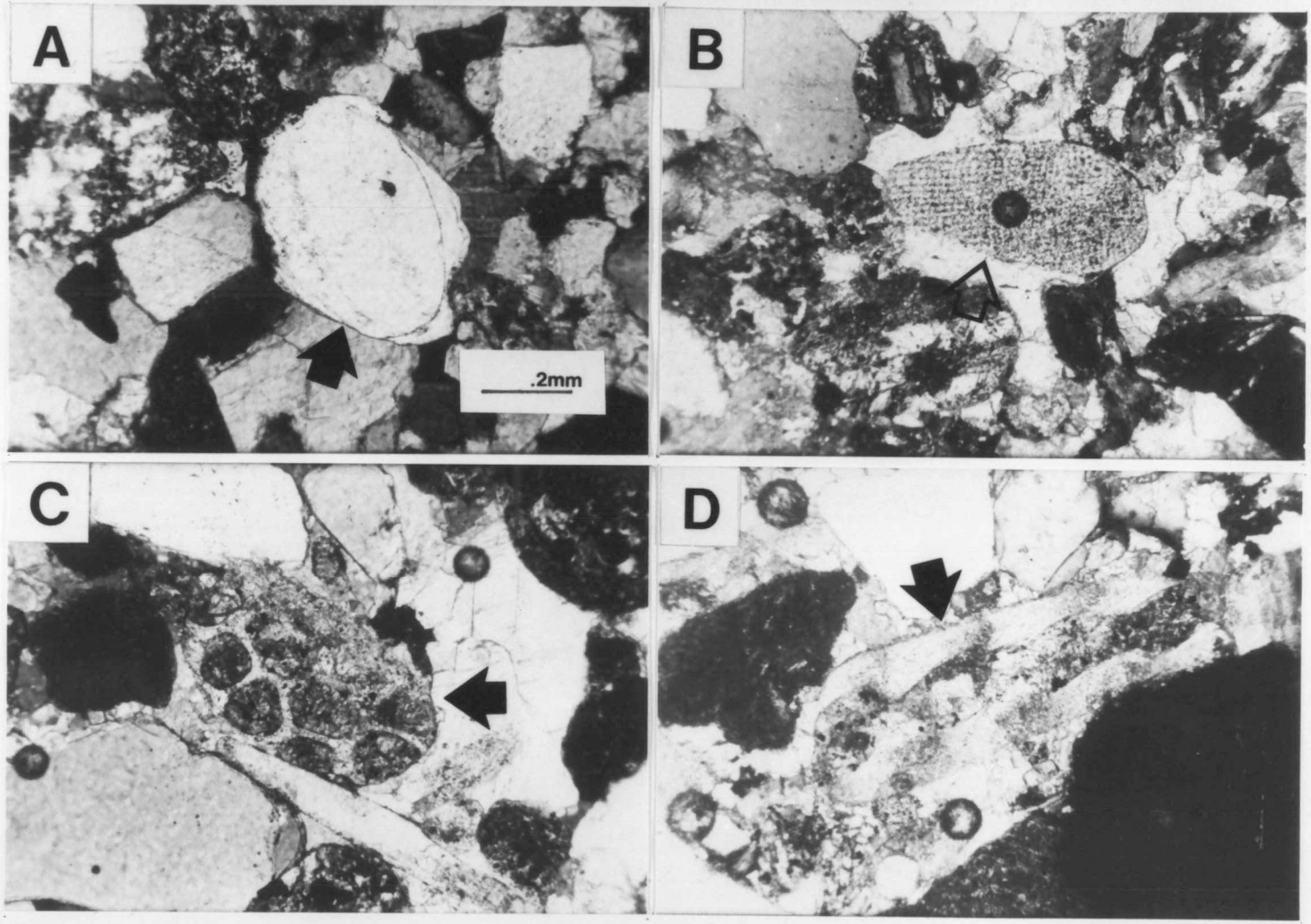

Figure 3.1.

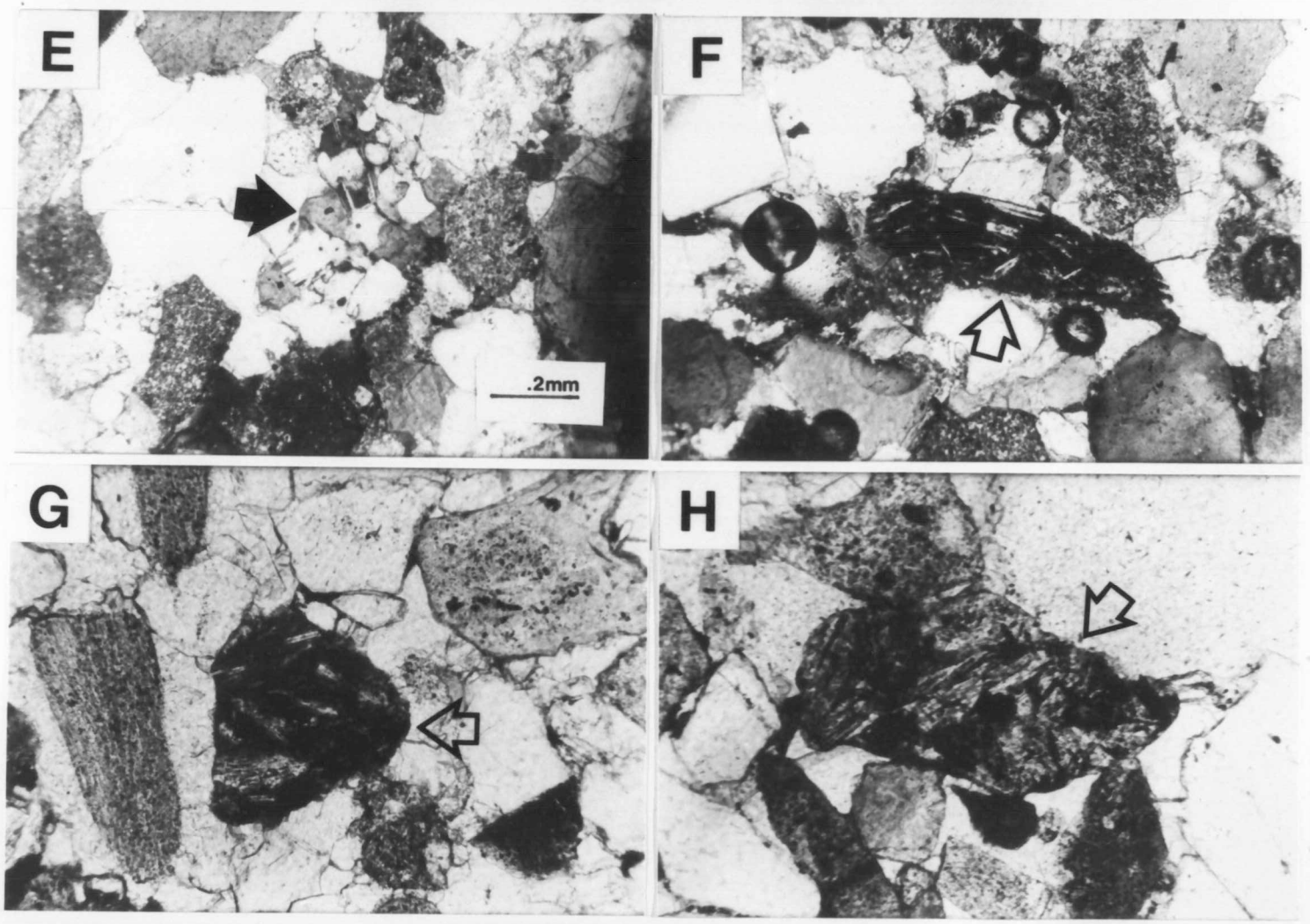

Figure 3.1. (Continued)

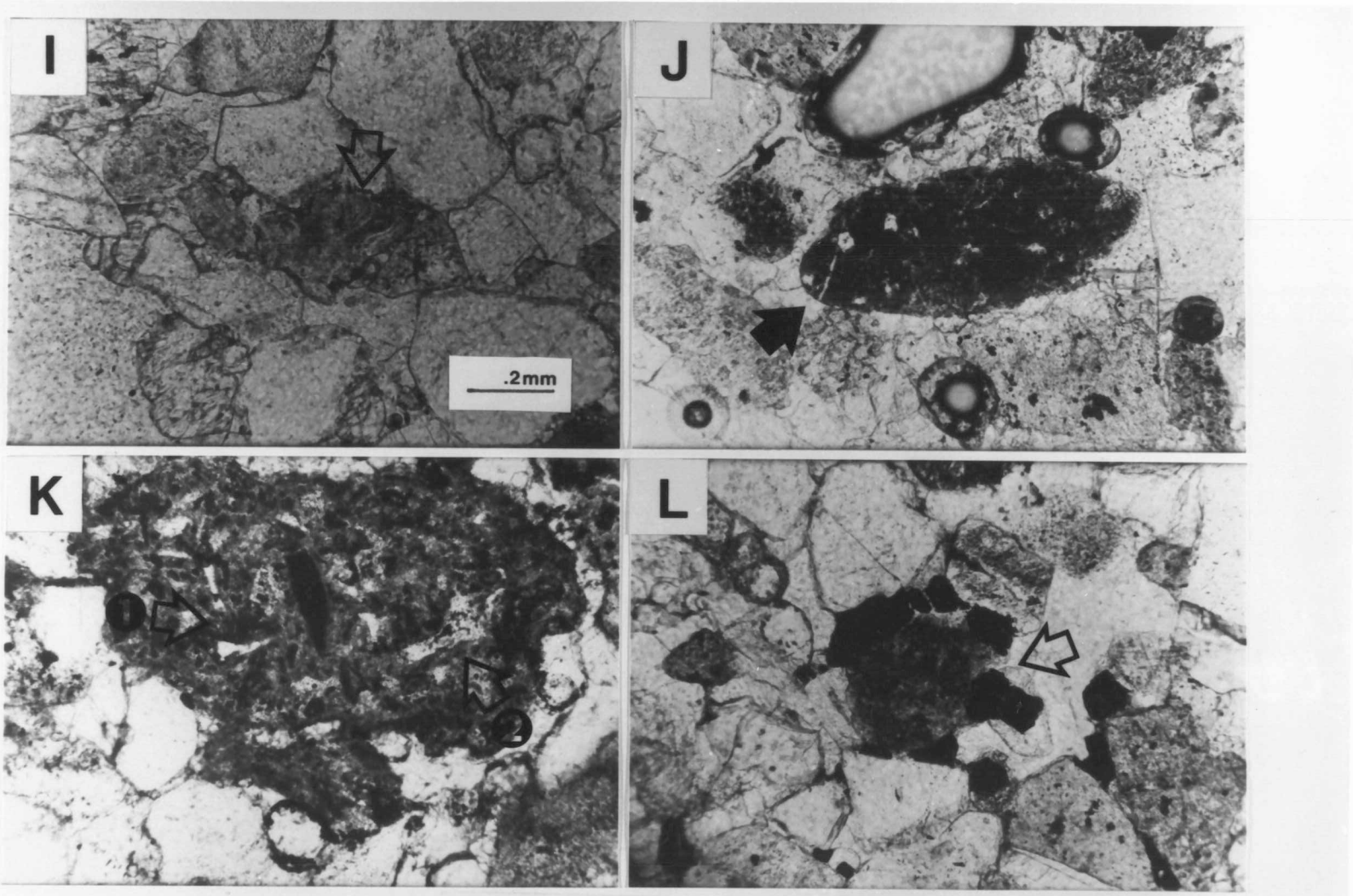

Figure 3.1. (Continued)

Individual limestone grains sometimes retain relict fossil structures. Alteration and size limitations preclude specific identification of fossil types; however, it appears mollusk-shell fragments and echinoderm plates are present (Figure 3.1, B, C, D).

Volcanic Rock Fragments (VRF's)

Volcanic constituents are divided into four categories, following Dickinson (1970). These include felsitic, microlitic, lathlike, and vitric grain types. VRF's tend to be rounded to well rounded. Alteration and grain size prevents quantitative identification of mineral species within the lithic grains; therefore, rock-type identifications are very general. Categorical separation of tuffs and other pyroclastics from ordinary volcanic detritus was not attempted.

Felsitic fragments are composed of quartz and feldspar in an anhedral to subhedral mosaic which is often indistinguishable from chert (Figure 3.1, E). The presence of microphenocrysts, crude laths, relict shards, or internal relief indicates a volcanic origin. Felsitic grains represent silicic volcanics, lavas, or tuffs. A generally equivalent rock type would be rhyolite.

Microlitic grains contain subhedral to euhedral plates or prisms (often plagioclase) with parallel to subparallel orientations, revealing flow at the source (Figure 3.1, F). These fragments represent intermediate compositions and frequently have undergone alteration, leaving aligned phenocrysts of plagioclase in a ground-mass of clay minerals. An equivalent rock type would be andesite or trachyandesite porphyry.

Lathlike VRF's are made up of abundant plagioclase plates in random orientation. The nonalignment of plagioclase laths form intergranular

and intersertal textures which are typical of basaltic rocks (Figure 3.1, G, H).

Vitric grains represent volcanic glass or their altered equivalents (Figure 3.1, I, J, K). Pronounced alteration of vitric tuffs to bentonite and "pseudochert" (Pettijohn, 1975, p. 308) makes identification difficult. Relict phenocrysts, glass shards, flow banding, and clots of opaque minerals may reveal their volcanic origin. Volcanics with extensive clay alteration and without phenocrysts are automatically categorized as vitric VRF's. Equivalent rock types are obsidian, vitric tuff, and crystal vitric tuff.

Authigenic Sulfides

Subhedral to anhedral aggregates of marcasite and pyrite are found clustered in and around VRF's, joining and penetrating them (Figure 3.1, L). These sulfides rarely are found attached to other grain types or "floating" in the cement. The association between authigenic sulfides and VRF's suggests a localized environment conducive to the nucleation of pyrite and marcasite.

Cement

Calcite is the dominant cement type, determined by alizarin red staining and x-ray diffraction. Cathodoluminescence petrography suggests two stages of calcite cementation, an early dull-red phase which appears to represent local dissolution of LRF's and reprecipitation of calcite, and a later bright yellow-orange phase which is independent of carbonate rock fragments.

Miscellaneous

Other framework grain types and cements are present in trace quantities. These include slate fragments, glauconite, chert, silicified dolomite rhombs, pyroxene, and chalcedony cement.

III. MODAL ANALYSES

Modal analysis was performed on 20 selected thin sections from the basal Oakville in the unmineralized portion of the Maclean Five exposure. These sections corresponded to 20 individual sampling stations within the barren zone. Seven grain and cement types adequately characterize the samples.

The analytical procedure was based on point-counting 200 grains per section, with a 30μ counting interval. A Swift stage coupled with a mechanical counter was used to maintain the proper interval and tabulate the results.

At this locality, the Oakville contains 32.2% quartz, 5.9% feldspar, 17.3% LRF's, 22.2% VRF's, 0.7% opaques, 19.4% calcite cement, and 2.3% miscellaneous (Figure 3.2; Table A-1, Appendix A). The mean overall composition plots well within the litharenite field of Folk's (1974) classification, as do 19 of the 20 individual compositions (Figure 3.3). Comparison of the means for the first ten sections measured against the final means reveal a maximum of 1.5% variation, usually less than 1%. This implies a relatively homogeneous sample, which is verified by the clustering of compositional data points on the QFR plot. The student's t-test was used to make error calculations for percentages of each grain type at the 95% confidence level (Appendix A).

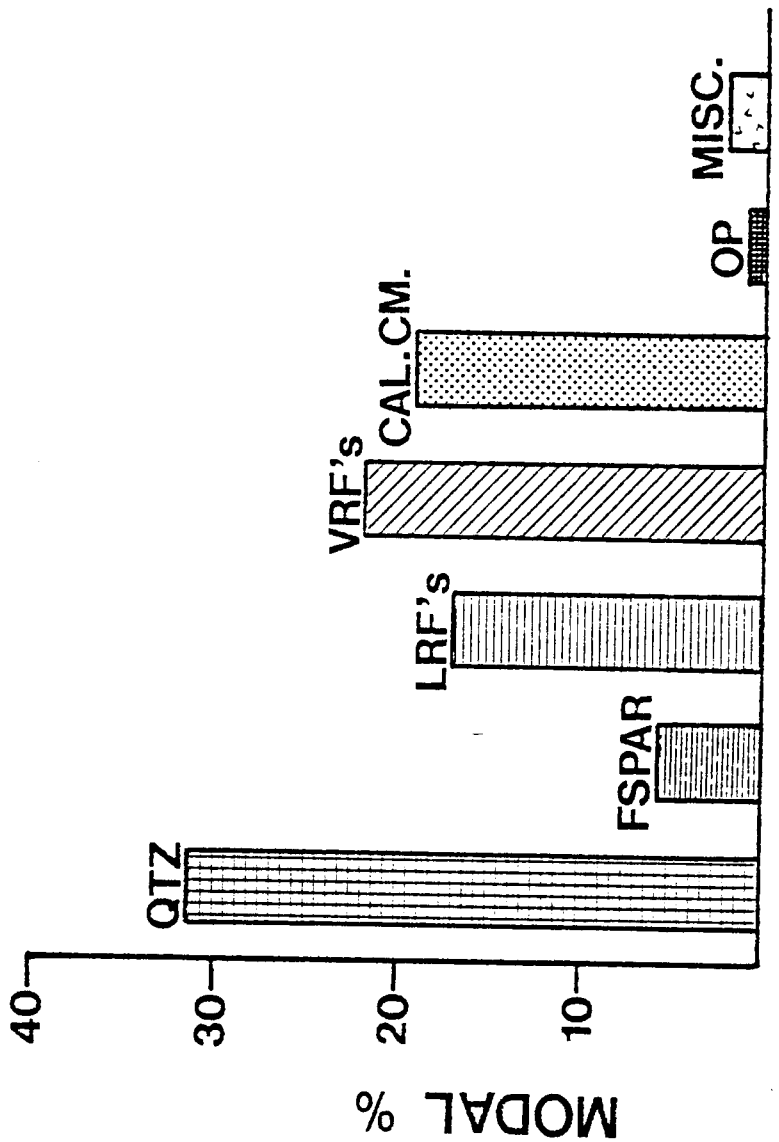

Figure 3.2. Histogram of framework grain types, Oakville Sandstone, Three Rivers, Texas.

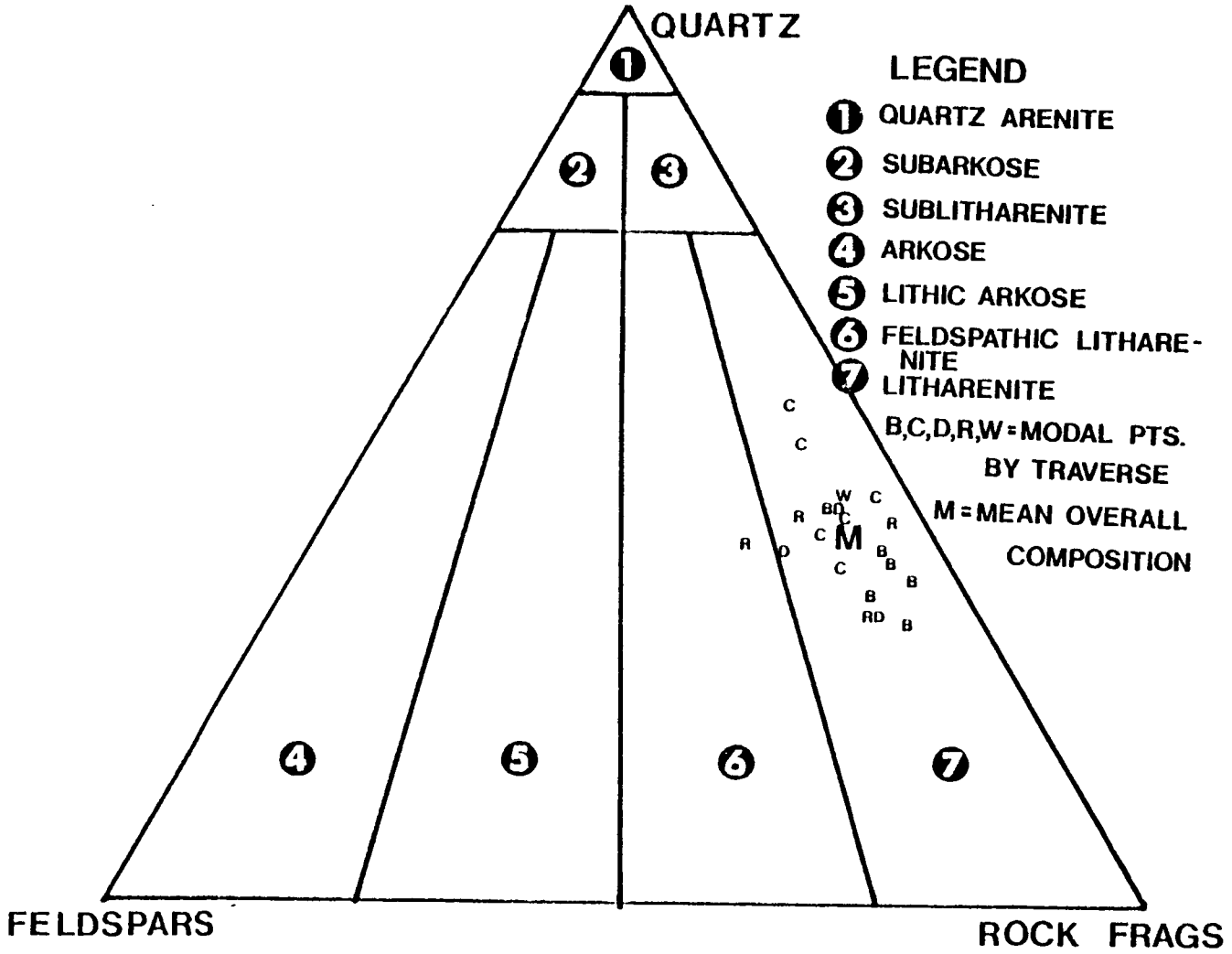

Figure 3.3. QFR compositions of Oakville Sandstone according to Folk's (1974) classification scheme.

IV. INTERPRETATION AND DISCUSSION

Chemical Alteration

Chemical processes involved with weathering of volcanoclastic sediments in South Texas were reviewed by Weeks and Eargle (1960). These authors identified chalcedony, montmorillonite and zeolites in association with altered tuffs and other volcanoclastics in the Karnes uranium district, which lies only a few miles northeast of the research area. This suite of secondary minerals is considered typical of arid to semi-arid weathering and diagenesis in volcanic terrains (Goodell, 1977; Walton, 1975).

Silicification. Some volcanic fragments in the Oakville may have undergone silicification and devitrification before deposition; however, there is some evidence for in situ deposition of silica. Thin quartz overgrowths are notable in the majority of thin sections examined, and overgrowths of chalcedony on quartz are also recognized. In Figure 3.4, A, silicification is evidenced by the growth of chalcedony on the north end of a VRF. VRF's nearby also exhibit chalcedonic alteration along their upper margins. The similar orientation of encroaching replacements is unlikely due to coincidental alignment during deposition; therefore, the alteration is post-depositional. Other cherty fragments retain relict phenocrysts (Figure 3.4, B). Some vitric grains have undergone alteration to both chalcedony and clay minerals (Figure 3.4, C). In some of these cases, chalcedony may represent devitrified glass.

The remarkable similarity between sedimentary cherts and "pseudochert" formed from silicification of volcanic debris can cause

Figure 3.4. Photomicrographs of chemical alterations (located by arrows), Oakville Sandstone.

A. VRF altered to chalcedony along upper margin. Note relict phenocrysts. Scale is representative of all photographs in this figure.

B. Cherty fragment with relict phenocrysts.

C. Vitric VRF altered to chalcedony and clay.

D. Crystal vitric tuff altered to clay and calcite.

E. Severely altered VRF with authigenic growth of clay in adjacent pore space.

F. Vitric VRF conforming to adjacent pore space.

G. Vitric VRF altered to clay with relict glass shards in parallel alignment.

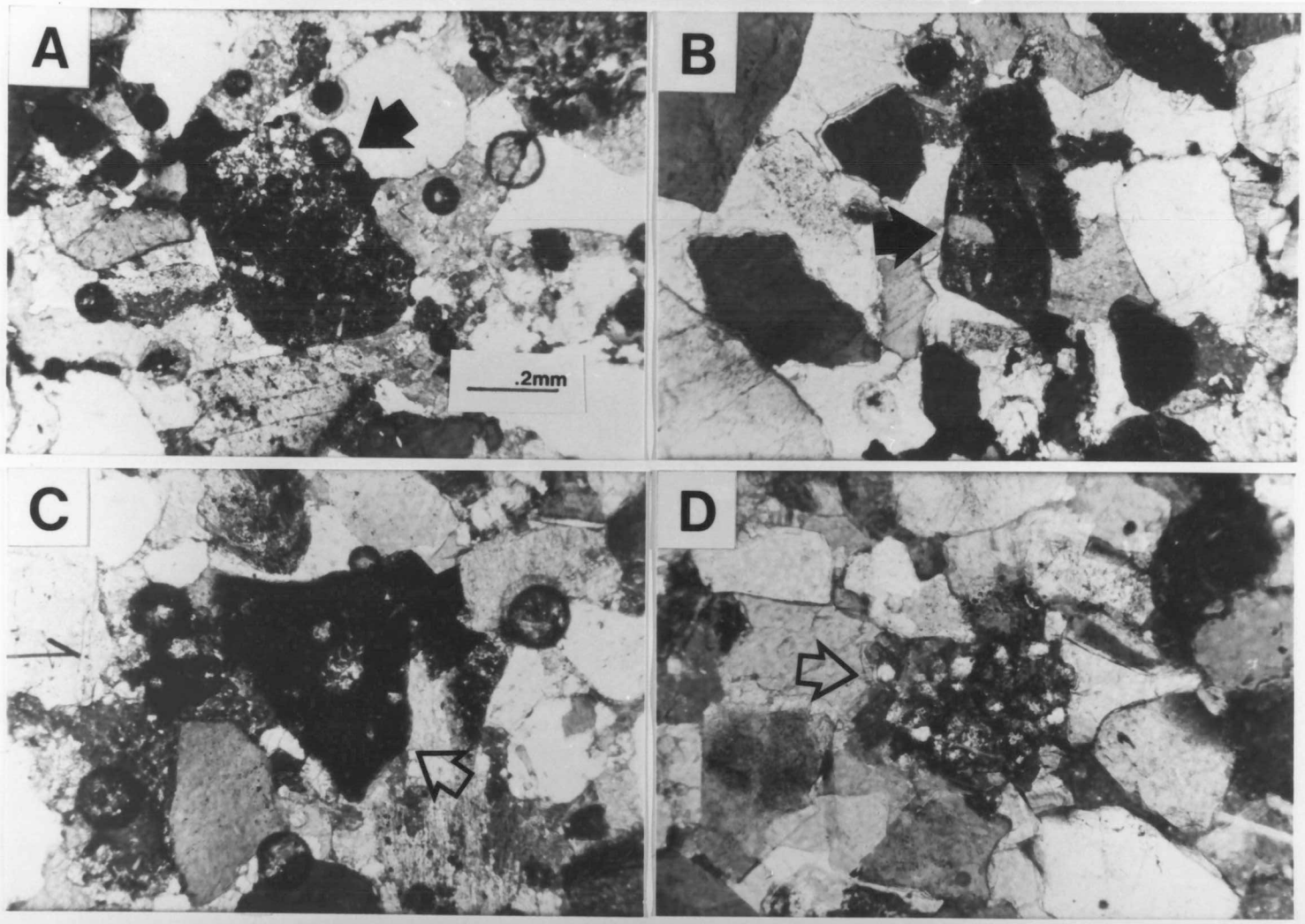

Figure 3.4.

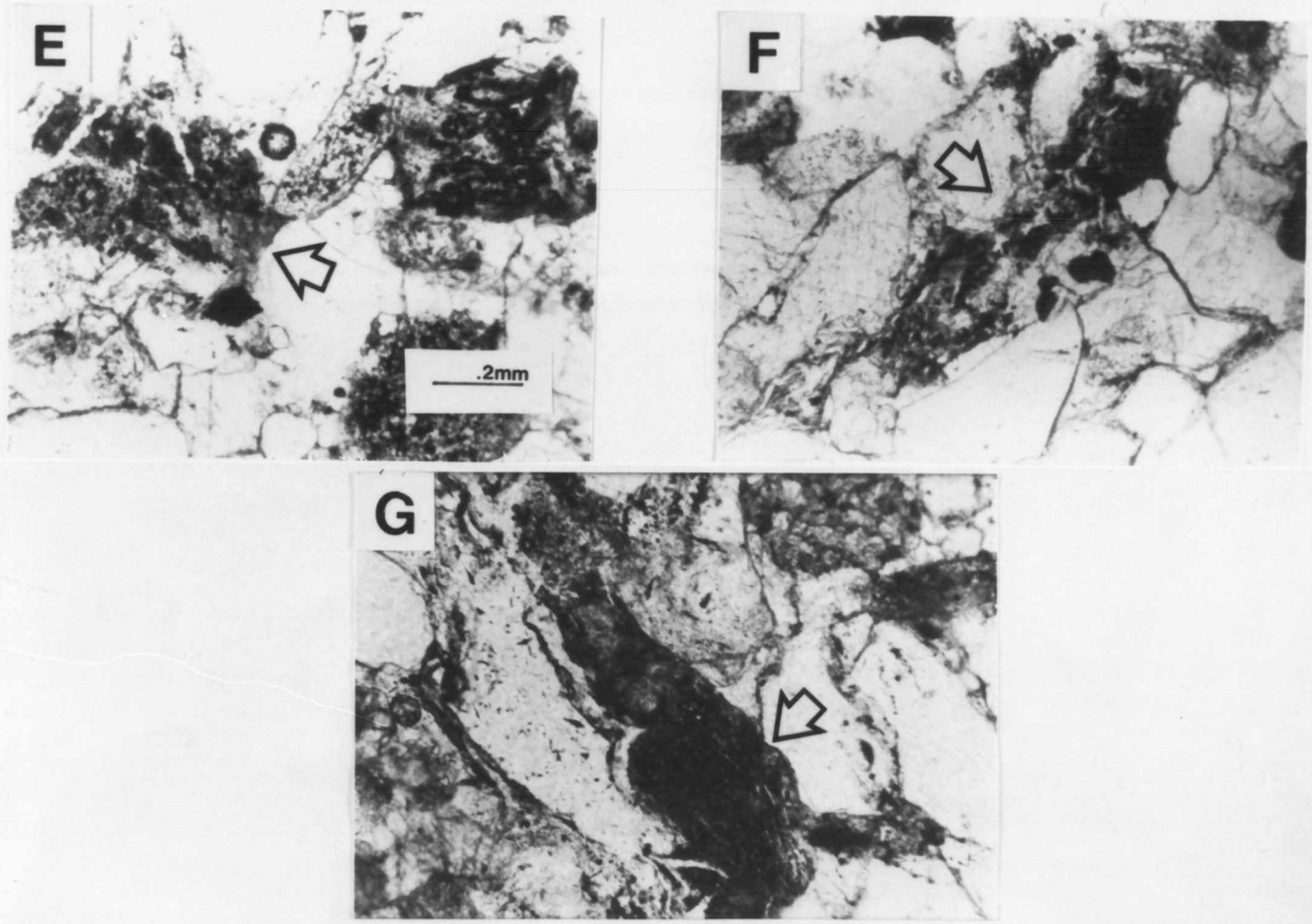

Figure 3.4. (Continued)

confusion. Undoubtedly, authors in the past may have reported erroneously high chert contents for the Oakville, based on this misconception.

Clay formation. Alteration of VRF's to brown, gray and black clays is prevalent. Although attempts at x-ray identification of clay alteration products failed in the present study, Garrels (1967) showed that kaolinite and montmorillonite are in equilibrium in volcanic rocks with greater than 200 ppm groundwater HCO_3^- concentrations. Since the mean HCO_3^- content of the Oakville is 286 ppm in the study area (Appendix B, Table B-1), both montmorillonite and kaolinite are most likely present.

In Figure 3.4, part D, crystal vitric tuff has undergone alteration to clay and calcite. Fibrous authigenic growths of clay were also observed around decomposed VRF's (Figure 3.4, E). Severely altered vitric grains (Figure 3.4, F) conformed to pore spaces between adjacent grains. Vitric tuffs, recognized by relict glass shards, seemed particularly susceptible to clay alteration (Figure 3.4, G).

The type and degree of clay alteration is apparently determined by grain size. Large phenocrysts may appear fresh although surrounded by a groundmass of clay byproducts. The differential in weathering rate is probably due to the increased surface area of fine-grained or glassy materials.

Sulfidization. Host-rock preparation is an essential step in creating a chemical environment conducive to uranium precipitation. After development of the Oakville fault, reducing gases seeped upward from the oil and gas deposits at depth and penetrated the Oakville

Sandstone (Klohn and Pickens, 1970). Clay beds, overlying the sandstones and draping the fault, formed a trap under which sour gases became concentrated. Some of these gases (H_2S, HS^-) supplied sulfide necessary for marcasite and pyrite formation.

Marcasite and minor pyrite are found clustered around altered VRF's. Marcasite formation is favored by acidic conditions; however, the restriction of marcasite nuclei to the proximity of VRF's suggest a localized control. It is plausible that clays with an overall negative charge (e.g., montmorillonite, Berner, 1971, p. 165) provided reactive sites for marcasite nucleation by attracting positively charged hydronium ions (H_3O^+) from solution and lowering pH at the grain boundary. Fe leached from the VRF's or supplied by groundwater combined with reducing gases and formed marcasite. In areas of higher pH, pyrite formed preferentially.

Cementation. Alkaline carbonate solutions dissolve detrital grains locally, corroding quartz, and cement the grains with calcite. Cementation is controlled by carbonate equilibria, which generally obeys these reactions (Brownlow, 1979):

$$\begin{array}{c} H_2O + CO_2\ (g) \\ \downarrow\uparrow \\ CaCO_3\ (s) + H_2CO_3 \rightleftharpoons Ca^{2+} + 2HCO_3^- \end{array}$$

Evidence presented in Figure 3.5 shows the bulk of cementing solution was introduced from the fault zone. The mean percentage of calcite cement by traverse displays a consistent decrease away from the fault plane. The student's t-test (Appendix A, Table A-2) demonstrates this

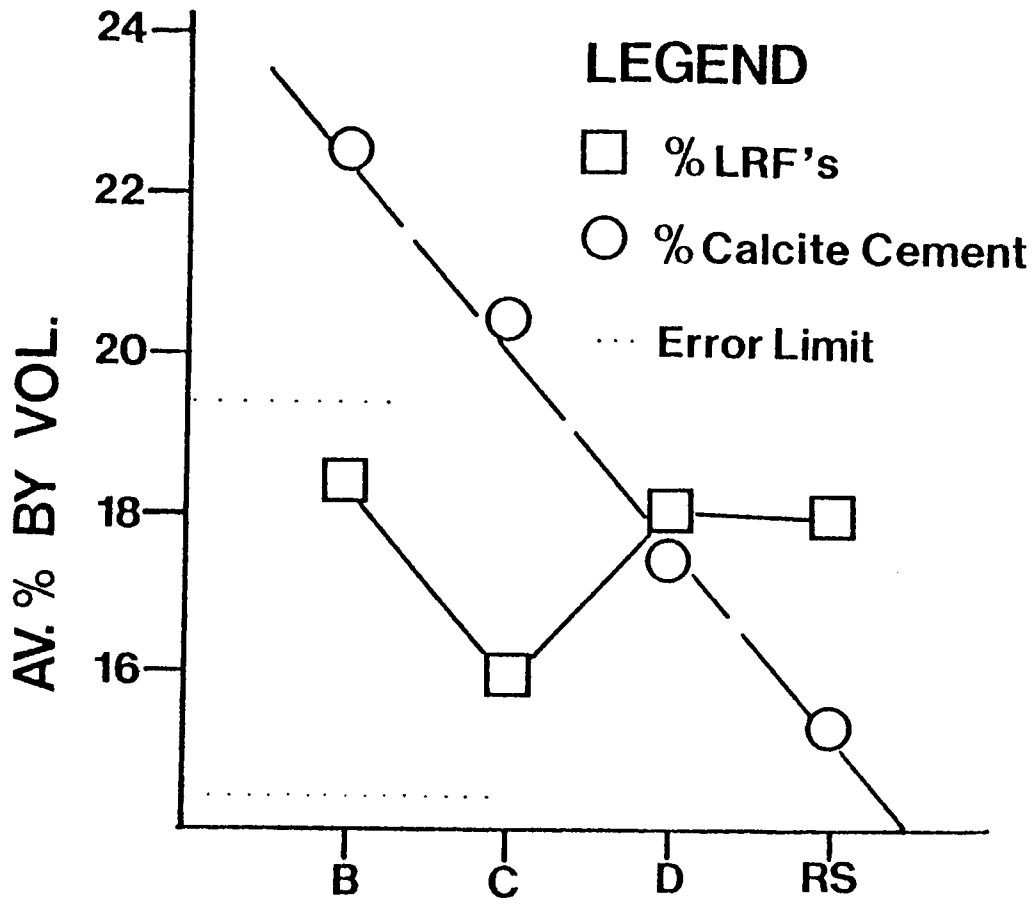

Figure 3.5. Average modal composition of carbonate grains by traverse. Error limit ±2.5%.

is a statistically valid variation in means at the 95% confidence level (Davis, 1970, p. 95-97). Although dissolution of LRF's contributed to the cement locally, their mean percentage by traverse remains constant relative to the calculated error (±2.5%). In addition, lithologic samples collected near the fault plane were well-indurated, while samples from traverses RS and WL were loose sand which had to be cemented with epoxy to make thin sections.

The cementation sequence appears to be as follows:

(1) dewatering of Catahoula clays opposite the fault plane during and after fault development, which formed calcareous solutions (evidenced by a rind of calcareous claystone along the fault);

(2) migration of solution into fault zone;

(3) saturation of HCO_3^- and Ca^{2+} with respect to calcite in presence of organic species, calcite precipitation (Donovan, 1974).

Pre-Ore Paragenetic Sequence

Although some of the alteration products observed in these thin sections undoubtedly formed during weathering or transport, diagenetic alteration and authigenesis is demonstrated by the following evidence:

(1) thin, fresh overgrowths of quartz and chalcedony on detrital quartz, presumably contemporaneous with leaching of silica from volcanics;

(2) minor fibrous growths of authigenetic clay in pore spaces around detrital VRF's;

(3) apparent Fe leaching from VRF's, providing localized sites for sulfide precipitation.

The pre-ore paragenetic sequence is represented by a bar diagram (Figure 3.6).

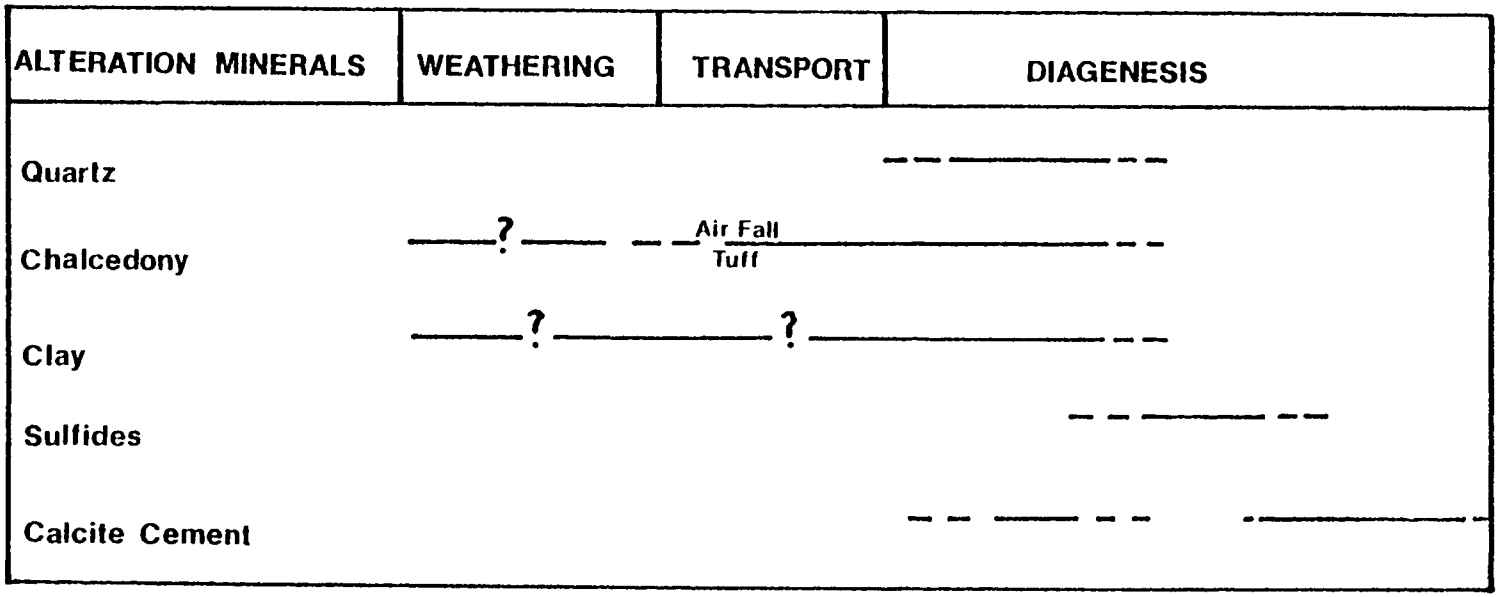

Figure 3.6. Pre-ore paragenetic sequence, Oakville Sandstone, Maclean Five pit.

Host Rock Geochemistry

Several lines of evidence strongly imply that weak to moderate alkaline conditions were prevalent during host rock deposition and diagenesis:

(1) quartz overgrowth and chalcedonic alteration of VRF's;

(2) remarkable preservation of LRF's, including delicate calcite fossil structures;

(3) calcite cementation.

Although Sevier (1962) determined that pH had no effect on silica solubility in the normal ranges of groundwater pH, Berner (1971) noted accelerated rates of dissolution of silica gel at higher pH. Alkaline conditions, therefore, favor migration of siliceous waters and chertification of sediments.

The most convincing evidence for alkaline conditions during transport and deposition of Oakville sediments is the high concentration of LRF's. Presumably, the carbonate fragments were eroded from the Edwards Plateau and transported tens of miles to their present location. Undoubtedly, alkaline conditions prevailed or the fragments would have been dissolved. In addition, the remarkable preservation of delicate calcite fossil structures (Figure 3.1, p. 26) demonstrates that pore waters remained alkaline during diagenesis. Calcite cementation also requires high HCO_3^- content and pH greater than 7.8 (Mason, 1966, p. 174), proving alkaline conditions during later diagenesis.

Groundwater geochemistry in the study area reflects alkaline conditions at present. The mean pH and HCO_3^- concentration from ten wells in the vicinity measured 8.52 and 286 ppm, respectively (Appendix B, Table B-1).

Uranium Source for the Oakville

The source of the uranium in South Texas has been debated for years, and at present, many local geologists consider the Catahoula Tuff as the major contributor. At some localities, however, its stratigraphic position makes this unfeasible or highly unlikely. Rather than resort to some exotic model explaining migration of uraniferous waters from the Catahoula, it seems more logical to first assess the Oakville as a uranium source.

Studies of contemporary volcanic suites in West Texas (Appendix B, Table B-2) reveal uranium concentrations of 3.3-19.5 ppm (Gottfried et al., 1962). Garrels (1967) surmised that devitrification of ash beds produced carbonate-rich waters capable of leaching uranium. DeVoto (1978, p. 67) reported uranium leaching from volcanoclastics during diagenetic alteration to clay minerals (kaolinite, montmorillonite). Zielinski (1979) showed that glassy lithic fragments release uranium in proportion to the weight of leached silica, providing an excellent long-term source of U. Since the Oakville contains nearly 23% VRF's with compositions analogous to those in the Big Bend area and in which the volcanic glass has been altered, it is quite possible that considerable uranium was leached out of Oakville sediments during diagenesis.

With this assumption one can make a bulk rock calculation to estimate the minimum amount of uranium released in a given area (Figure 3.7). For example, consider a wedge of rock 1 km × 4 km × 100 m and assume a U content of 5 ppm for the volcanics. If the VRF's have a density of 2.7 g/cm^3, then they will contain 0.0031 kg U/m^3. Assuming a 50% leaching efficiency, it is possible to introduce 310,000 kg U into

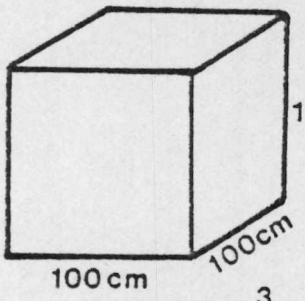

$$= 1m^3 =$$

$$100cm \times 100cm \times 100cm$$

$$\frac{100^3 cm^3}{1m^3} \times \frac{2.7g}{cm^3} = 2.7 \times 10^6 \frac{g}{m^3}$$

$$2.7 \times 10^6 \frac{g}{m^3} \div 1000 \frac{g}{kg} = 2700 \frac{kg}{m^3}$$

$$2700 \frac{kg}{m^3} \times 5 \times 10^{-6} U \times .23 \text{ VRF's} =$$

$$.0031 \frac{kg U}{m^3}$$

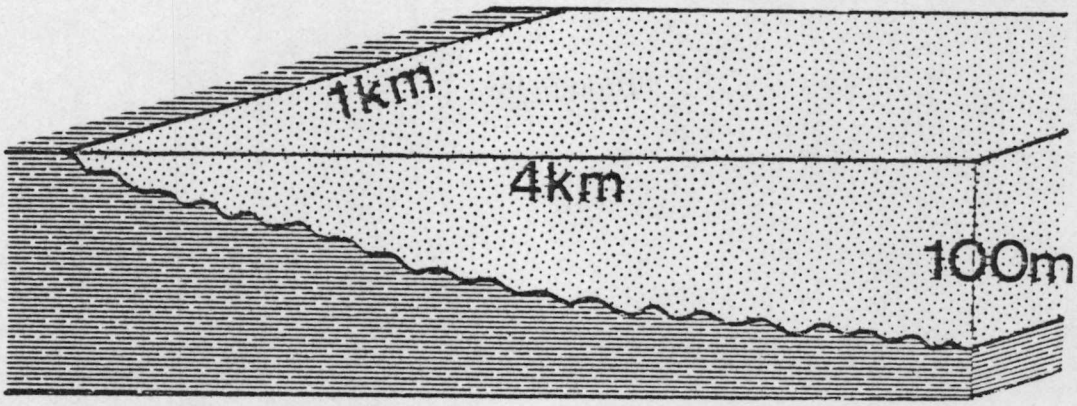

$$1000m \times 4000m \times 100m = 4 \times 10^8 m^3$$

$$\frac{4 \times 10^8 m^3}{2} \times .0031 \frac{kg U}{m^3} = 620{,}000 kgU$$

$$50\% \text{ leaching} = 310{,}000 kgU$$

Figure 3.7. Bulk-rock calculation for uranium availability in Oakville sediments.

solution. Since the Oakville and its equivalents extend for hundreds of kilometers and reach hundreds of meters in depth, the original amount of uranium contained in the volcanoclastics was enormous and could account for all known uranium deposits hosted by the Oakville Sandstone.

CHAPTER IV

ORE PETROLOGY

I. MINERALOGY

Sampling limitations precluded determination of the ore assemblage from the rock samples alone, since they represented only three levels in the mine. Six high-grade powdered core samples were selected for x-ray diffraction analysis, representing the 5, 53, 81, 85, and 86 ft (1.5, 16.2, 24.7, 25.3, 25.9, and 26.2 m) intervals of the deposit. Diffraction patterns revealed a uniform ore assemblage of uraninite and coffinite for the entire reduced section of the mine; therefore, the sample suite is considered fairly demonstrative of the deposit as a whole.

The ore minerals of the Maclean Five deposit consist of uraninite, coffinite, sphalerite, and marcasite with rare pyrite. Umohoite has been reported by mine geologists, although it was not recognized in the present study. The high molybdenum content of the ore, however, suggests that umohoite and molybdenite (or jordisite) were probably present and have been altered to mineraloids in the samples which were analyzed. Garrels (1957) reports that umohoite should be a stable phase under reducing conditions when Mo is available, and Granger (1963) notes that hydrated uranium minerals such as jordisite or illsemenite are often x-ray amorphous. A thin layer of oxidized uranium minerals (autinite, carnotite ?) capped the deposit before mining operations began, indicating gradual oxidation at the surface level. Samples from this horizon were not available during the field season.

II. ORE TEXTURES

Textural evidence is indicative of dissolution, replacement, and precipitation in voids. Uranium minerals fill the interstices between detrital grains (Figure 4.1, A). Numerous sections exhibit stringers and veinlets of mineralization corresponding to zones of permeability and crystalographic and structural weaknesses.

Dissolution

Irregularly-shaped, corroded chunks of detrital quartz are observed suspended in calcite cement, apparently dissolved by the invading carbonate solutions. Megascopic evidence of dissolution processes is also recognized in hand specimen. Rock samples from stations A-4, A-6, and A-12 (99 ft or 30 m contour level) exhibit veinlets and stringers of mineralization, hinting that pre-existing calcite was dissolved and replaced by uranium minerals. At station A-5 (79 ft or 24 m contour level) marcasite is found concentrated along fractures and microfaults. Solution bands are also evident, demonstrating several successive phases of solution, migration, and deposition.

Replacement

Uraninite, coffinite, sphalerite, and marcasite are observed replacing calcite cement and detrital grains. These minerals may appear disseminated or in patterns corresponding to cleavage planes of the invaded minerals (Figure 4.1, B). Some grains experience replacement by all four ore minerals, while others are replaced by only one mineral type. VRF's appear most susceptible to replacement and quartz the

Figure 4.1. Ore textures (reflected light), Maclean Five deposit. Local textures denoted by arrows.

A. Uranium minerals filling interstices between detrital grains (transmitted light).

B. Marcasite filling cleavage in gangue. Scale is representative of remiander of photographs in this figure.

C. Uraninite (light phase) replacing calcite cement and surrounding embayed quartz grain. Also note uraninite replacing quartz.

D. Aggregate of twinned marcasite replacing calcite and detrital gangue.

E. Detrital gangue shredded by ore solutions and marcasite crystallization.

F. Marcasite rimming cavity in uraninite-coffinite intergrowth.

G. Marcasite "floating" in calcite cement (C) and along calcite grain boundaries.

H. Ribbon-like intergrowth of uraninite and coffinite (U-Cf) filling large void formed by dissolution.

I. Uraninite and coffinite (U-Cf) replacing calcite.

J. Colloform intergrowth of uraninite and coffinite filling dissolution zone in calcite cement.

K. Boyryoidal marcasite (M) with pyrite core (P).

L. Lateral sequence of ore deposition controlled by pH: calcite (left of photo), uraninite-coffinite (U-Cf), sphalerite (S), and marcasite (M).

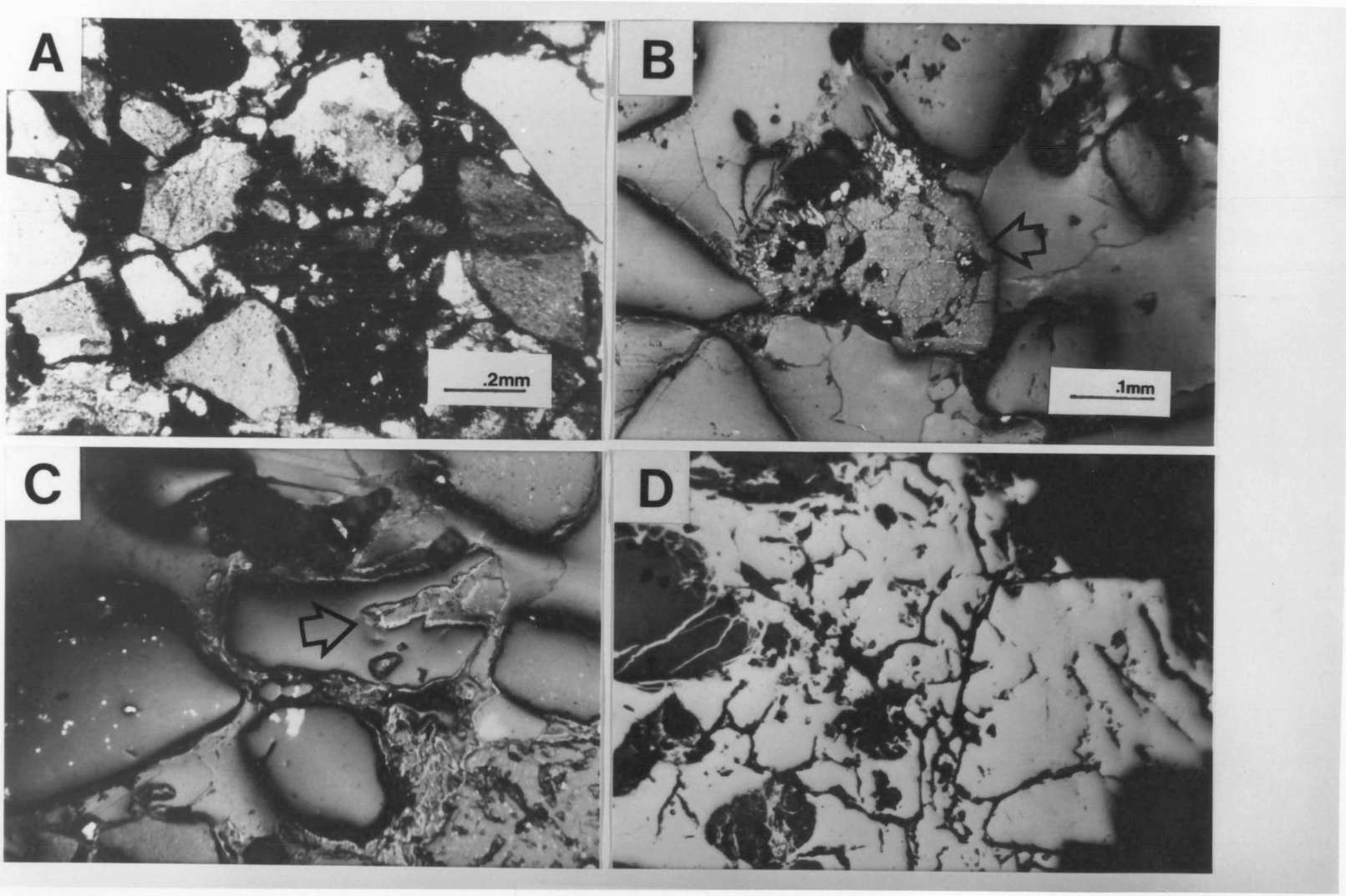

Figure 4.1.

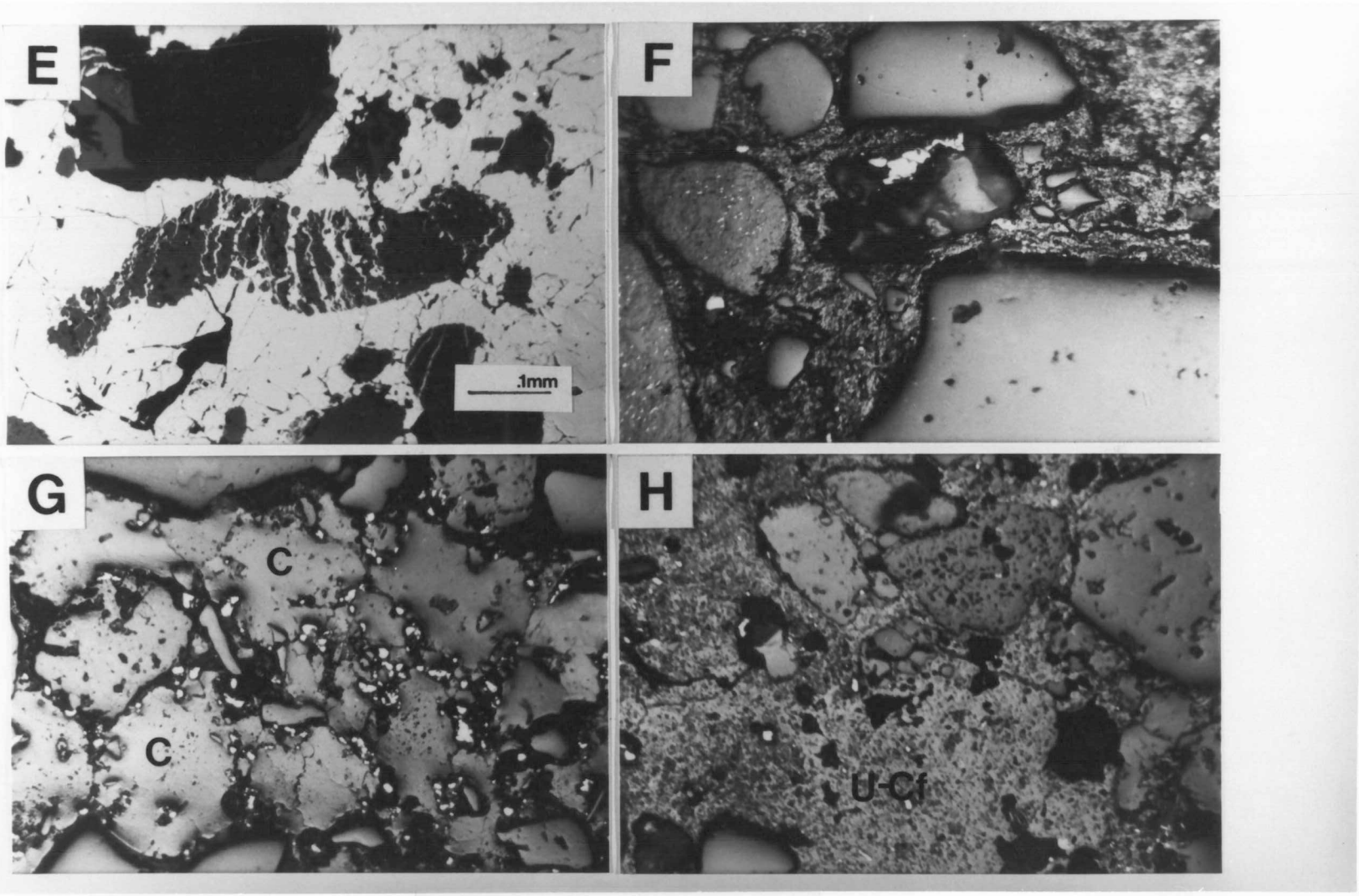

Figure 4.1. (Continued)

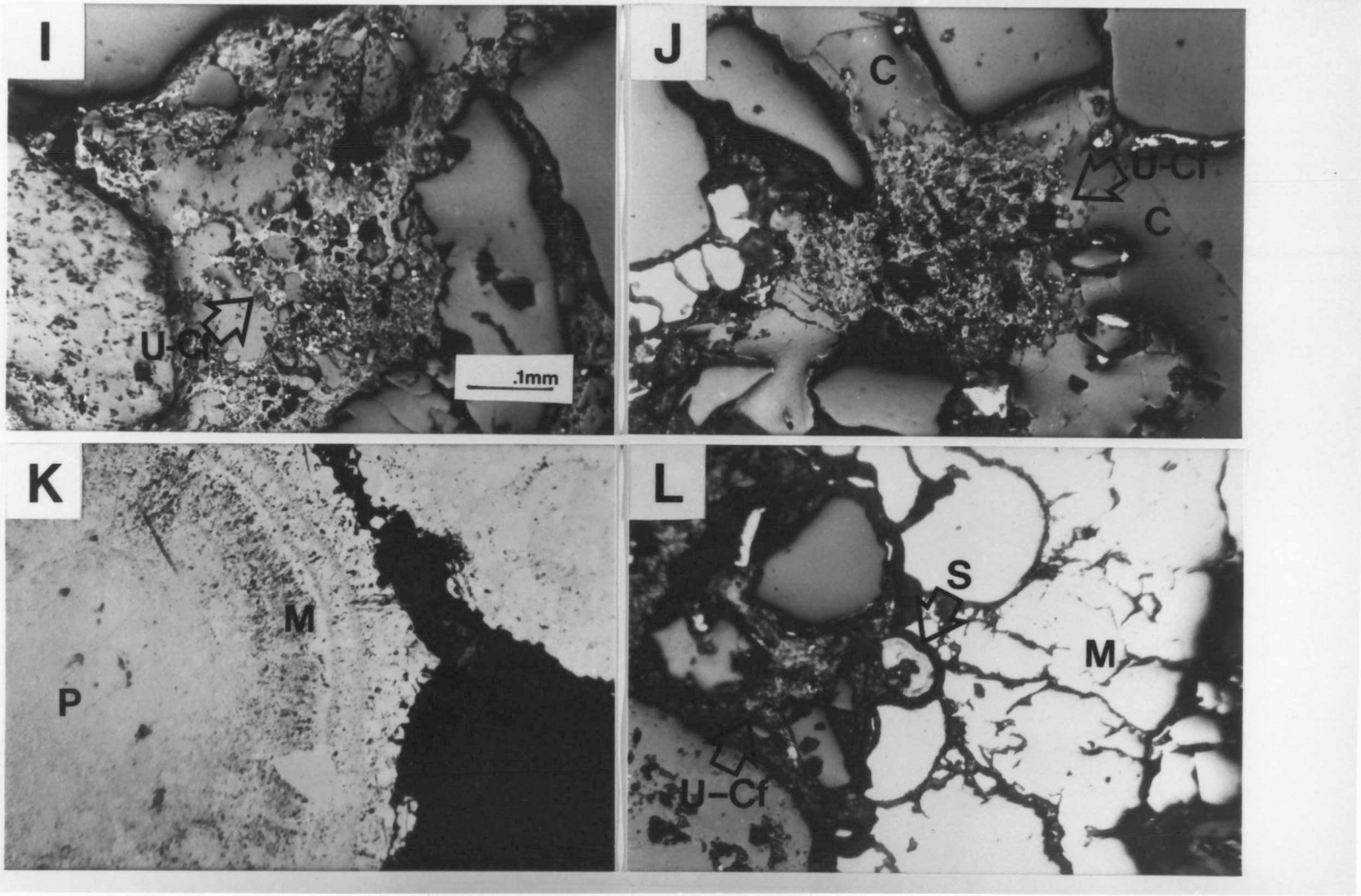

Figure 4.1. (Continued)

least, although marcasite seems to attack grains indiscriminantly. Uraninite and coffinite also replace calcite along zones of weakness, such as boundaries between other calcite grains or detrital grains (Figure 4.1, C).

Aggregates of twinned marcasite are also found replacing calcite and detrital grains (Figure 4.1, D), sometimes forming a sulfide cement. The aggregate morphology implies several periods of deposition around the original nucleus. Solutions depositing marcasite seem to have been exceptionally corrosive, as numerous detrital grains appear shredded during marcasite crystallization (Figure 4.1, E). Occasionally, sphalerite is seen embedded in twinned marcasite; however, no uranium mineralization was noted in this phase of marcasite deposition.

Stringers and veinlets of marcasite clearly replace ribbon-like intergrowths or uraninite and coffinite. Marcasite also rims cavities in uraninite-coffinite masses (Figure 4.1, F). Other marcasite is interspersed through the uraniferous phases, and is less diagnostic in relation to the sequence of deposition. Disseminated marcasite is also noted "floating" in calcite and along calcite grain boundaries, although in this case FeS_2 is obviously a replacement (Figure 4.1, G). Chemical stability relations preclude the co-precipitation of calcite and marcasite (Beurger, 1934; Mason, 1966).

Co-Precipitation

Uraninite and coffinite form ribbon-like intergrowths in interstitial spaces between detrital grains and sometimes replace calcite (Figure 4.1, H, I). Sphalerite inclusions are present locally

and are apparently contemporaneous. Twinned marcasite also contains inclusions of sphalerite.

Deposition in Voids

Uraninite, coffinite, sphalerite, and marcasite exhibit colloform and crustiform textures (Figure 4.1, J), indicating precipitation in open spaces (Ramdor, 1969). Occasionally colloform uraninite and sphalerite fill dissolution pores in calcite cement. In one instance (station A-4, at 90 ft or 27 m contour) colloform marcasite was found with a pyrite core, evidencing a pH reduction during sulfide deposition (Figure 4.1, K).

Sequential Deposition

At station A-4 (99 ft or 30 m contour) two polished sections demonstrated a lateral sequence of ore deposition in response to local pH reductions, beginning with calcite deposition. Later, uraninite and coffinite formed contemporaneous intergrowths in the interstices, followed by colloform growths of sphalerite, giving rise to crustiform marcasite (Figure 4.1, L).

III. ORE-STAGE PARAGENETIC SEQUENCE

Several lines of evidence support an initial pre-ore period of carbonate dissolution and calcite deposition, which restricted permeability along the fault plane to zones of dissolution and structural weakness:

(1) dissolved and brecciated quartz in calcite cement;

(2) replacement of calcite cement by all other types of ore minerals;

(3) uniformity of the second stage of calcite cement introduced through the fault plane, determined by CL.

Mineralizing solutions entered permeability pockets and precipitated calcite, which was followed by contemporaneous uraninite, coffinite, and sphalerite. Since mineralizing fluids such as these became acidic locally (Garrels, 1957), calcite dissolved slightly where in contact with solution and uraninite, coffinite, and sphalerite replaced calcite. Residual solutions became more acidic as carbonate complexes diminished, and sphalerite and marcasite crystallized, often replacing uranium minerals, calcite and detrital minerals.

Local variations in pH exerted strong influence on the mineralizing process, evidenced by colloform marcasite with pyrite cores, and lateral sequences of ore deposition in relation to pH sensitivity (Figure 4.1, L). The paragenetic sequence becomes confusing in sections with overlapping pulses of mineralization (i.e., solution banding). In general, however, textural relationships reflect precipitation according to a sharp pH gradient. Ore paragenesis is represented in Figure 4.2.

IV. MINERAL STABILITIES

Mineral phase relations are in good agreement with these petrologic interpretations. Langmuir (1978) demonstrated that uraninite and coffinite intergrowths are equilibrium assemblages in rocks with siliceous groundwaters (>60 ppm), and Brookins (1977) introduced phase diagrams which show overlapping stability fields for these minerals. Marcasite

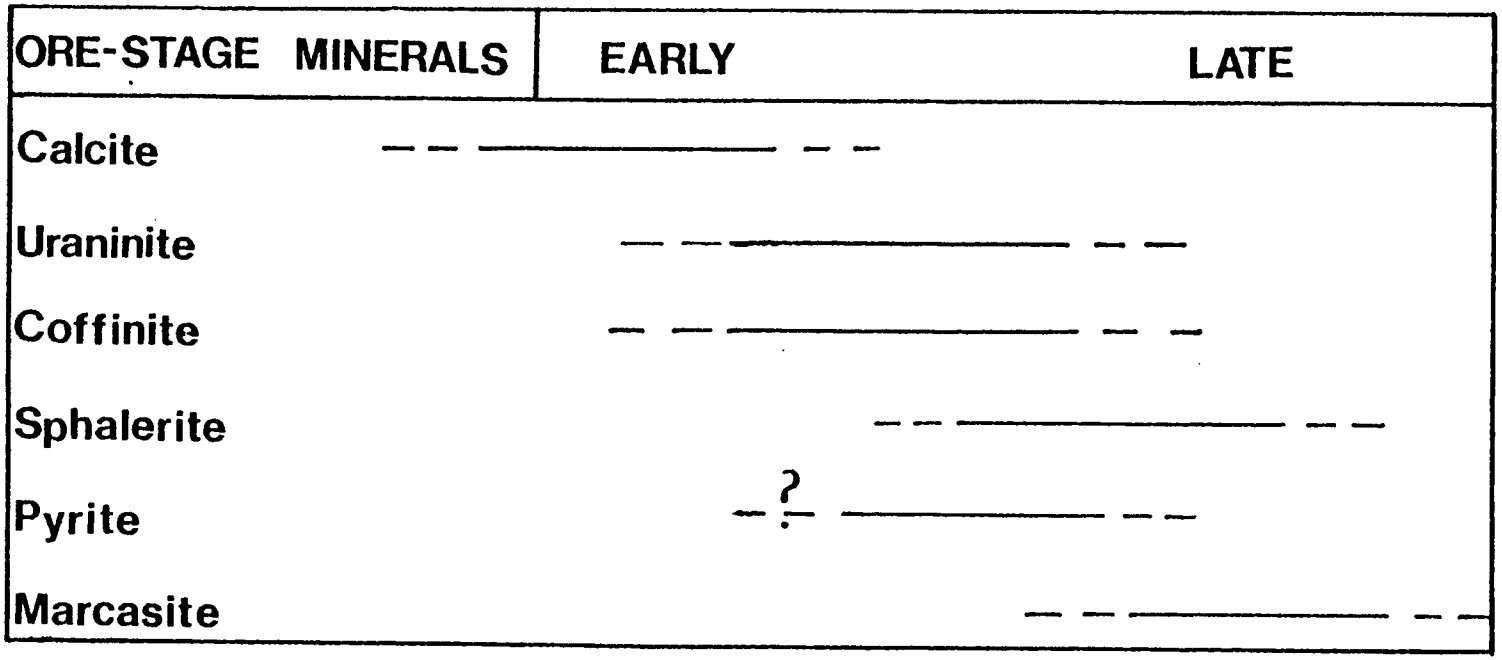

Figure 4.2. Ore-stage paragenetic sequence, Maclean Five deposit.

preferentially forms at low pH (Buerger, 1934). The sequence of ore deposition can be explained by sharp reductions in pH with relatively constant Eh (Figure 4.3).

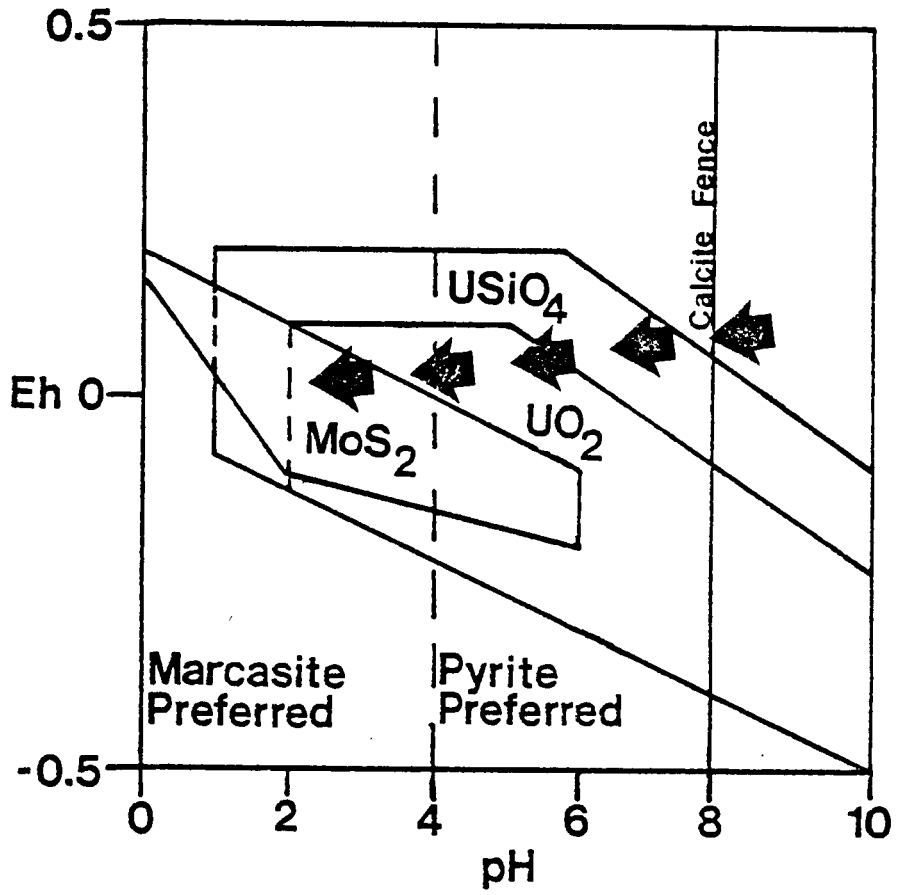

Figure 4.3. Schematic overlay of pertinent mineral stability fields.

Sources: Brookins, 1977 (uraninite and coffinite); Wedepohl, 1969 (molybdenite); El-Dahhar and Barnes, 1979 (marcasite-pyrite).

CHAPTER V

TRACE ELEMENT ANALYSIS

I. INTERPRETATION OF ELEMENT DATA

Twelve elements were identified and measured in the core samples, including U, Ba, Mn, Na, K, Al, Dy, Sm, Ce, As, Nd, and Mo. The significance of values for Ba and the rare earth elements (REE) is unclear and is discussed in Appendix C, along with the NAA procedures and element concentrations (Tables C-3, C-4). Computer analyses were performed on the data using the Statistical Analysis System, 1979 (Barr et al., 1979).

Error Analysis

Values reported in the text were validated by comparison with several recognized standards (Appendix C, Table C-4). Absolute error was calculated from the formula

$$E_3 = \sqrt{E_1^2 + E_1^2} ,$$

and is reported in Table 5.1.

Summary Statistics

Summary statistics for the element populations were calculated. Na, K, and Al exhibit means which fall approximately in the middle of their respective distributions (ranges), implying a normal or pseudo-normal distribution of these elements. The other element populations are all positively skewed, suggesting lognormal distribution (Levinson,

Table 5.1

Error Calculations for Element Data

Element	Standard Error (E_1)	Mean Relative Error (E_2)	Absolute Error (E_3)
U	1.5%	1.94%	2.45%
As	7.0%	11.28%	13.28%
Na	2.0%	0.77%	2.14%
K	3.0%	6.06%	6.76%
Al	21.0%	3.35%	21.27%
Mn	2.0%	0.64%	2.10%
Mo	3.0%	7.22%	7.82%

1974, p. 471). Uranium, Mn and Mo display standard deviations greater than their corresponding means, also indicative of non-normal relationships. The summary statistics are tabulated in Table 5.2. Histograms of the element data support these observations (Figure 5.1). Lognormal groups of values show high contrast, and are particularly useful in the delineation of unusual chemical and physical phenomena.

Depth-Concentration Plots

Elemental concentrations were plotted against depth to test the data for vertical trends. Uranium, As, and Mo display three corresponding zones of significant enrichment, the first zone from 3-10 ft (0.9-3 m), the second zone from 48-60 ft (15-18 m), and the third zone from 80-87 ft (24-27 m) (Figure 5.2). Within these intervals, an increase or decrease in U almost invariably results in an increase or decrease in As and Mo. This would seem to indicate a significant relationship between these elements and the chemical parameters which

Table 5.2

Summary Statistics for Maclean Five Element Data (ppm)

VARIABLE	N	N MISSING	MEAN	STANDARD DEVIATION	MINIMUM VALUE	MAXIMUM VALUE	RANGE	SKEWNESS
U	50	1	2654.50	5559.55	20.00	24927.00	24907.00	2.98
MO	43	8	5674.14	10613.94	243.00	50712.00	50469.00	3.29
AS	36	15	66.17	55.23	10.00	197.00	187.00	0.89
MN	50	1	731.92	757.82	99.00	3643.00	3544.00	2.80
NA	51	0	5734.33	877.85	3993.00	7759.00	3766.00	0.32
K	48	3	12947.52	3012.69	7949.00	21972.00	14023.00	0.77
AL	39	12	41874.44	17518.10	14637.00	83343.00	68706.00	0.93

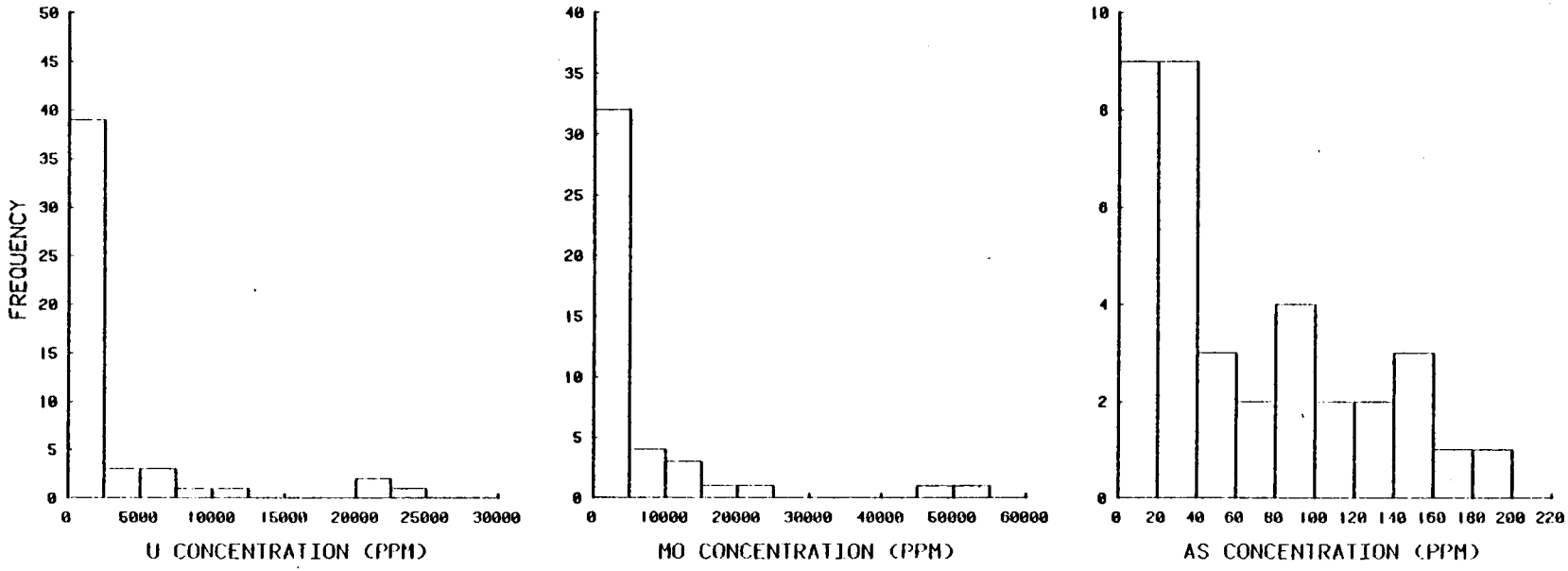

Figure 5.1. Histograms of element data from a vertical suite of core samples, Maclean Five deposit.

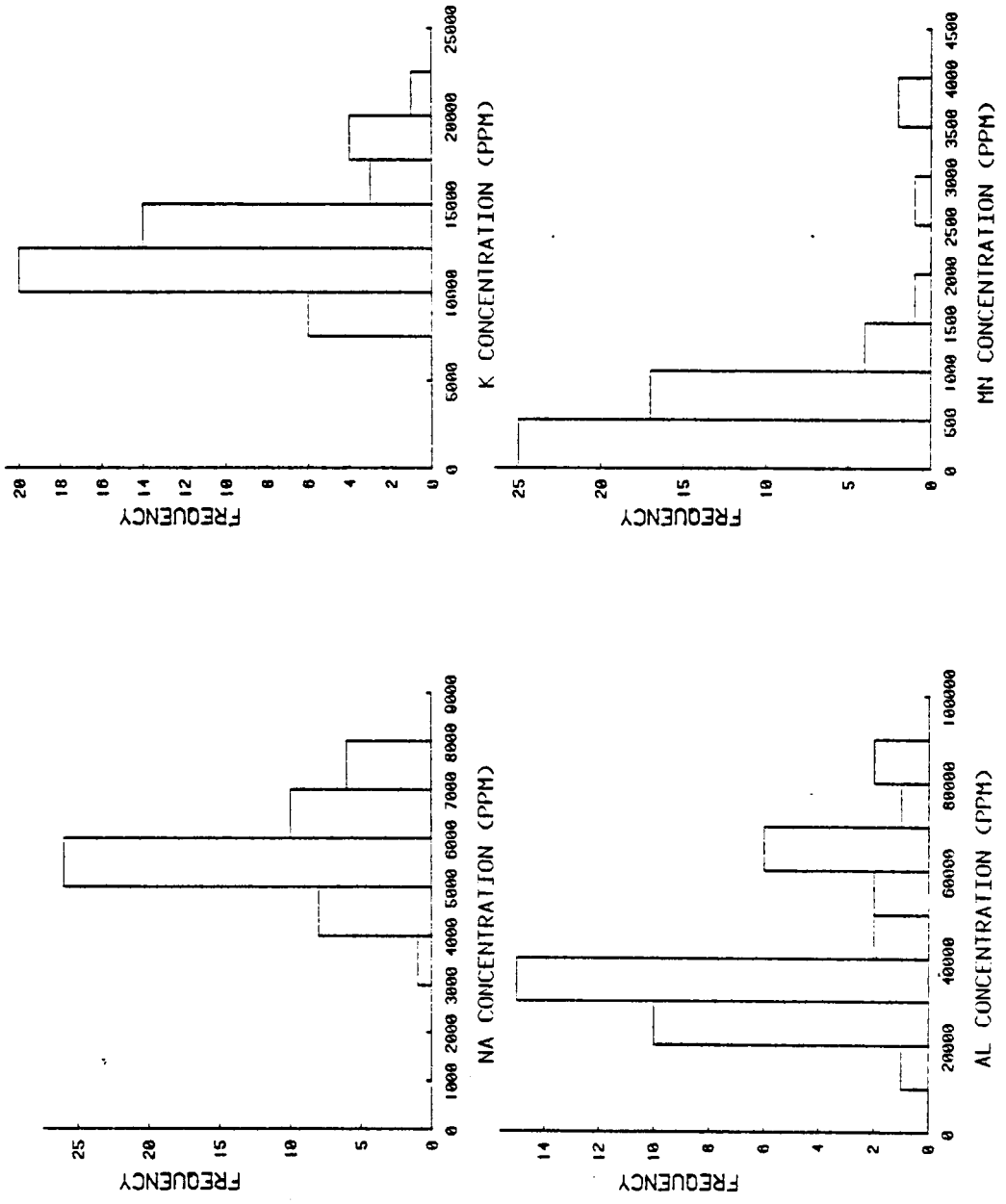

Figure 5.1. (Continued)

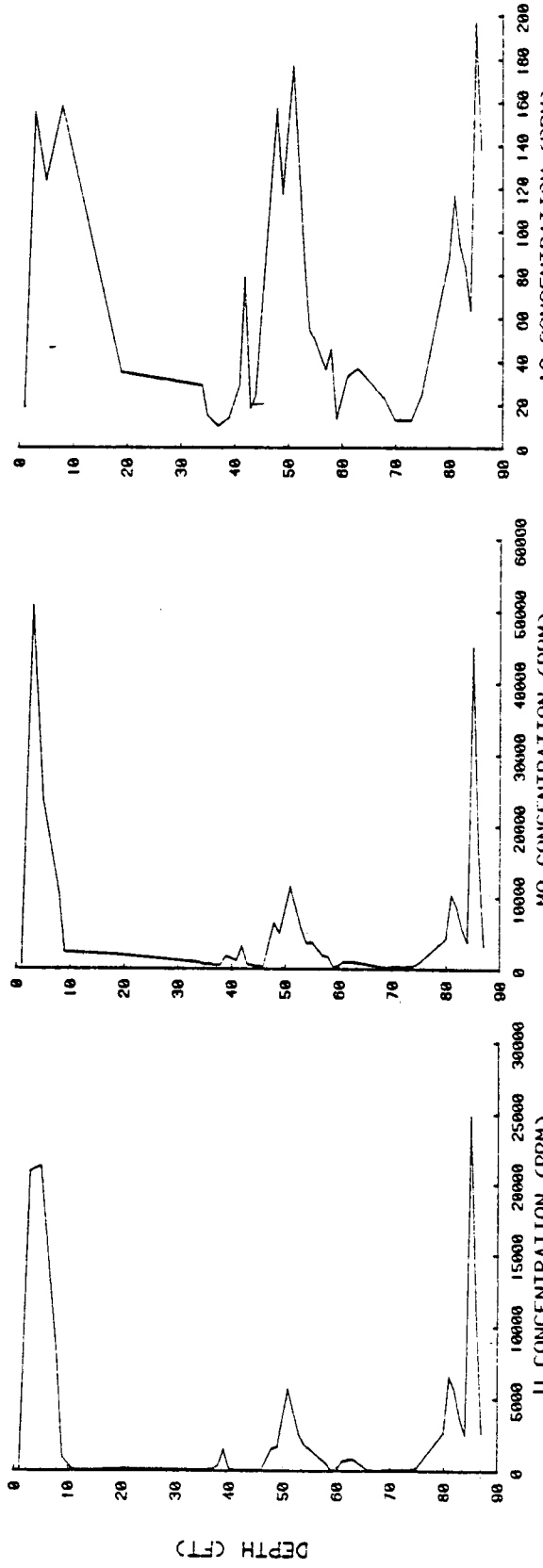

Figure 5.2. Depth-concentration plots for element data, Maclean Five deposit.

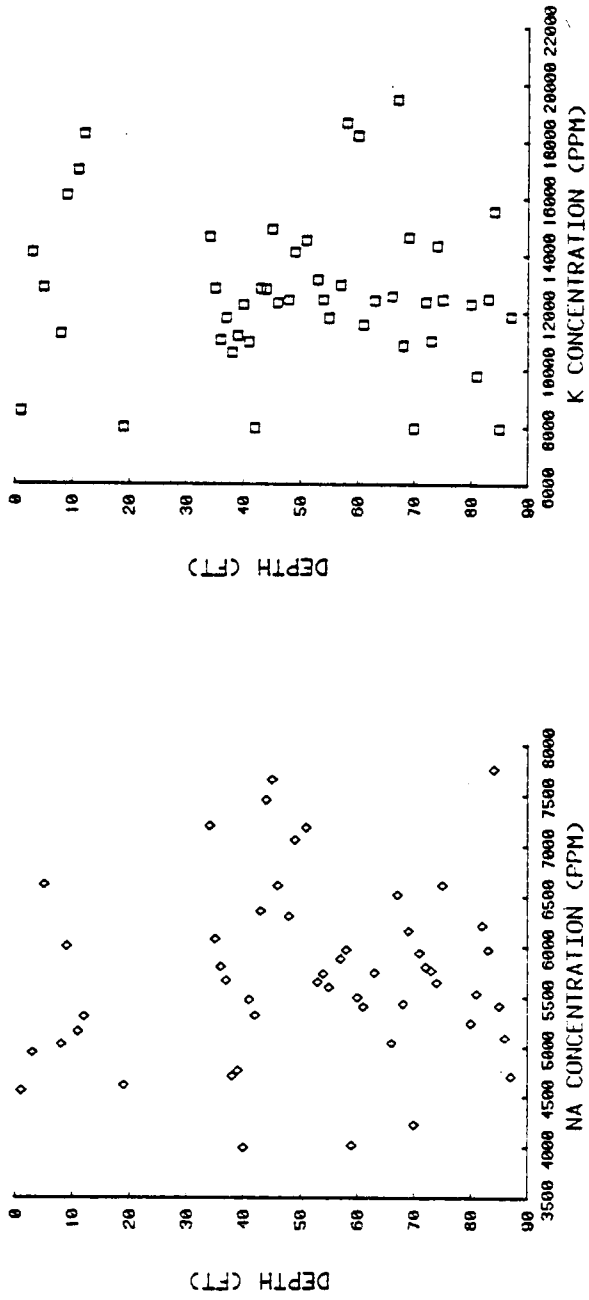

Figure 5.2. (Continued)

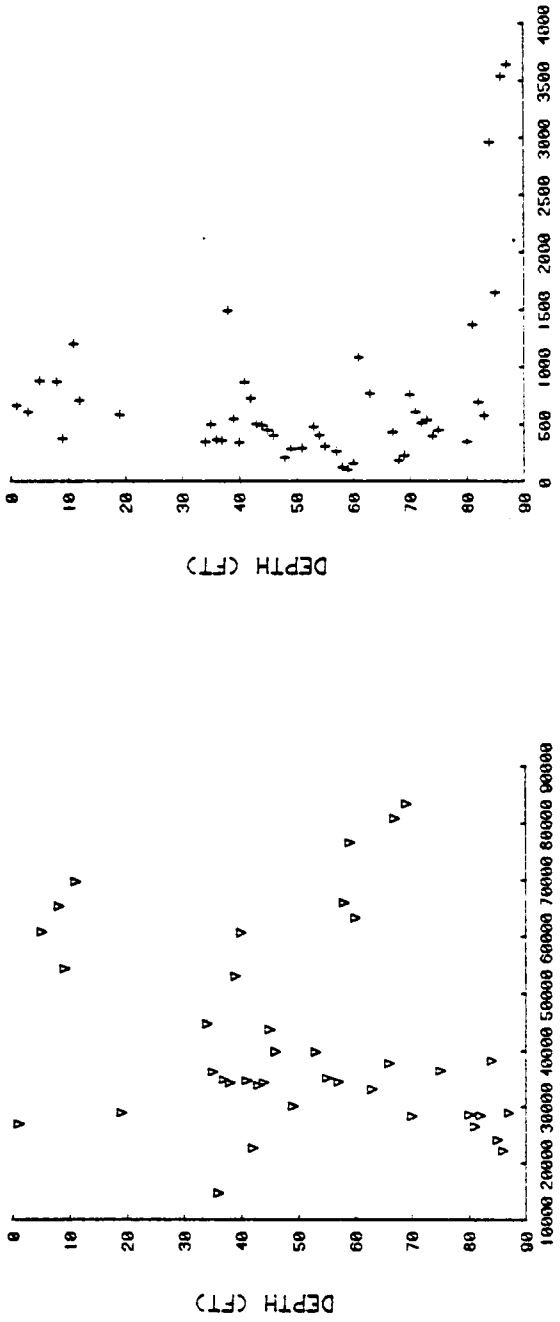

Figure 5.2. (Continued)

control their precipitation. Mn, K, Na, and Al values appear scattered in relation to depth, and apparently bear no relation to U.

Pearson Correlation Matrix

The Pearson or product-moment correlation of data reveals the influence of one variable on another, as measured in terms of covariance and variance of the individual elements. The correlation coefficient, r, may be represented by the following mathematical formula (Nie et al., 1970, p. 280):

$$r = \frac{\sum_{i=1}^{N} (X_i-\bar{X})(Y_i-\bar{Y})}{\left\{\left[\sum_{i=1}^{N} (X_i-\bar{X})^2\right]\left[\sum_{i=1}^{N} (Y_i-\bar{Y})^2\right]\right\}^{\frac{1}{2}}}$$

The coefficient r is the fitness measure of the data to a linear regression line, and r^2 is the ratio of variance in one variable explained by variance in the other.

A Pearson correlation matrix of the element data is reproduced in Table 5.3. It includes bivariate correlations, their significance levels, and the number of observations used in the calculations. Corresponding elements with high correlation coefficients and low significance levels are boxed in for emphasis.

As might have been expected from the depth-concentration plots, U shows a strong correlation with Mo and As. K, Na, Al, and Mn exhibit no appreciable correlation with U or its associated elements, suggesting that these elements are concentrated in detrital minerals natural to the

Table 5.3

Correlation Matrix for Element Data, Maclean Five Deposit[a]

	DEPTH	U	MO	AS	MN	NA	K	AL
DEPTH	1.00000	-0.06035	-0.10662	-0.00288	0.29658	0.10819	-0.03324	-0.21217
	0.0000	0.6772	0.4962	0.9867	0.0365	0.4498	0.8226	0.1947
	51	50	43	36	50	51	48	39
U	-0.06035	1.00000	0.95106	0.74012	0.30734	-0.02821	-0.17494	-0.09841
	0.6772	0.0000	0.0001	0.0001	0.0317	0.8458	0.2395	0.5511
	50	50	43	35	49	50	47	39
MO	-0.10662	0.95106	1.00000	0.74114	0.22643	-0.09853	-0.11232	-0.11241
	0.4962	0.0001	0.0000	0.0001	0.1443	0.5296	0.4844	0.5268
	43	43	43	35	43	43	41	34
AS	-0.00288	0.74012	0.74114	1.00000	0.30437	0.12879	-0.05649	-0.10477
	0.9867	0.0001	0.0001	0.0000	0.0711	0.4541	0.7510	0.6030
	36	35	35	36	36	36	34	27
MN	0.29658	0.30734	0.22643	0.30437	1.00000	-0.11182	-0.19598	-0.30834
	0.0365	0.0317	0.1443	0.0711	0.0000	0.4395	0.1868	0.0596
	50	49	43	36	50	50	47	38
NA	0.10819	-0.02821	-0.09853	0.12879	-0.11182	1.00000	0.24865	-0.00255
	0.4498	0.8458	0.5296	0.4541	0.4395	0.0000	0.0884	0.9877
	51	50	43	36	50	51	48	39
K	-0.03324	-0.17494	-0.11232	-0.05649	-0.19598	0.24865	1.00000	0.73850
	0.8226	0.2395	0.4844	0.7510	0.1868	0.0884	0.0000	0.0001
	48	47	41	34	47	48	48	37
AL	-0.21217	-0.09841	-0.11241	-0.10477	-0.30834	-0.00255	0.73850	1.00000
	0.1947	0.5511	0.5268	0.6030	0.0596	0.9877	0.0001	0.0000
	39	39	34	27	38	39	37	39

[a] Correlation coefficients/probability > |R| under HO:RHO = 0/number of observations.

host rock, such as orthoclase, plagioclase, or clays. The correlation of K and Al lends evidence to this assumption.

It is evident from the statistical treatment of the data that U and the associated elements are responsive to an analogous set of chemical conditions along the fault plane.

Element-Element Plots for Linear Correlation

X-Y plots of data are useful in delineating linear trends among data pairs. Element-element plots were prepared for those elements which demonstrated significant linear correlation with uranium in the preceding matrix (Table 5.3). Visual analysis of the data spread around a hypothetical correlation line may prevent spurious conclusions about the linearity of data relationships.

Examination of the data plots verify a strong linear relationship between U and Mo (Figure 5.3). The relationship between U and As does not conform to a linear model.

Both correlation coefficients and data plots demonstrate a strong correspondence in some interelement relationships. Outlying points, therefore, may reveal important deviations from the overall trend and reflect unusual conditions within certain zones. Visual analysis of these deviations reveals a depletion in U relative to Mo at the 3 ft (0.9 m) level (Figure 5.3). Uranium was leached at the surface during weathering and redistributed to intervals below, enriching basal zones. It is evident that remobilization processes, including solution, vertical migration, and redeposition, are important secondary factors in the genesis of the Maclean Five uranium deposit.

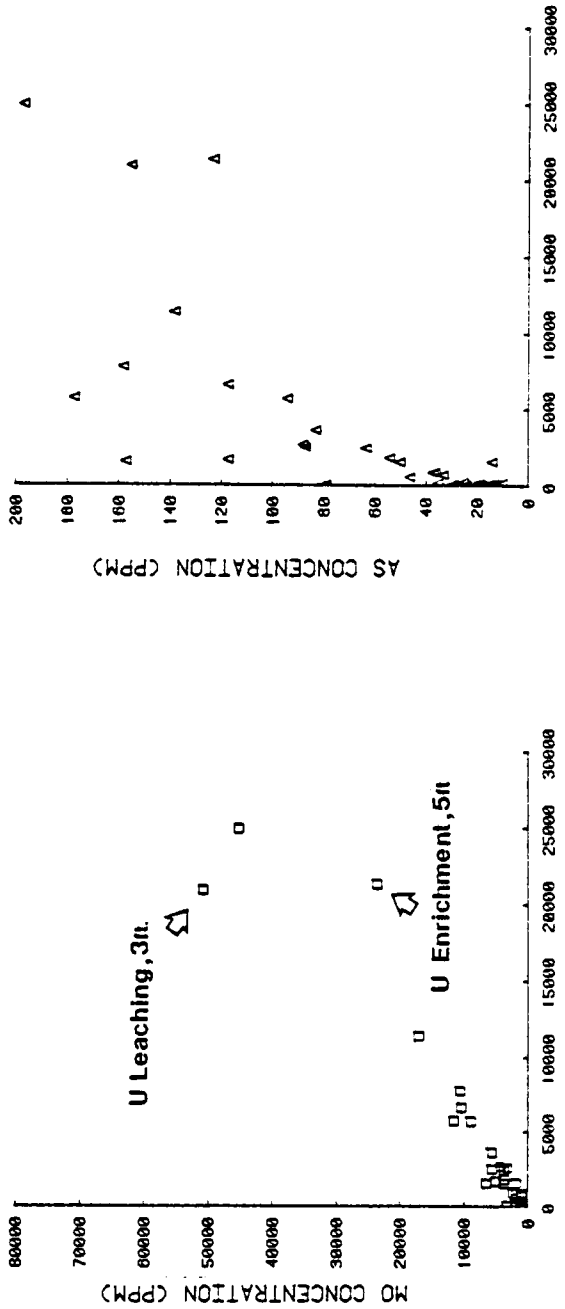

Figure 5.3. Correlation plots of uranium with associated elements.

II. COMPARISON OF MACLEAN FIVE DEPOSIT WITH SOME OTHER URANIUM DEPOSIT-TYPES

Trends in Common Types of Uranium Deposits

Roll-front deposits. Roll-front uranium deposits occur in sandstone host rocks along sinuous geochemical fronts controlled by gradual horizontal changes in Eh. Except for local fluctuation, pH is maintained at a relatively constant level by the buffering effect of carbonate solutions. The pH may be lowered for short distances near the redox boundary in response to remobilization processes, as is evidenced by marcasite overgrowths on pyrite in some roll-front ores (Goldhaber, et al., 1978); however, Harshman (1974) demonstrated the distribution of trace elements associated with roll-front uranium in several major provinces (Gas Hills, Shirley Basin, Black Hills, and Texas Gulf Coast) may be explained by horizontal migration of pH-constant solutions across a gentle Eh gradient (Figure 5.4).

Of particular importance is the horizontal trace element zonation reported by Harshman (1974). Se, V, Mo, U, and the mineral pyrite show persistent relations in regard to the redox front, although representing widely dispersed geographic areas. This is an indication that the geochemical controls causing roll-front deposition are relatively uniform and widespread. Se precipitates in a narrow zone near the redox front, and is indicative of the shift from oxidizing to reducing conditions. V and U precipitate at or slightly downdip from the roll boundary, depending on the local Eh gradient. Pyrite occurs consistently throughout the deposits studied, and Mo drops out at a considerable

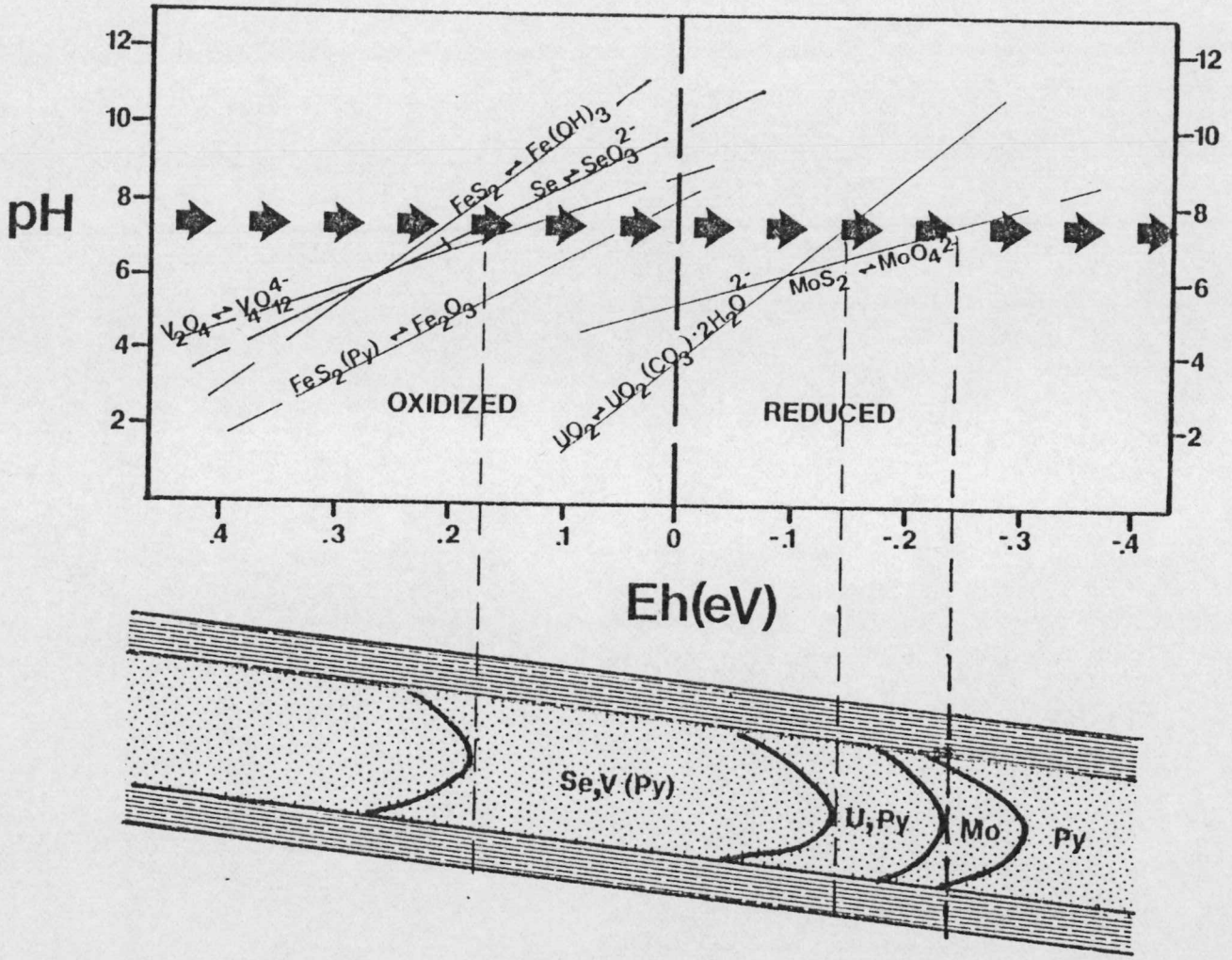

Figure 5.4. Trace element zonation in a typical roll-front uranium deposit. Data from Harshman, 1974.

distance downdip from zones of uranium enrichment. The segregation of U and Mo in roll-front deposits is of particular significance in relation to the Maclean Five deposit (Figure 5.5).

Tabular deposits. Shawe (1966) and Brooks and Campbell (1976) reported trace element distributions for tabular ores on the Colorado Plateau. Tabular deposits demonstrate a vertical distribution of trace elements, with segregation between zones of U and Mo enrichment and Se and V concentrations. In general, Ba, calcite, U, and Mo are enriched at the top of the tabular orebody, while Se and V reach maximum concentrations at a lower interval (Figure 5.6).

Brooks and Campbell (1976) suggested that this reflects an inversion of the roll-front phenomena, that is the upper levels were more reducing, and the lower intervals more oxidizing. This interpretation, however, is only valid if the mineralizing solutions migrated upward into overlying reduced zones. Since enrichment from surficial processes figures heavily in the formation of these deposits (Motica, 1968), this seems unlikely. In addition, Fe fixed in pyrite and marcasite reaches a maximum in the lower zone, as does organic carbon, implying that reducing conditions were also prevalent there.

Since calcite and Ba concentrations experience a fifty-fold increase above and in the U zone, a more plausible model for uranium deposition may be postulated. Uranium migrated downward through the sediments, complexed by carbonate ions. Calcite became saturated and then precipitated, along with barite and witherite. Removal of a significant amount of carbonate ions from solution reduced the pH, and molybdenum

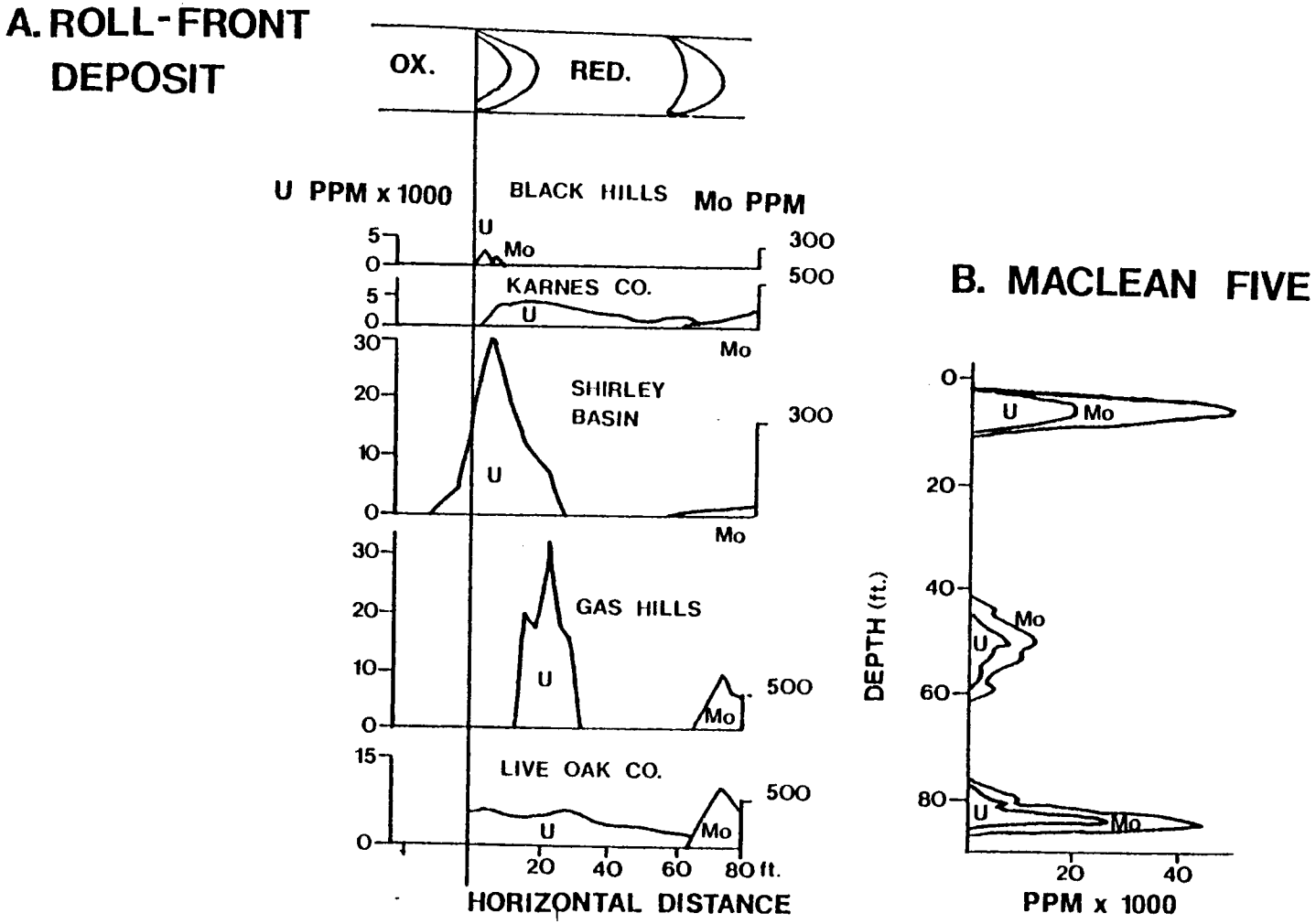

Figure 5.5. Comparison of U-Mo distributions in roll-front deposits (Harshman, 1974) with that of the Maclean Five deposit.

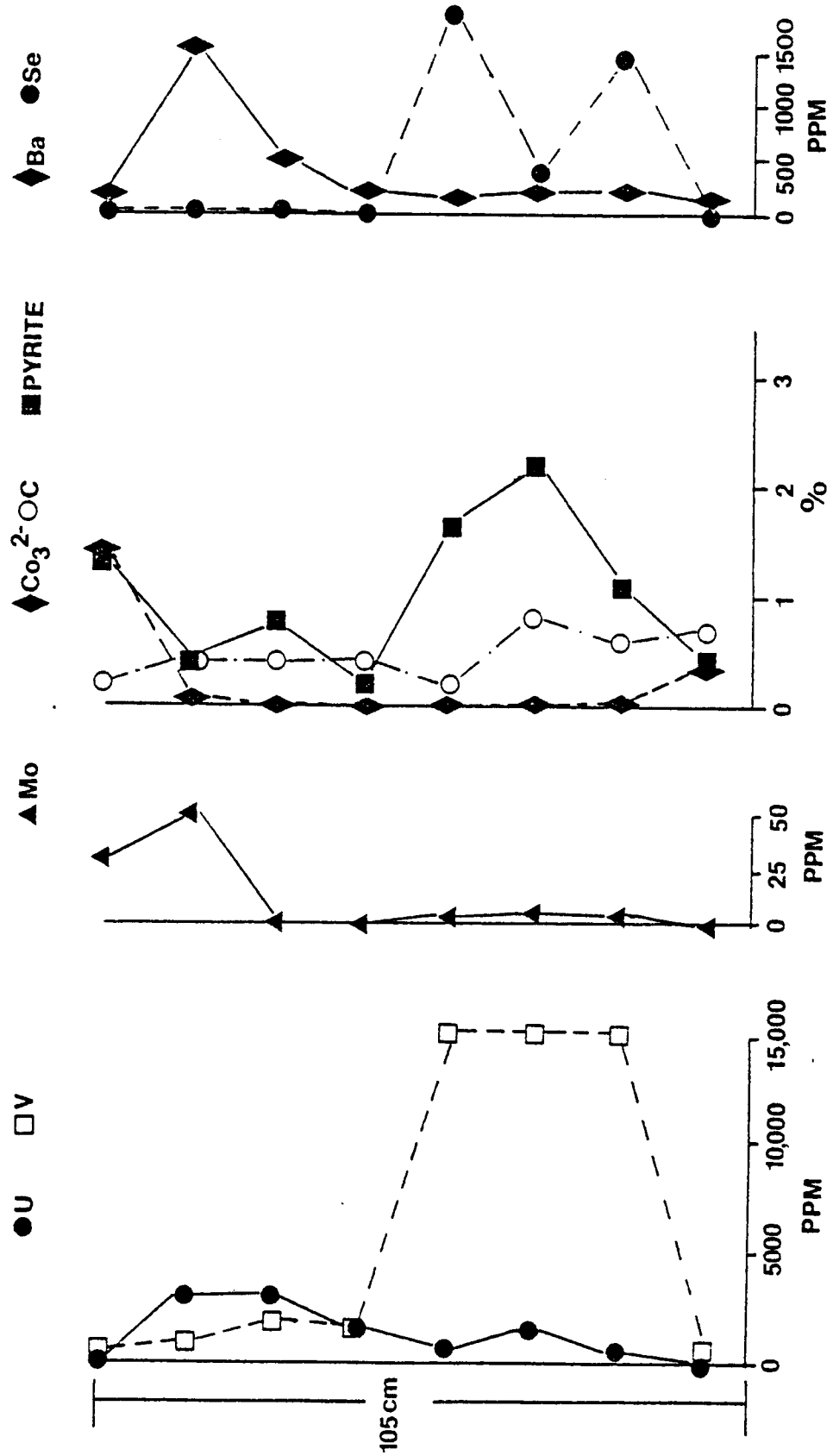

Figure 5.6. Vertical variations of elements in a tabular orebody. Data from Brooks and Campbell, 1977.

and uranium minerals precipitated, followed by pyrite and marcasite. An Eh gradient as well as a pH gradient existed, as shown by the segregation of U and Mo. Later, the upper zone became partially oxidized and Se, which is highly sensitive to Eh changes (Granger and Warren, 1974), was redistributed in the lower zone, incorporated in late stage pyrite and ferroselite ($FeSe_2$). Alternatively, tabular deposits may represent the wings of a denuded roll-front deposit.

Trends in the Maclean Five Deposit

The Maclean Five deposit differs from roll-front and tabular deposits in both the spatial distribution of the uranium ore and its associated elements. The uranium-molybdenum mineralization forms a "dike-like" orebody of very narrow horizontal extent (<25 ft or 7.6 m), extending 87 ft (26.5 m) vertically. In addition, U and Mo are not separated, but rather display a linear correlation throughout the deposit. Deviations from this linear trend may be explained by secondary enrichment processes.

In the Maclean deposit ore is much more concentrated in both U and Mo than nearby roll-front deposits such as the Felder (0.05-0.35% U_3O_8), although the Maclean contains less extensive reserves. At the Felder deposit Mo reaches a maximum several hundred feet downdip from the roll-front. The maximum concentration of Mo reported by Harshman (1974) was 1000 ppm (Gas Hills area), while the mean concentration of Mo in the Maclean deposit is 5674 ppm. Mo data from uranium ores in the Karnes District (Weeks and Eargle, 1963) ranged from 7-3000 ppm; whereas, the Maclean deposit contains 243-50,712 ppm Mo.

The highly restricted spatial distribution of the ore coupled with anomalously high concentrations of U and Mo, even for uranium ores, indicates a sharp gradient of deposition. In addition, the uniform coexistence of U and Mo suggests a relatively static Eh through time, and a low pH for ore formation (Figure 5.3, p. 71). Eh-sensitive Se was detected by qualitative XRF analysis at both the 8 ft (2.4 m) and 80 ft (24.4 m) intervals, also supporting a stationary Eh. The coexistence of ore-stage marcasite and calcite reflects the alternation of alkaline and acidic conditions.

Dissimilarities between the Maclean Five deposit and typical roll-front orebodies can be explained in terms of the redox budget. Roll-front deposits occur in permeable aquifers with free groundwater movement in which reductants dissipate rapidly in a large volume of porous rock, developing a horizontal Eh gradient. In the Maclean, permeability and porosity has been restricted by calcite cement, and reductants have become concentrated in the pore water. Depletion of reducing gases is resisted by overlying permeability barriers and a constant influx of fresh gases from hydrocarbon deposits at depth.

Apparently the fault zone provided a sealed environment with relatively constant Eh, a chemical solution baffle in which ore-deposition was controlled by carbonate equilibria. A new model of ore formation is required to explain the unusual characteristics associated with the Maclean Five uranium deposit.

CHAPTER VI

MODEL FOR FAULT-TRAP MINERALIZATION

I. BACKGROUND INFORMATION

Genetic Evidence

The disposition of uranium deposits near and along the Oakville fault suggests a genetic link between them. In the Felder ore trend, typical roll-front deposits occur in the upthrown fault block at some distance from the fault; however, in the Maclean One deposit to the southwest, the roll front has migrated nearly to the edge of the fault plane (Figure 6.1).

In the Maclean Five deposit, mineralization is entirely restricted to the downthrown block of the fault, with only vestiges of uranium mineralization (radioactive daughters) recognizable in the upthrown sands. In addition, Sulphur Creek to the north has almost entirely eroded the Oakville sediments from the upthrown portion of the fault zone, leaving a thin layer of sediment capping the Catahoula on the northwest side which is incapable of conducting large volumes of solution. This means that the uranium was emplaced when the Oakville was thicker than at present, and thus predates the final erosional phase.

It is evident that uranium mineralization in the Maclean Five deposit bears some genetic relation to the roll-front ores to the north and northeast, and that development of the Sulphur Creek drainage system has exerted influence on the disposition of local redox cells, resulting in redistribution of the uranium.

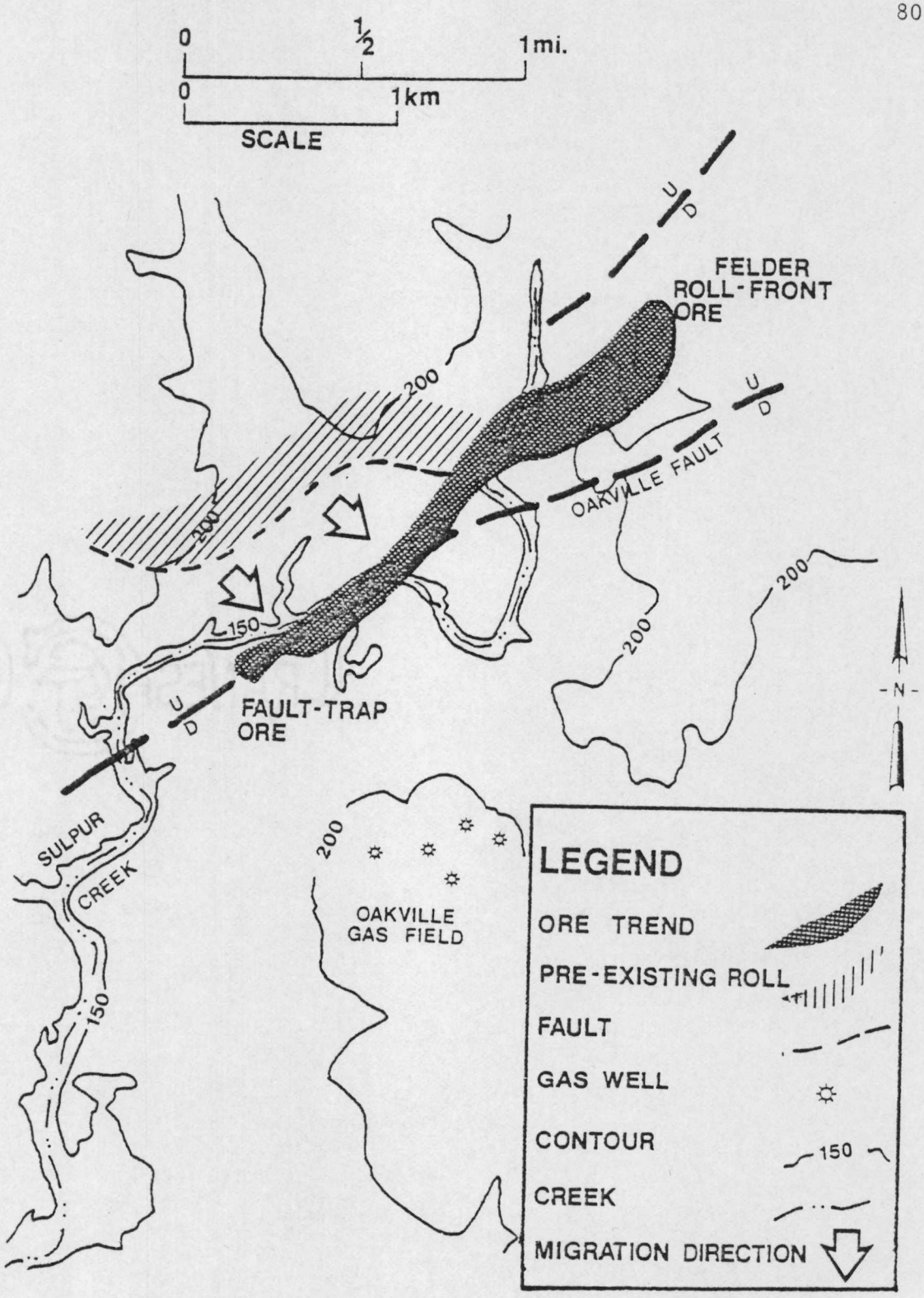

Figure 6.1. Map view of the Felder roll-front and fault-trap uranium ores showing influence of Sulphur Creek drainage on their dispositions.

Reductant Source

Except for a thin cap of oxidized mineralization, uranium ore in the Maclean deposit is in the reduced state (U^{+4}). This means a reductant must be supplied to reduce uranium and precipitate uraninite and coffinite. Although rotting vegetation which produces CH_4 and H_2S (Rackley, 1972) is an efficient source of reductant, the lack of organic debris in many Tertiary stratigraphic units in South Texas has led authors to propose that uranium was reduced by sour gases emanating from faults which penetrate petroleum reservoirs at depth (Eargle and Weeks, 1961; Klohn and Pickens, 1970).

In Maclean Five, sour gases were evolved as groundwater entered the open pit and equilibriated with the atmosphere. H_2S fumes were obvious, and CH_4 and C_2H_6 were also detected by analytical methods (Louis Pogorski, personal communication, 1979, Chemical Projects Ltd., Rexdale, Ontario, Canada). Presence of H_2S and CH_4 in the present groundwater, however, is not necessarily diagnostic of past reductants, as these gases may form near the surface from recently deposited vegetal matter and percolate down into the host rock. In addition, H_2S may form from weathering and bacterially catalyzed oxidation of ore-stage sulfides, rather than originating deep within the fault zone (Rackley, 1972).

Aqueous Hydrocarbon Associations

In order to determine the source of sour gases emanating from the Maclean deposit, ten groundwater samples from the pit were collected and analyzed for gases of the light hydrocarbon series. This procedure was based on patented sampling and analytical techniques developed by

Pogorski and Quirt (1976) in geochemical exploration for hydrocarbons and uranium. Exxon Minerals Company, U.S.A., donated analytical results from 20 additional samples from the surrounding Live Oak County area. These data sets are summarized in Appendix D.

Statistical analyses were performed on the data and are reported in Tables 6.1, 6.2, and 6.3. Since ethane is less likely to be associated with recent vegetal decay, it is useful to determine its correlation with methane. Both these hydrocarbons are found in natural gas deposits overlying oil fields; a strong correlation between these variables would imply a petroleum origin. In this instance ethane and methane groundwater values show good correlation ($r = 0.69, 0.87$ respectively), both in the mine and the surrounding county. Ethane and methane concentrations exhibit their strongest correlation with depth ($r = 0.77, 0.84$ respectively), again supporting a petroleum source for the reductant. In addition, Eargle et al. (1977) reported that bitumens and hydrocarbon seeps were notable in the mine area before oil and gas production lowered the reservoir pressure. The nearby location of the Oakville gas field (Figure 6.1) provides strong circumstantial evidence for petroleum reductants.

II. MODEL OF ORE GENESIS

Geochemical Considerations

Experimental and theoretical thermodynamic calculations show that uranium can be transported by most all common anionic complexes, and that temperature, pressure, and concentration of metals drastically affect the determination of the predominant aqueous species. In the

Table 6.1

Summary Statistics for Hydrocarbon Data[a]

Variable	N	Mean	Standard Deviation	Minimum Value	Maximum Value	Range
Methane 1	11	8,001.27	3,003.57	3,848.00	11,733.00	7,885.00
Ethane 1	11	81.45	68.88	14.00	171.00	157.00
Methane 2	20	406,682.50	632,906.10	330.00	1,777,653.00	1,777,323.00
Ethane 2	10	267.10	191.24	16.00	566.00	550.00
Depth	20	167.00	118.42	45.00	400.00	355.00

[a]Units equal cc/liter, NTP.

Table 6.2

Correlation Matrix for Maclean Data

	Methane 1	Ethane 1
Methane 1	1.00000 0.0000	0.68832 0.0192
Ethane 1	0.68832 0.0192	1.00000 0.0000

Table 6.3

Hydrocarbon Correlation Matrix for Live Oak County[a]

	Methane 2	Ethane 2	Depth
Methane 2	1.00000 0.0000 20	0.86979 0.0011 10	0.83689 0.0001 20
Ethane 2	0.86979 0.0011 10	1.00000 0.0000 10	0.77369 0.0086 10
Depth	0.83689 0.0001 20	0.77369 0.0086 10	1.00000 0.0000 20

[a]Correlation coefficients/probability > |R| under HO:RHO = 0/number of observations.

sedimentary environment, however, standard temperature and pressure (STP) conditions prevail, and pH and concentration become overwhelming factors. Langmuir (1978) constructed several plots of mole percent uranyl species versus pH. In pure water uranyl-hydroxy complexes are important, whereas, in groundwater with significant dissolved CO_2 (10^{-2}atm), carbonate complexes are dormant (pH 5-9). Addition of Cl^-, $SO_4^=$, and F^- adds further complexity, although equilibrium-constant expressions reveal these complexes to be negligible in the presents of abundant carbonate at STP. Phosphate radicals lower the solubility of uranyl-carbonate complexes (Romberger, 1978), but few groundwaters contain enough $PO_4^=$ to be of significance.

In the Oakville Sandstone petrologic evidence and recent groundwater chemistry reflect moderately alkaline conditions during deposition and diagenesis. The high calcite content of the rock (up to 40% by volume) reflects the activity of carbonate solutions and lends evidence to the presumption that uranium was transported as a carbonate complex.

Host Rock Preparation

After deposition of the Oakville sediments, dewatering and compaction of Catahoula clays below produced zones of weakness which led to compactional faulting. Deformation pierced hydrocarbon traps at depth, and sour gases (CH_4, H_2S, HS^-) began to migrate upward along the fault plane, saturating the permeable, overlying sandstones. Weathering of the Oakville along its outcrop leached uranium from reactive pyroclastic debris and set the redox cycle into motion. Sands along the fault plane opposite the Catahoula Tuff were cemented by calcareous

solutions from dewatering of clays, seepage along the fault, and oxidation of hydrocarbons (Donovan, 1974).

The fault-trap mechanism of ore formation is a three stage process, involving deposition, remobilization, and redeposition of uranium and associated minerals. These processes are represented in graphical form in Figure 6.2 and 6.3.

Stage I: Roll-Front Development

During the generation of the redox front, moderately alkaline uraniferous carbonate solutions (pH below the calcite fence, reflected by scarcity of cemented rock) migrated through porous sandstones between impermeable clay beds. Reducing gases invaded the sands contemporaneously, and dissipated rapidly away from the fault-source, creating a horizontal Eh gradient. The pH-constant, buffered solutions (dark arrow, Figure 6.2) continued to migrate through the porous medium until a critical redox potential was reached and uraninite began to precipitate. Due to the gentle, horizontal Eh gradient (Figure 5.4, p. 73) and relatively constant pH, molybdenum minerals such as jordisite or molybdenite precipitated a considerable distance downdip from the uranium ore-roll, and the iron sulfide pyrite formed preferentially relative to marcasite. The roll-front sequence can be traced through reactions 6 and 2, or 2 or 3 (Figure 6.2), depending on the initial pH and the slope of the mineralization path in regard to slight pH fluctuations.

Stage II: Weathering and Stream Erosion

Stage II can be envisioned as the roll-front sequence in reverse. Streams (e.g., Sulphur Creek) began to incise into sediments on the

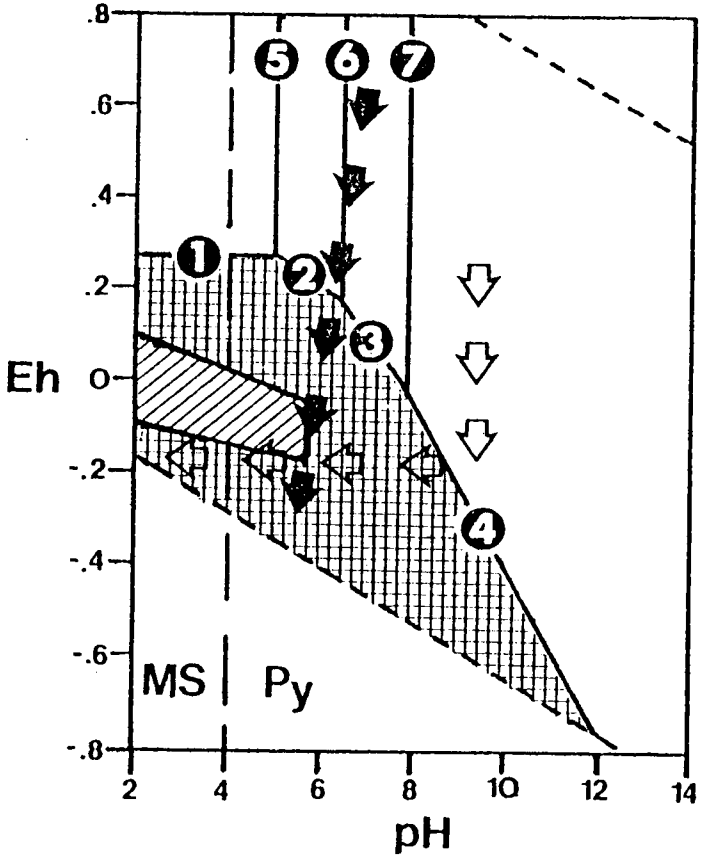

ORE STAGE REACTIONS

1 $UO_2^{2+} + 2e^- = UO_2$

2 $UO_2CO_3^\circ + 2H^+ + 2e^- = UO_2 + CO_2 + H_2O$

3 $UO_2(CO_3)_2^{2-} + 4h^+ + 2e^- = UO_2 + 2CO_2 + 2H_2O$

4 $UO_2(CO_3)_3^{4-} + 6H^+ + 2e^- = UO_2 + 3CO_2 + 3H_2O$

5 $UO_2CO_3^\circ + 2H^+ = UO_2^{2+} + CO_2 + H_2O$

6 $UO_2(CO_3)_2^{2-} + 2H^+ = UO_2CO_3^\circ + CO_2 + H_2O$

7 $UO_2(CO_3)_3^{4-} + 2H^+ = UO_2(CO_3)_2^{2-} + CO_2 + H_2O$

CARBONATE EQUILIBRIA

$$\begin{array}{c} H_2O + CO_2(g) \\ \updownarrow \\ CaCO_3(s) + H_2CO_3 \rightleftharpoons Ca^{2+} + 2HCO_3^- \end{array}$$

Figure 6.2. Evolution of Eh-pH conditions for fault-trap ore model. Eh-pH diagram constructed from data by Langmuir, 1978. MoS_2 field (cross-hatched) shown for reference.

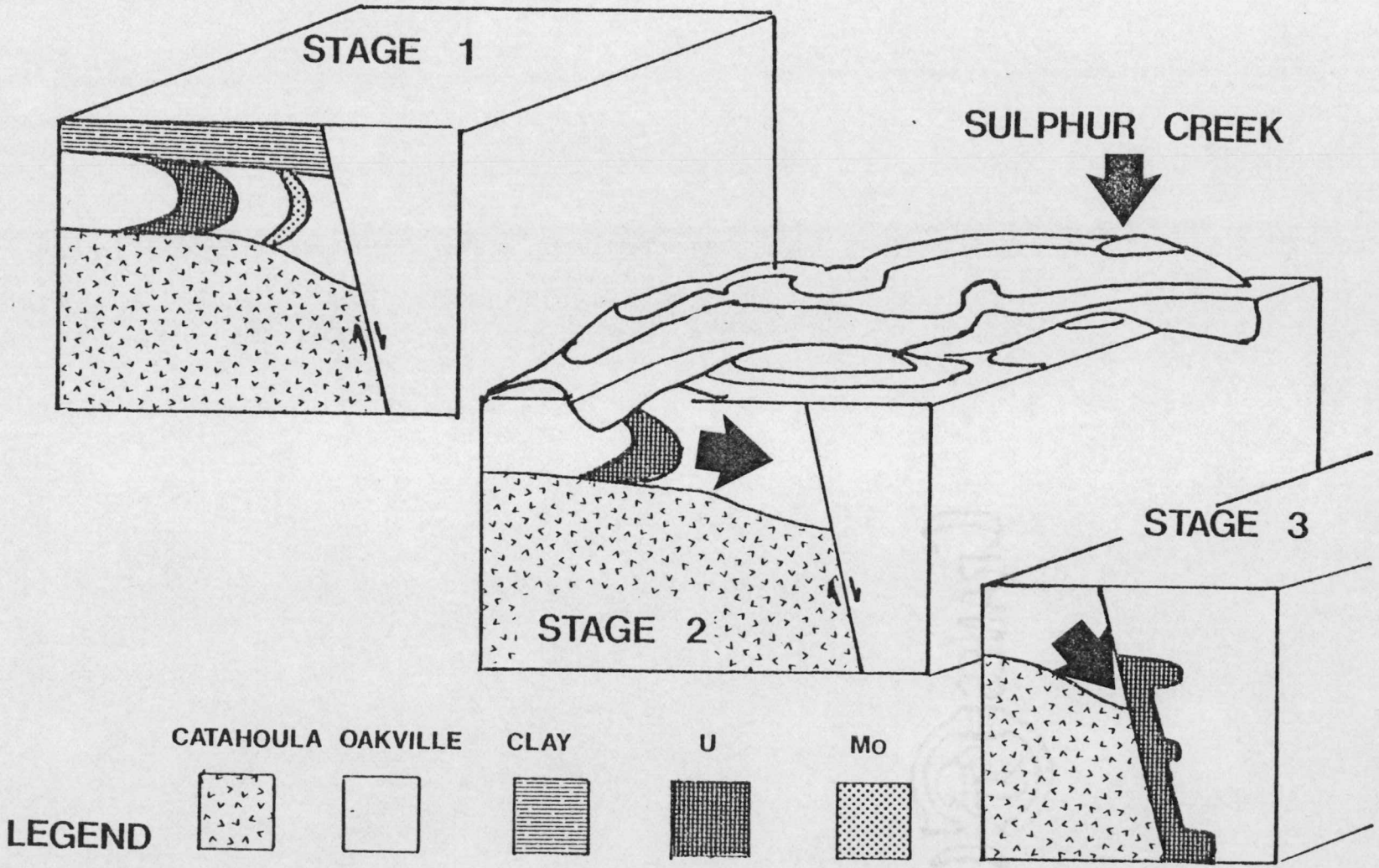

Figure 6.3. Time-space diagram for model of fault-trap uranium mineralization.

upthrown block (Figure 6.3). Eventually the overlying clay layers which protected the reduced zone began to wear thin and oxidation prevailed (reactions 1, 2, 3, or 4, Figure 6.2). The preferred reactions depended on the Eh and pH of encroaching waters, the composition of the host rock, and the oxidation rate. For instance it was possible to produce acidic waters from the weathering of ore-stage sulfides. If uraninite was oxidized in acidic conditions, UO_2^{2+} or $UO_2CO_3^{\circ}$ complexes formed; however, the calcite content of the Oakville would have only allowed local acidity, and uranyl-carbonate complexes were most likely preferred in the long term. Possible sequences of reactions include: 1, 5, 6, and 7; 2, 6, and 7; 2 and 6; 3 and 7; or simply 2, 3, or 4 (Figure 6.2). Uraniferous solutions moved downdip toward the fault, eventually encountering the molybdenum halo and becoming Mo-enriched.

Stage III: Fault-Trap Mineralization

As uraniferous carbonate solutions entered the fault zone, carbonate equilibria became of primary importance (Figure 6.2). Eh was maintained at a relatively constant level by the influx of reducing gases from hydrocarbon deposits at depth. Conditions of pH were above 8 (white arrow, Figure 6.2), demonstrated by ore-stage calcite deposition. Highly concentrated solutions entered microenviornments in the pre-existing calcite cement and became saturated, forming more calcite. Calcite precipitation shifted the carbonate equilibria to the left, resulting in the generation of H_2CO_3 and sharp local reductions in pH. Lowering of the pH destabilized the carbonate complexes and allowed formation of uranium minerals. Marcasite precipitation was preferred

over pyrite due to the drastic drop in pH (El-Dahhar and Barnes, 1979). These sharp local pH reductions resulted in the entire ore sequence across a few millimeters (Figure 4.1, L, p. 50). The sharp depositional gradient prevented the segregation of uranium and molybdenum. The sequence of reactions for fault-trap mineralization include 7 and 3, or simply 4, depending on the Eh level within the fault zone (Figure 6.2).

Oxidation and Supergene Enrichment

Geochemical and mineralogical evidence indicates recent surficial oxidation of the deposit in response to erosion, resulting in oxidation at the surficial level and formation of oxidized uranium minerals. Uranium and Mo were leached from the surface, migrated in solution down the fault plane, and enriched basal zones. Overprints of oxidation and supergene enrichment are distinct from the original ore-forming process.

Timing of Ore Emplacement

Since fault-derived reductants are presumed responsible for roll-front development in South Texas, ore rolls must then postdate deformational episodes that form the controlling faults and open conduits for migration of reducing gases. The Oakville fault in particular seems to represent a phase of compactional faulting that began after deposition of the unit was completed in the Miocene. This stage of faulting is truncated by the Pliocene unconformity, which implies faulting terminated in the late Miocene. The Maclean Five deposit obviously postdates the Oakville fault. Intense oxidation and presence of radioactive daughters in the sands of the upthrown fault-block indicates migration of ore-forming fluids along the base of the Oakville and into the fault zone.

The overlying Plio-Pliestocene sands and gravels do not exhibit the same degree of oxidation, nor do they contain significant uranium; therefore, mineralizing solutions must have entered the fault when the Oakville was much thicker in the mine area than at present. Ore-genesis must then predate development of the unconformity, restricting the age of mineralization to the late Miocene.

III. APPLICATION TO EXPLORATION

The fault-trap model of uranium mineralization is an exciting new concept for exploration in Texas. At present most all local exploration programs are based on the search for roll-front type deposits which have characteristic suites of trace elements and zonation corresponding to horizontal Eh gradients. Fault-trap deposits, while narrow in horizontal extent, are rich in metallic concentrations (some ore 32% U_3O_8 reported) and display a simple correlation between U and associated elements, rather than horizontal zonation.

Several characteristics of fault-trap deposits should serve as aids in designing exploration programs:

(1) fault and hydrocarbon association;

(2) narrow linear ore distribution, resulting in narrow linear geochemical anomalies;

(3) surface anomalies of radioactive daughter products.

Halos of trace elements around fault-trap mineralization would presumably be very narrow and elongated in strike direction, generally conforming to the shape of the host fault. Although the geochemical zonation surrounding two proximal deposits may overlap (e.g., the Felder

roll-front and the Maclean Five fault zone), fault-trap mineralization should be recognized by highly anomalous concentrations of U, Mo, and As in the sampling media.

Application of the fault-trap model will require innovations in regional exploration philosophy. Recognition of regional normal faults becomes essential and will necessitate application of shallow seismic and remote sensing (pre-dawn infrared) technologies. Of foremost importance is the delineation of fault trends which serve as conduits for reducing gases and in which erosion on the upthrown block has been severe. This search may begin directly in areas of uranium production, as most drilling programs presently stop short of controlling faults. Areas with poorly developed roll fronts which lie updip from fault zones may also be considered favorable, since in these cases reduction is not strong enough to stabilize uranium and the solutions pass on downdip.

Considering the prolific number of regional normal faults in uranium bearing units, the potential for additional deposits of this type is enormous. Only time will tell whether the Maclean Five deposit is a "freak of nature," or a common type of uranium occurrence along the Texas Gulf Coast.

CHAPTER VII

SUMMARY AND CONCLUSIONS

I. SUMMARY

Interpretations and conclusions reported below are based on examination of 85 thin-sections, 33 polished sections, and chemical analyses of 51 core samples from the Maclean Five deposit. Radiometric readings from the 99 ft (30.2 m) level of the mine helped elucidate the spatial distribution of the ore. Chemical data from several sources aided determination of the host rock geochemistry. The findings are summarized as follows:

(1) radiometric readings at the 99 ft (30.2 m) level reveal a very narrow horizontal distribution of the uranium ore (<25 ft or 7.6 m), restricted to the immediate vicinity of the fault plane and implying fault-control; sampling procedures were based upon this hypothesis;

(2) in the study area the Oakville Sandstone comprises 32.2% quartz, 5.9% feldspar, 17.3% LRF's, 22.2% VRF's, 0.7% opaques, 2.3% miscellaneous, and 19.4% calcite cement;

(3) VRF's display textures typical of rhyolite, andesite, trachyandesite, basalt, and vitric tuff rock types; VRF's have undergone alteration to chalcedony and clays;

(4) the percentage of calcite cement increases toward the fault zone;

(5) remarkable preservation of delicate calcite fossile structures and present groundwater geochemistry indicate alkaline conditions during weathering, transport, and deposition of the Oakville sediments;

(6) bulk rock calculations reveal considerable amounts of uranium may have been leached from the Oakville during diagenesis, providing an internal source for mineralizing fluids;

(7) the ore assemblage is predominantly uraninite and coffinite with accessory sphalerite and marcasite (rare pyrite);

(8) the paragenetic sequence, calcite → uraninite-coffinite → sphalerite → marcasite, is indicative of sharp reductions in pH during ore formation. Co-existing calcite and marcasite, along with colloform marcasite with pyrite cores, support this observation. Overlapping pulses of mineralization may confuse the order of precipitation;

(9) ore textures reflect, dissolution, replacement, and precipitation in voids;

(10) summary statistics from trace element concentrations in the core samples demonstrate inherent host rock constituents are pseudo-normally or normally distributed, while elements associated with uranium appear lognormally distributed;

(11) depth-concentration plots show three zones of uranium enrichment, including the 3-10 ft (0.9-3 m), 48-60 ft (14.6-18.3 m), and 80-87 ft (24.4-26.5 m) intervals;

(12) U in the core samples displays a simple linear correlation with Mo; and U also correlates with As, although it does not conform to a linear model; Na, K, Al, and Mn have no correlation with U, and are apparently fixed in detrital minerals.

(13) outlying points revealed by X-Y correlation plots denote zones of surficial leaching (3 ft or 0.9 m level) and supergene enrichment (85 ft or 25.9 m level);

(14) the correlation between U and Mo contrasts vividly with the segregation of these elements in Eh-controlled roll-front and tabular ores, but may be explained by sharp local reductions in pH at a constant Eh;

(15) ethane and methane exhibit good correlation in mine waters, reflecting a hydrocarbon source for the reductant;

(16) the fault-trap model for uranium mineralization can be envisioned as a three stage process: Phase I - roll-front development; Phase II - weathering and stream erosion; and Phase III - fault-trap mineralization;

(17) field evidence implies ore emplacement took place in late Miocene;

(18) application of the fault-trap model to uranium exploration may lead to new discoveries of uranium among the numerous regional normal faults along the Gulf Coast; anomalous concentrations of U, As, and especially Mo in the geochemical sampling media should serve as potential pathfinders for this deposit type; groundwater halos around such deposits would presumably be narrow along dip and elongate in the strike direction, generally conforming to the shape of the host fault.

II. CONCLUSIONS

The Maclean Five deposit is a non-typical fault-related uranium occurrence in which pre-existing calcite cement along a fault and

reducing gases formed a chemical solution baffle, resulting in a highly restricted, high-grade, "dike-like" orebody. Precipitation of ore minerals was triggered when carbonate complexes transporting uranium and associated metals entered permeable zones in the cement and became saturated with respect to calcite. Precipitation of calcite reduced the pH and prompted deposition of uraninite, coffinite, and other minerals such as marcasite. Textural evidence reflects these sharp local reductions in pH. Uranium and associated trace elements show highly significant linear correlations, rather than segregation, and unusually high concentrations, also indicative of a sharp depositional gradient. Considering the numerous regional normal faults along the Gulf Coast, it seems highly probable that similar deposits exist elsewhere. Application of the fault-trap model of uranium mineralization may lead to exciting new discoveries, even in areas of extensive previous exploration.

REFERENCES

REFERENCES

Adler, H. H., 1974, Concepts of uranium ore formation in reducing environments in sandstones and other sediments, in Formation of uranium ore deposits: Vienna, Internat. Atomic Energy Agency, Prov., p. 141-166.

Bailey, R. V., and Childers, M. O., 1977, Applied mineral exploration with special respect to uranium: Boulder, Co., Westview Press, 542 p.

Barnes, H. L., and Czmanske, G. K., 1967, Solubilities and transport of ore minerals, Chapter 8, in Barnes, H. L., ed., Geochemistry of hydrothermal ore deposits, New York, Holt, Rinehart, and Winston.

Barr, A. J., Goodnight, J. H., and Sall, J. P., 1979, Statistical analysis system user's guide: Raleigh, North Carolina, SAS Institute, Inc., 494 p.

Berner, R. A., 1971, Principles of chemical sedimentology, McGraw-Hill, New York, 240 p.

Boyle, R. W., Hornbrook, E. H. W., Allen, R. J., Dyck, W., and Smith, A. Y., 1971, Hydrogeochemical methods-application in the Canadian shield; CIM Bull. 64, p. 60-71.

Brookins, D. G., 1977, Geochemical genesis of uranium in the southern San Jan Basin: Bendix Field Engineering Corp., NURE Geology Uranium Symposium, Sedimentary Host Rock Session, p. 8-27.

Brooks, R. A., and Campbell, J. A., 1976, Preliminary investigation of the elemental variation and diagenesis of a tabular uranium deposit, La Sal mine, San Juan County, Utah: U.S.G.S. Open-File Report, p. 76-287.

Brownlow, A. H., 1979, Geochemistry: Englewood, N.J., Prentice Hall, 498 p.

Bruce, C. H., 1972, Pressured shale and related sediment deformation: mechanism for development of regional contemporaneous faults: Am. Assoc. Petroleum Geologists Bull., vol. 57, p. 878-886.

Buerger, M. J., 1934, The pyrite-marcasite relation, Am. Mineral., vol. 19, p. 37.

Bunker, C. M., and MacKallor, J. A., 1973, Geology of the oxidized uranium ore deposits of the Tordilla Hill - Deweesville area, Karnes County, Texas: a study of a district before mining: U.S. Geol. Survey Prof. Paper 765, 37 p.

Davis, J. C., 1973, Statistics and data analysis in geology: New York, John Wiley and Sons, 550 p.

De Voto, R. H., 1978, Uranium geology and exploration, Golden, Colorado, Colorado School of Mines, 396 p.

Dickinson, W. R., 1970, Interpreting detrital modes of graywacke and arkose: Jour. Sed. Pet., vol. 40, p. 695-707.

Donovan, T. J., 1974, Petroleum microseepage at cement, Oklahoma: evidence and mechanism: Am. Assoc. Petroleum Geologist Bull., vol. 58, no. 3, p. 429-446.

Eargle, D. H., Dickenson, K. A., and Davis, B. O., 1975, South Texas uranium deposits: Am. Assoc. Petroleum Geologists Bull., vol 59, p. 766-779.

Eargle, D. H., and Weeks, A. D., 1961, Possible relation between hydrogen sulfide-bearing hydrocarbons in fault-line fields and uranium deposits in the southeast Texas coastal plain: U.S. Geol. Survey Prof. Paper 424-D, p. D7-D9.

El-Dahhar, M. A., and Barnes, H. L., 1979, Transactions, American Geophysical Union, No. 18, vol. 60, p. .

Folk, R. L., 1974, Petrology of sedimentary rocks: Austin, Texas, Hemphill Publishing Co., 182 p.

Garrels, R. M., Hostetler, P. B., Christ, C. L., and Weeks, A. D., 1957, Stability of uranium, vanadium, copper, and molybdenum minerals in natural waters at low temperatures and pressures (abs.): Geol. Soc. America Bull., vol. 68, p. 1732.

Garrels, R. M., 1967, Genesis of some groundwaters from igneous rocks, in Albelson, P. H., Researches in geochemistry, vol. 2, Wiley, New York, p. 405-420.

Gleason, G., and Reed, B. H., 1977, Gamma spectra and nuclide identification catalog: Oak Ridge, Oak Ridge Associated Universities.

Goldhaber, M. B., Reynolds, R. L., and Rye, R. O., 1978, Origin of a South Texas roll-type uranium deposit: II. Sulfide petrology and sulfur isotope study: Econ. Geol., vol. 73, p. 1690-1705.

Goodell, P. C., 1977, Uranium and the diagenesis of volcanic sediments: Bendix Field Engineering Corp. NURE Geology Uranium Symposium, Igneous Host Rock Session, p. 24-35.

Gottfried, D., Moore, R., and Caemmerer, A., 1962, Thorium and uranium in some alkalic igneous rocks from Virginia and Texas, in short papers in geology, hydrology, and topography: U.S. Geol. Survey Prof. Paper 450-B, p. B70-B72.

Grandstaff, D. E., 1976, A kinetic study of the dissolution of uraninite: Econ. Geol., vol. 71, no. 8, p. 1493-1506.

Granger, H. C., 1963, Mineralogy, in Kelley, V. C., ed., Geology and technology of the Grants uranium region: New Mexico Bur. Mines and Mineral Resources Men. 15, p. 21-37.

Harshman, E. N., 1974, Distribution of elements in some roll-type uranium deposits, in Formation of uranium ore deposits, International Atomic Energy Agency, p. 169-183.

Kleinbaum, P. G., and Kupper, L. L., 1978, Applied regression analysis and other multivariate methods: North Scituate, Mass., Duxbary Press, 556 p.

Klohn, M. L., and Pickens, W. R., 1970, Geology of the Felder uranium deposit, Live Oak County, Texas: Paper presented at A.I.M.E. Meeting, Denver, Colorado, Feb. 15-19, 1970: Mining Engineers Soc. pre-print no. 70-1-38, 19 p.

Langmuir, D., 1978, Uranium solution-mineral equilibrium at low temperatures with applications to sedimentary ore deposits: Geochem. Cosmochem. Acta, vol. 42, p. 547-569.

Levinson, A. A., 1974, Introduction to exploration geochemistry, Applied Publishing Ltd.: Maplewood, Illinois, 614 p.

Lyon, W. S., Jr., 1964, Guide to activation analysis, D. Van Nostrand Company, Inc., New York, 186 p.

Mason, B., 1966, Principles of geochemistry: New York, John Wiley and Sons, 329 p.

Motica, J. E., 1968, Geology and uranium-vanadium deposits in the Uravan Mineral Belt, southwestern Colorado, in "Ore deposits of the United States, 1933-1967," vol. 1, Am. Inst. Mining, Metall., and Petroleum Engineers, p. 805-813.

Nichols, C. E., Butz, T. R., Cagle, G. W., and Kame, V. E., 1977, Uranium geochemical survey in the Crystal City and Beeville quadrangles, Texas: Oak Ridge, Union Carbide, U.S. Gov. Contract W-7405, 132 p.

Nie, N. H., Hull, C. H., Jenkins, J. G., Steinbrenner, K., and Bent, D. H., 1970, Statistical package for the social sciences: New York, McGraw-Hill, 675 p.

Pettijohn, F. J., 1975, Sedimentary rocks, 3rd ed., Harper and Row, New York, 628 p.

Pogorski, L. A., and Quirt, S. G., 1976, Helium surveys emerging in explorations: The Northern Miner, Annual Review Number, p. D1 and D19.

Rackley, R. I., 1972, Environment of Wyoming Tertiary uranium deposits: Am. Assoc. Petroleum Geologists Bull., vol 56, no. 4, p. 755.

Radiological Health Handbook, 1970, U.S. Government Printing Office, Washington, D.C.

Ramdor, P., 1969, The ore minerals and their intergrowths: New York, Pergammon Press, 1174 p.

Romberger, S. B., 1978, Uranium geochemistry, Golden, Colorado, Colorado School of Mines, 168 p.

Sellards, E. H., Adkins, W. S., Plummer, F. B., 1932, The geology of Texas, vol. 1, Stratigraphy: Univ. of Texas Bull., no. 3232, 6th ed., 1975, 1007 p.

Sevier, R., 1962, Silica solubility, 0-200° C, and the diagenesis of siliceous sediments, Journal of Geology, vol. 70, p. 127-150.

Shawe, D. R., 1966, Zonal distribution of elements in some uranium-vanadium roll and tabular orebodies on the Colorado Plateau: U.S. Geol. Survey Prof. Paper 550-B, p. 239-241.

Walton, A. W., 1975, Zeolitic diagenesis in Oligocene volcanic sediments, Trans-Pecos Texas: Geol. Soc. America Bull., vol. 86, p. 615-624.

Wedepohl, K. H., ed., 1969, Handbook of geochemistry, vol. II: New York, Springer Verlag, p. 1-A-1 to 90-O-1.

Weeks, A. D., and Eargle, D. H., 1960, Uranium at Palangana salt dome, Duval County, Texas: U.S. Geol. Survey Prof. Paper 400-B, p. B48-B52.

Weeks, A. D., and Eargle, D. H., 1963, Relation of diagenetic alteration and soil-forming processes to the uranium deposits of the southeast Texas coastal plain, in clays and clay minerals, vol. 10, 10th Natl. Conf. Clays and Clay Minerals, 1961, Proc.: New York, Macmillan and Co., p. 23-41.

Zielinski, R. A., 1979, Uranium mobility during interaction of rhyolitic obsidian, perlite, and felsite with alkaline carbonate solution: Chemical Geology, vol. 27, p. 47-63.

APPENDICES

APPENDIX A

ERROR CALCULATION FOR MODAL ANALYSIS

It is useful to assign practical limits to reported values in the sedimentary petrology section. Through modal analysis, estimates were made as to the percentage of various sandstone constituents in a number of samples. Assuming the samples are representative of the same population, a range of mean values is generated which should approximate the normal distribution. From the Chi-square test, it is determined that the lithologic constituents are indeed normally distributed.

Statistical parameters characteristic of the normal distribution and other similar distributions are known. The limits of error of an arithmetic mean may be determined from a t-table if the estimated standard deviation and degrees of freedom (i.e., in this case, the number of samples) have been determined. The general form of the equation is:

$$\overline{X} \pm t_{n-1,1-\alpha/2} \, S/\sqrt{n}$$

where $\overline{X}$ represents the arithmetic mean, t_{n-1} symbolizes the t-statistic for the desired confidence level (CL), based on the student's t-distribution, α equals 1-CL/100, S is the approximate standard deviation, and n equals the number of samples (Kleinbaum and Kupper, 1978). The limits of error were calculated at the 95% confidence level for ten of the grain categories (Table A-1).

Table A-1

Modal Analysis by Grain Type

Sample No.	Quartz	Fspar	Plag.	Kspar	LRF	VRF	VRF-Fel.	VRF-Micro.	VRF-Lath.	VRF-Vitric	Cal. Cm.	Opaques	Misc.
BRN	26	6.5	0.5	6	18	23	8	2	9	4	25	1.5	--
B-2	30	4	2	2	14	27	5	1	15	6	22	--	3
B-4	30	3	2	1	27	20	3	4	10	3	15	--	5
B-6	24	5	2	3	24	22	7	1	7	7	24	--	1
B-8	25.5	26	1	25	14.5	22	7.5	1	8	5.5	30	1.5	3
B-10	34	6	1.5	4.5	12.5	23.5	9	2	5.5	7	19.5	0	4.5
C-2	36.5	2	0.5	1.5	13	28	5.5	2	6	14.5	18	1	1.5
C-4	33	8.5	2	6.5	15	23	3.5	1.5	4.5	13.5	21.5	--	--
C-6	44	5	2	3	12	22.5	3.5	0.5	4.5	14	15	0.5	1
C-10	42	4.5	0.5	4	12.5	14.5	5	1	5	3.5	23	2	0.5
CRS	29	8	--	8	22	18	6	2	5	5	22	1	--
C-S	34	5	--	5	21	16.5	6	5	2.5	3	23	--	1.5
D-4	30.5	4.5	0.5	4	15	20	2.5	--	9	6.5	17.5	0.5	12
D-6	28	8	2	6	22	27	9	2	12	4	15	--	--
D-8	31	12	2.5	9.5	17	19	8	1	6	4	19.5	1	0.5
RS-2	33	3.5	0.5	3	20.5	22	3.5	3	5	10.5	15	1	5
RS-4	26	1.5	0.5	1	25.5	27	3	5	8	11	18	1	1
RS-6	37	16	1	15	15	22	5.5	1	10	5.5	10	0	--
RS-10	34	8	2.5	5.5	10.5	24.5	4.5	1.5	9	9.5	18	2.5	2.5
WL-2	36	5	4	1	15	22	6	1	6	9	17	1	4
Average First Ten	32.9	6	--	--	18	22.3	5.9	1.8	6.8	8.1	20.9	--	--
Average Total	32.2	5.9	1.3	4.6	17.3	22.2	5.6	1.9	7.4	7.3	19.4	0.7	2.3
Error, 95%	±2.72	--	±0.53	±0.74	±2.5	--	±1.05	±0.71	±1.52	±1.9	±2.3	±0.38	--

T-Test for Variation in Means

The t-test can also be used as a measure of statistically valid variation between two populations with unlike means. The test is based on two alternative hypotheses: Ho: $\overline{X}_1 = \overline{X}_2$ or Ho: $\overline{X}_1 \neq \overline{X}_2$. The test statistic is calculated as follows:

$$t = \frac{\overline{X}_1 - \overline{X}_2}{Sp\ 1/n_1 + 1/n_2},$$

where

$$Sp^2 = \frac{(n_1-1)S_1^2 + (n_1-1)S_2^2}{n_1 + n_2 - 2}$$

and $\overline{X}$ equals mean, n equals number of samples, and S equals standard deviation. If the t-statistic exceeds a certain critical level at the desired degree of confidence (percent), then Ho: $\overline{X}_1 \neq \overline{X}_2$, and then it is a valid deviation between the means.

This test was used to check the observation that calcite cement decreased away from the fault plane. The decrease held true at the 95% confidence level. Statistics used for this test are listed below in Table A-2.

Table A-2

Statistics for T-Test Comparison
of Means, Calcite Cement

N (Number Obs.)	$\overline{X}$ (Mean)	S (Std. Dev.)	Cricital T-Statistic	Calculated T-Statistic
$N_B = 6$	$\overline{X}_1 = 22.58$	$S_1 = 5.1$	1.943	2.43
$N_{RS} = 4$	$\overline{X}_2 = 15.25$	$S_2 = 3.77$	2.132	2.43
--	--	$S_p = 4.65$	--	--

APPENDIX B

HOST ROCK GEOCHEMICAL DATA

Table B-1

Live Oak County Groundwater Data, Oakville Formation[a]

No.	pH	HCO_3^-	$SO_4^=$
1	8.3	276	102
2	8.7	242	223
3	8.9	264	228
4	8.7	284	684
5	9.0	260	157
6	7.9	400	30
7	9.6	248	263
8	8.0	294	407
9	8.1	336	5
10	8.0	256	32
Mean	8.52	286	213

[a]From Nichols and others, 1977, Uranium Geochemical Survey in the Crystal City and Beeville Quadrangles, Texas.

Table B-2

Uranium Concentrations for Some Extrusive Igneous Rock Types, Big Bend Area, Texas[a]

Rock Type	U (ppm)
Rhyolite	16.4
Trachyte	19.5
Trachyandesite porphyry	6.2
Trachyandesite	4.3
Basalt porphyry	3.3

[a]Gottfried, D., R. Moore, and A. Caemmerer, 1962, Throium and uranium is some alkalic igneous rocks from Virginia and Texas, in Short papers in geology, hydrology, and topography: U.S. Geol. Survey Prol. Paper 450-B, p. B70-B72.

APPENDIX C

NEUTRON ACTIVATION PROCEDURE AND DATA PRESENTATION

Theory

Neutron activation analysis (NAA) is based on utilization of characteristic gamma radiation emitted by induced radionuclides (Lyon, 1964). Samples are irradiated by low energy (<0.2 eV), thermal neutrons in a reactor. The radioactive samples are then analyzed by gamma ray detection to determine the activities of radioisotopes produced by neutron bombardment. Since the predominant reaction incurred is simple addition of neutrons (X^{y} (n,γ) X^{y+1}), the activities of parent isotopes are proportional to that of their radioactive analogues. Only elements which produce radionuclides upon irradiation may be measured by NAA.

Radionuclide activity obeys the following relation:

$$A = N\sigma\phi S \ ,$$

where A equals radioisotope activity, N equals number of parent atoms available for reaction, σ equals thermal cross-section, ϕ equals neutron flux, and S equals saturation factor (Lyon, 1964, p. 8-9). The saturation factor is further defined by another relation:

$$S = (1 - e^{-\lambda t}) \ ,$$

where λ = 0.693/half-life isotope and

t = irradiation time.

Examination of the principles governing NAA procedures reveals several important limitations. To undergo appreciable neutron capture, an isotope must exhibit:

(1) a large thermal neutron cross-section (σ);

(2) significant relative isotopic abundance.

The relative importance of these factors will vary according to the absolute amount of analyte in the sample.

Detection limits also depend upon the properties of the radionuclide produced. To reach acceptable detection levels, a radionuclide must:

(1) reach saturation quickly (i.e., have short $T_{\frac{1}{2}}$);

(2) emit characteristic gamma radiation within the counting spectrum of the detector;

(3) produce gamma rays at a rate which can be accurately measured.

Application

NAA analyses were performed on 51 powdered core samples representing an 87 ft vertical interval within the Maclean deposit. Laboratory and CF^{252} reactor facilities were provided by Oak Ridge Associated Universities.

Sample preparation. Sample materials were placed in polyethylene rabbits, labeled, and weighed on a Metler balance. Sample weights were recorded and noted on the plastic containers.

Irradiation. Sample rabbits were suspended on strings and lowered into plastic tubes or "holes" in the reactor vessel while the source was dormant. The source was then brought up and the sample parameters

recorded (sample number, weight, hole number, time) in the irradiation log book.

Initially, irradiation times were varied from 80 minutes to seven days to determine the number of measurable elements present. A three day or greater irradiation term proved optimum. Pertinent sample parameters are listed in table form (see Table C-1).

Analysis. NAA was performed by a sophisticated analysis system composed of a PDP-11 computer, a GeLi detector, and a 4200 channel pulse height analyzer. The procedure was sequenced by program input through a teletype terminal.

Samples were removed from the reactor and placed in a sample holder above the detector (distance varies from 10-158 cm, by virtue of choice). Gamma-counts were initiated precisely one minute after the irradiations were terminated, except in cases of equipment failure or other unusual circumstances. After expiration of the counting interval, a peak search and analysis program was used to locate, identify, and measure representative peaks recorded on the monitor. The program requires input of sample parameters, while compensating internally for all other variables associated with the NAA procedure.

Error Analysis

The analysis program is equipped with a built-in measure of relative error. When a peak is integrated, the program first transforms the observed count to a Gausian distribution. The deviation of the observed peak from the normal curve is calculated in terms of relative error (percent).

Table C-1

Sample Parameters for Neutron Activation Analysis

Sample No.	Irrad.	Hole	Ct. Dist.	Wait T.	Live T.
1	4464	6	10	1	2000
3	3456	6	108	21	2000
5	4110	4	158	61	1000
5	4110	4	158	111	2000
8	5400	4	10	1	1000
8	7230	2	10	1	500
9	3554	4	108	1	2000
11	5173	4	10	1	2000
12	5431	6	10	15	2000
19A	4621	4	10	1	2000
34	5106	4	10	1	2000
35	5313	3	10	1	2000
36	15744	3	10	1	1000
37	5305	3	10	1	2000
38	4300	4	10	1	2000
39	5434	6	10	1	2000
40	4679	3	10	1	2000
41	5382	6	10	1	2000
42A	4354	3	10	1	2000
43	5783	4	10	1	2000
44A	2702	2	10	1	1000
45	5718	4	10	1	2000
46	4417	3	10	1	2000
48	5431	6	10	62	2000
49	6134	3	108	1	2000
51	6010	3	10	55	2000
53	4403	6	10	1	2000
54	3604	3	10	60	2000
55	6191	6	10	1	2000
57	4545	6	10	1	2000
58	6189	6	10	1	2000
59	8146	4	10	1	2000
60	1384	2	10	1	1000
61	80	5	10	1	1000
63	3604	3	10	1	2000
66	4483	6	10	1	2000
67	8146	4	10	1	2000
68	3604	6	10	170	2000
69	3840	3	10	4	500
69	3840	3	10	228	2000
70A	4564	4	10	1	2000
71	3840	3	10	23	200
72	3604	6	10	121	2000

Table C-1 (continued)

Sample No.	Irrad.	Hole	Ct. Dist.	Wait T.	Live T.
73	3840	6	10	36	200
73	3840	6	10	160	2000
74	3840	6	10	49	200
74	3840	6	10	63	2000
75	4276	3	10	1	2000
80	4336	3	10	1	2000
81	3830	4	158	1	2000
82	3900	4	108	1	2000
83	3970	3	108	1	2000
83	3970	3	10	122	2000
84	4035	3	10	215	200
85	4737	3	148	694	120
85A	250	2	108	1	2000
86	4330	6	108	1	2000
87	4390	6	108	1	2000
87	4390	6	10	50	2000

Error may arise from several other factors. Element concentrations in this procedure are determined by the measurement of radionuclides; however, to calculate the absolute abundance of an element in a sample, one must account for all the isotopes present. This requires the assumption that natural materials are in isotopic equilibrium, or that the ratio of isotopes in the whole earth is representative of those in the sample. This may not always be the case, as numerous processes of isotopic fractionation have been described. Radioisotopes with a low target nuclide abundance are particularly susceptible to this error, as any relative isotopic enrichment will result in an erroneously high value for the total element concentration. In addition, detector distance can drastically affect counting rates for an isotope, depending on the energy and intensity of the characteristic gamma radiation.

In order to interpret the element data effectively, factors which contribute error must be considered. A table of isotopes used in this study has been prepared, including a list of factors which control their reliability (Table C-2, C-3). Replicate analyses of several samples produced results within the predicted MRE range.

Discussion of REE Concentrations

REE elements were measured in inordinantly high concentrations. These values were not reported in the text because of probable large error factors:

(1) a good portion of these elements may represent artifacts from the NAA procedure (fission products);

(2) standards containing U and REE in this concentration range were unavailable;

Table C-2

Chart of Pertinent Radionuclides

Parent Nuclide	Isotopic %	γ X-Section	Radioisotope	Char. γ (KeV)	γ %	Half-Life ($T_{\frac{1}{2}}$)	M.R.E. (%)
U^{238}	99.27	2.73	U^{239}	74.6	51	23.5 min	1.94
Ba^{138}	71.66	0.38	Ba^{139}	165.9	23	82.7 min	10.53
Mn^{55}	13.3	13.3	Mn^{56}	846.8	99	2.58 hr	0.64
Na^{23}	100	0.53	Na^{24}	1368.6	100	15.0 hr	0.77
K^{41}	6.91	1.5	K^{42}	1524.7	18	12.4 hr	6.06
Al^{27}	100	0.234	Al^{28}	1779.0	100	2.27 min	3.35
Dy^{164}	28.18	2600	Dy^{165}	94.6	4	1.26 min	10.8
Sm^{152}	26.72	208	Sm^{153}	103.2	28	46.8 hr	--
Sm^{154}	22.71	5	Sm^{155}	104.3	73	22.3 min	3.02
Ce^{142}	11.07	0.96	Ce^{143}	293.2	46	1.37 days	10.29
As^{75}	100	4.3	As^{76}	559.1	43	26.3 hr	11.28
Nd^{146}	17.22	1.4	Nd^{147}	91.1	28	11.1 days	10.62
Nd^{150}	5.62	1.3	Nd^{151}	116.8	40	12.0 min	11.07
Mo^{98}	23.78	0.14	Mo^{99}	140.5	2	66.2 hr	7.22

Table C-3

Table of Standards for NAA Data

Element	Reported (ppm)	NAA/ORAU	% Error	Reported (ppm)	NAA/ORAU	% Error
		NBL 42-4			NBL 76-B	
U	5,200	5,184	1	100	98	2
		USGS WL-1			NBS COAL #1632	
As	--	--	--	5.91	5.5	1
Na	1,600	1,500	2	--	--	--
K	5,300	5,160	3	--	--	--
Al	78,600	62,155	21	--	--	--
Mn	1,280	1,300	2	--	--	--
		Spiked Standard				
Mo	52,233	50,712	3			

(3) concentration levels of REE an order of magnitude greater than previously reported in sandstones requires thorough documentation.

Interpretation of these values remains ambiguous. Richard Delle Valle, University of New Mexico; and Geoffrey Gleason, Oak Ridge National Laboratory (personal communication, 1980); have observed increasing concentrations of REE in NAA with increasing U concentration, and have proposed that fission products from the NAA procedure may be responsible; however, published data on fission yields suggests that only minor amounts of these elements can be made in a low-flux reactor, such as the Cf^{252} reactor used for these analyses. It is possible that these physical parameters, based on research from the 40's and 50's, are in error. The strong similarity between U and REE distributions and highly significant correlations between these elements may reflect the production of REE from fission of U^{235} (Tables C-4, C-5, C-6; Figures C-1, C-2, C-3). However, this does not detract from the valid correlation between U and Mo, which is obviously present in the samples.

At present neither argument can be totally disregarded. Possible interpretations are:

(1) REE are fission products, and their lognormal distributions reflect exponential increases in these elements with increases in U content;

(2) REE trends are real because of the scarcity of fissionable U^{235} in the samples and the low flux of the reactor, combined with a relatively short three-day irradiation term.

Table C-4

Element Data for Maclean Five Deposit (ppm)

OBS	DEPTH	U	BA	MN	SR	K	AL	DY	SM	CE	AS	ND	MO
1	1	153	279	664	4561	8531	26849	1.7	360	.	19	3915	640
2	3	20915	17815	608	4946	14080	.	31.5	69977	41582	155	.	50717
3	5	21321	.	880	6621	12947	60712	.	45166	72816	123	99699	23499
4	8	7756	5140	869	5036	11220	65247	9.4	490	7327	158	.	10564
5	9	927	.	375	6337	16967	54256	3.2	1534	.	.	15179	2338
6	11	78	368	1203	5163	16958	67632	3.8	490	.	.	902	.
7	12	35	.	706	5309	18235	.	4.0	10	.	.	.	.
8	19	176	350	585	4616	7968	28882	1.8	384	.	35	.	1987
9	36	93	724	346	7199	34624	44649	2.1	8	.	29	1320	915
10	35	97	429	499	6376	12822	36253	1.6	9	.	15	.	638
11	36	116	372	364	5802	11009	14637	1.7	11	.	.	2298	762
12	37	162	404	358	5667	11785	34791	2.3	13	.	10	.	469
13	38	384	580	1492	4707	10569	34145	1.6	871	739	.	.	611
14	39	1553	1248	543	4760	11159	52938	1.8	98	1514	14	.	1851
15	40	152	363	361	3923	12248	60577	2.1	347	.	.	.	.
16	41	69	.	865	5475	10965	34581	1.5	4	.	29	.	1163
17	42	45	315	723	5319	7951	22570	1.7	93	.	79	.	3288
18	43	51	417	503	6356	12825	33648	1.7	6	.	18	.	634
19	44	51	395	493	7453	12795	34222	1.7	6	.	24	.	569
20	45	47	661	450	7654	14890	43653	2.0	4	.	.	.	392
21	46	50	495	401	6609	12327	39814	1.8	95	.	.	.	363
22	48	1537	1362	208	6303	12623	.	1.4	132	1912	157	.	6402
23	49	1675	.	286	7060	14098	30021	.	3584	.	117	.	4937
24	51	5712	3926	290	7183	14510	.	1.7	369	7135	172	.	11553
25	53	2487	1645	477	5653	13137	39772	1.2	5692	2378	87	.	5553
26	54	1799	1688	403	5735	12435	.	1.8	.	2358	54	.	3563
27	55	1538	1225	306	5539	11396	35039	1.4	.	1309	50	.	3788
28	57	854	899	262	5881	12952	34296	1.7	1650	.	36	.	1863
29	58	551	560	122	5970	18642	65902	3.5	.	.	46	.	1746
30	59	53	622	93	4018	21972	76509	3.2	9	.	13	1386	244
31	60	20	1048	157	5499	18191	63241	3.5	6	.	.	.	.
32	61	707	651	1084	5406	11560	.	1.7	62	.	33	.	1035
33	63	846	846	767	5244	12414	32968	1.7	66	.	37	.	999
34	66	31	1122	.	5945	12586	37820	2.4	4	.	.	.	.
35	67	22	4373	431	6518	19457	80807	4.7	5	.	.	.	.
36	68	.	.	182	5435	10835	.	3.1	5	.	23	.	.
37	69	50	.	228	6157	14629	83343	3.3	6	.	.	.	243
38	70	119	373	358	4272	7953	28233	1.5	120	.	13	.	372
39	71	86	.	604	5938	.	.	2.2	150	.	.	.	.
40	72	96	.	509	5901	12368	.	2.1	13	.	13	.	371
41	73	112	.	538	5762	10999	.	2.7	188	.	13	.	454
42	74	138	595	327	5444	14317	.	1.9	.	.	.	.	507
43	75	219	636	450	6611	12443	36474	2.1	494	.	25	.	832
44	80	2660	1873	366	5245	12707	28691	1.5	5932	3339	88	.	4252
45	81	6400	8453	1369	5533	9777	26396	.	12395	10433	117	201176	10376
46	82	5670	3575	692	4211	.	28354	.	9300	6916	94	207912	8870
47	83	3607	3183	576	5369	12477	.	1.9	6010	4101	83	100132	5517
48	84	2435	2031	2959	7759	15544	38309	1.9	4167	3540	63	63682	3722
49	85	24927	19758	1649	5515	7359	24040	19.5	2083	57932	157	26138	45816
50	86	11379	6274	3598	5099	.	22128	.	22027	15867	138	258278	17007
51	87	2564	1996	3649	4705	11861	28904	1.7	4220	2971	.	.	9199

Table C-5

Summary Statistics for Supplementary Data

VARIABLE	N	N MISSING	MEAN	STANDARD DEVIATION	MINIMUM VALUE	MAXIMUM VALUE	RANGE	SKEWNESS
BA	41	10	2412.15	4167.13	279.00	19758.00	19479.00	3.28
CE	18	33	13565.50	21222.61	739.00	72816.00	72077.00	2.09
SM	47	4	4226.81	12322.83	4.00	69977.00	69973.00	4.33
DY	46	5	3.27	4.86	1.20	31.50	30.30	4.95
ND	13	38	75155.00	90912.66	902.00	251278.00	250376.00	1.00

Table C-6

Correlation Matrix for Supplementary Data[a]

	BA	CE	SM	DY	ND	U
BA	1.00000	0.97542	0.66286	0.88581	0.25153	0.97003
	0.0000	0.0001	0.0001	0.0001	0.4556	0.0001
	41	17	37	38	11	41
CE	0.97542	1.00000	0.64294	0.82682	-0.44093	0.94810
	0.0001	0.0000	0.0072	0.0003	0.3221	0.0001
	17	18	16	14	7	18
SM	0.66286	0.64294	1.00000	0.86513	0.54335	0.74104
	0.0001	0.0072	0.0000	0.0001	0.0550	0.0001
	37	16	47	42	13	46
DY	0.88581	0.82682	0.86513	1.00000	-0.04001	0.85059
	0.0001	0.0003	0.0001	0.0000	0.9186	0.0001
	38	14	42	46	9	45
ND	0.25153	-0.44093	0.54335	-0.04001	1.00000	0.31474
	0.4556	0.3221	0.0550	0.9186	0.0000	0.2949
	11	7	13	9	13	13
U	0.97003	0.94810	0.74104	0.85059	0.31474	1.00000
	0.0001	0.0001	0.0001	0.0001	0.2949	0.0000
	41	18	46	45	13	50

[a]Correlation coefficients/probability > |R| under HO:RHO = 0/number of observations.

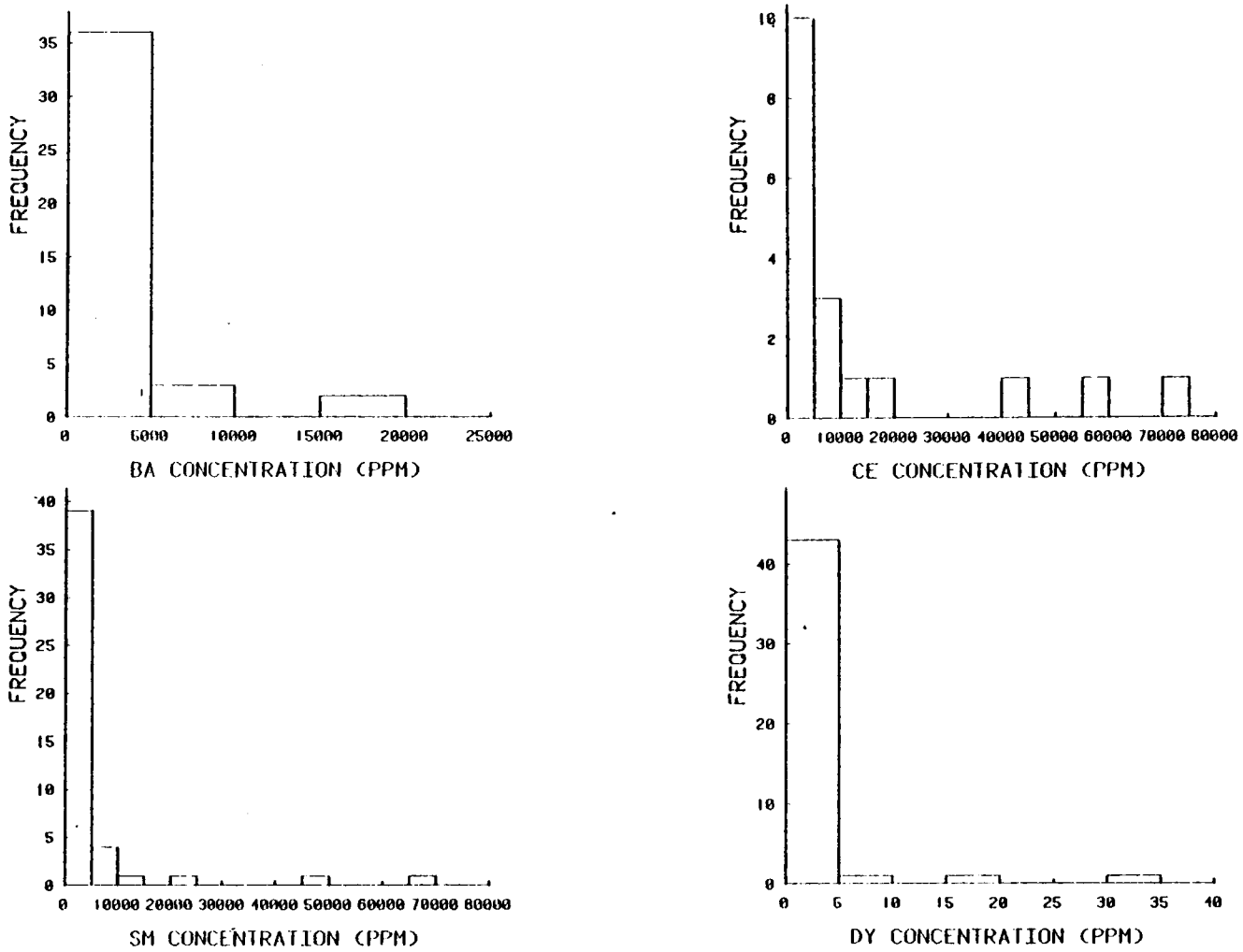

Figure C-1. Histograms of supplementary element data.

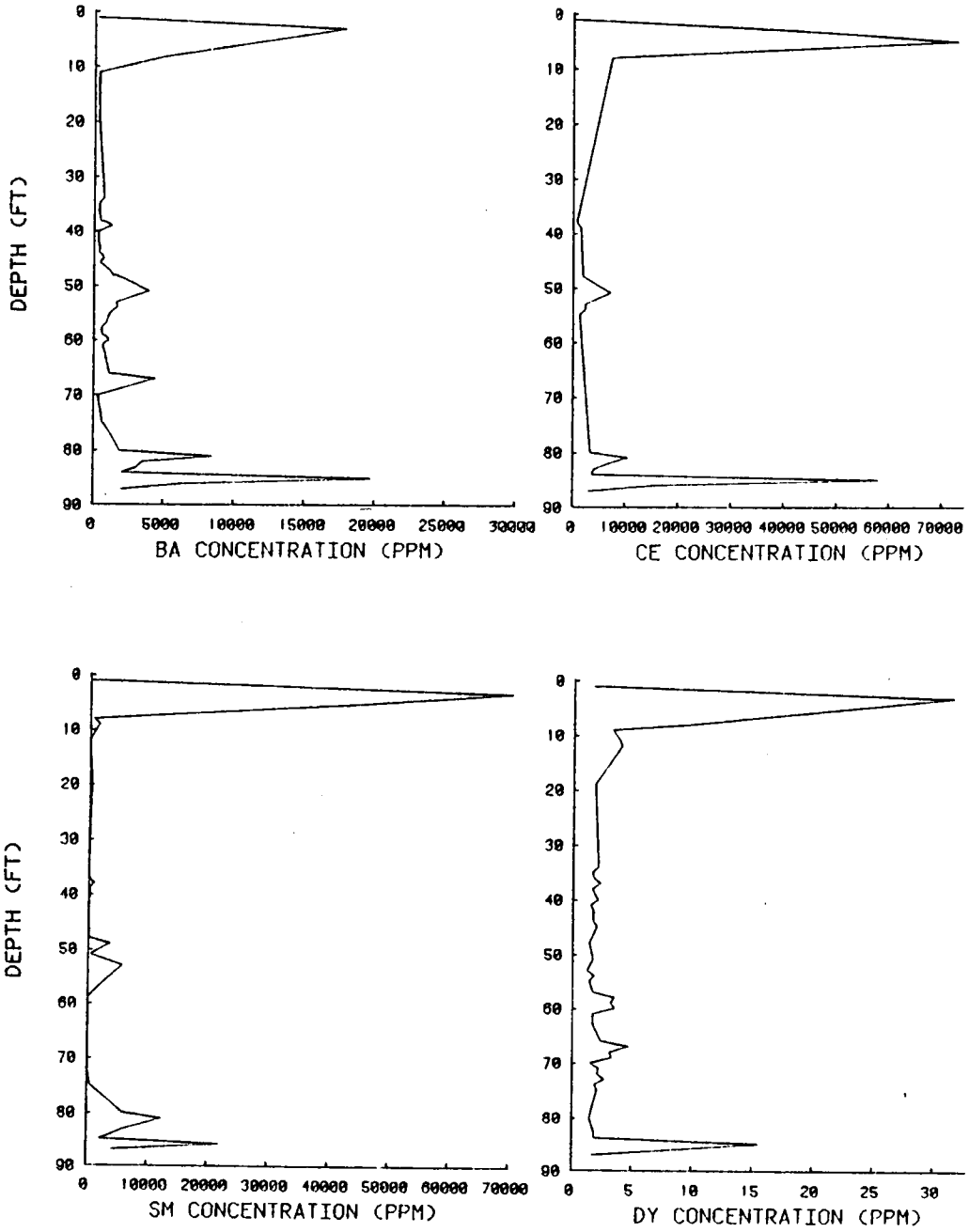

Figure C-2. Depth concentration plots for supplementary data.

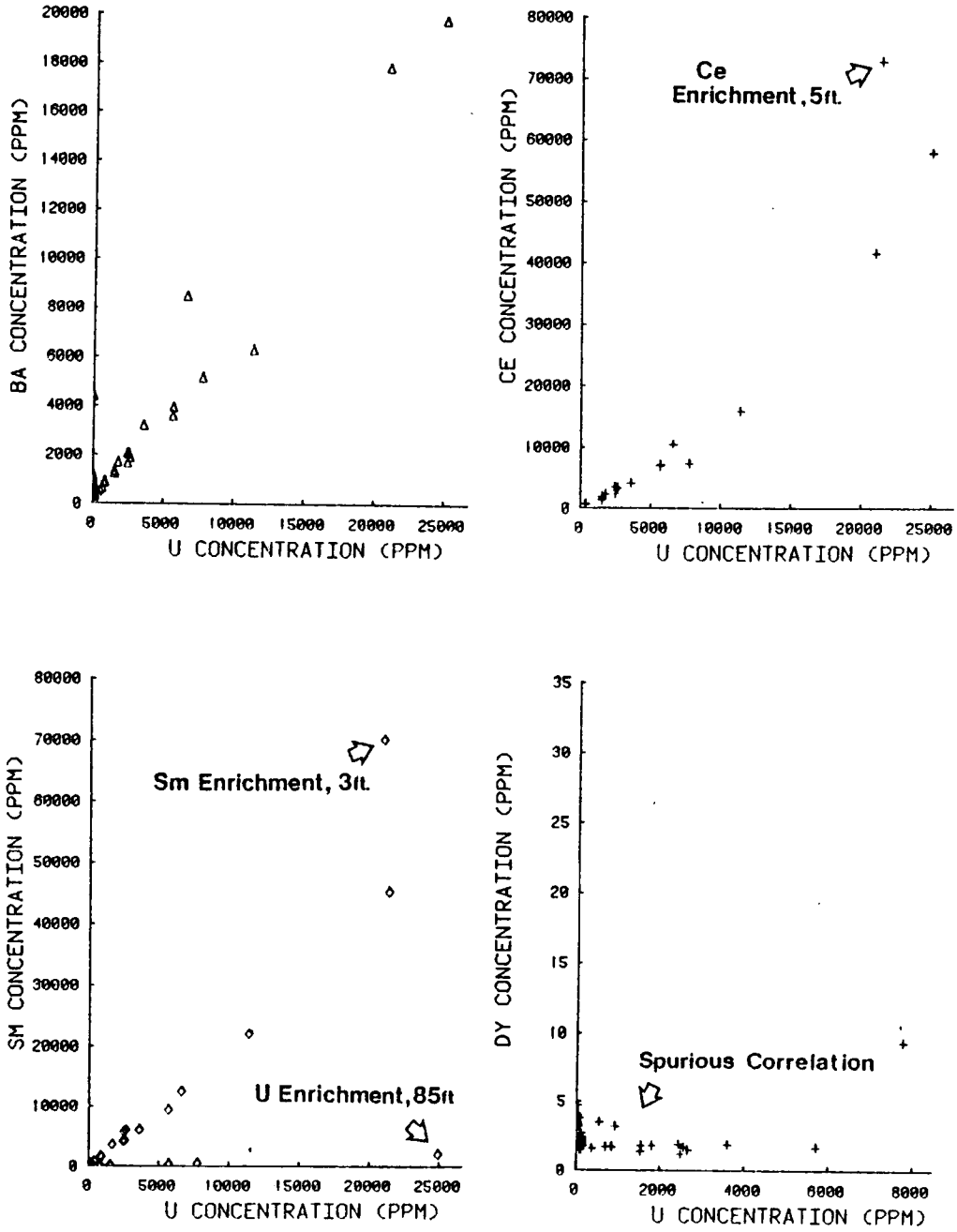

Figure C-3. Correlation plots for supplementary data.

APPENDIX D

AQUEOUS HYDROCARBON DATA

Table D-1

Hydrocarbons

Source	Methane	Ethane	Depth
Maclean Five Pit[a]	5361	139	-
	10236	143	-
	11277	149	-
	11324	161	-
	11733	171	-
	6475	15	-
	5037	29	-
	6461	14	-
	5704	31	-
	3848	15	-
	10558	29	-
Live Oak County[b]	1735663	368	315
	730003	348	387
	22415	-	68
	2036	16	160
	842683	393	300
	699750	371	312
	19934	-	70
	1231	-	65
	1601	-	45
	455	-	85
	25962	68	98
	418431	119	123
	5182	-	80
	784	-	30
	1777653	566	275
	1675908	392	400
	167359	30	190
	938	-	95
	330	-	60
	5332	-	132

[a]Analyses performed by Chemical Projects Ltd., Rexdale, Ontario, Canada.

[b]Data supplied by Exxon Minerals Company, U.S.A., Corpus Christi, Texas.

VITA

William Blair Cathey was born in Columbia, Tennessee, on November 30, 1954, and was raised on a farm near his ancestral home, Hampshire, Tennessee. He graduated from Central High School in Columbia, Tennessee, in June of 1972. On October 18, 1974, he married Victoria Ann Russell of Williamsport, Tennessee. In 1975 he entered The University of Tennessee, Knoxville, to study geology, and completed his degree with high honors on June 10, 1977. In the fall of the following year, he entered The University of Tennessee graduate school to study geology. Upon completion of his degree, he was employed by Continental Oil Company as an oil and gas exploration geologist.